OPTICAL ARBITRARY WAVEFORM GENERATION USING CHROMATIC DISPERSION IN SILICA FIBERS

A Thesis
Presented to
The Academic Faculty

by

Elric O. Von Eden

In Partial Fulfillment
of the Requirements for the Degree
Master of Science in the
School of Electrical and Computer Engineering

Georgia Institute of Technology
August 2007

OPTICAL ARBITRARY WAVEFORM GENERATION USING CHROMATIC DISPERSION IN SILICA FIBERS

Approved by:

Dr. Ali Adibi, Advisor
School of Electrical and Computer Engineering
Georgia Institute of Technology

Dr. Gee-Kung Chang
School of Electrical and Computer Engineering
Georgia Institute of Technology

Dr. Stephen E. Ralph
School of Electrical and Computer Engineering
Georgia Institute of Technology

Date Approved: February 9, 2007

This is dedicated to my family and everyone else who helped me along my way just so they could see me succeed. This is also dedicated to the innocent students and faculty who lost their lives at Virginia Tech on April 16, 2007 doing what I am doing now: pursuing a higher education.

ACKNOWLEDGEMENTS

I would like to thank Dr. Ali Adibi for being my advisor, for always being accommodating and willing to provide me with any help and resource that I may need with my project or any other endeavors. I also appreciate the opportunity to be a part of his group and to do research in an area in which I am interested. I would especially like to thank Dr. Siva Yegnanarayanan for serving as a mentor and providing me with invaluable and necessary assistance during the course of my work and research. My research and thesis would not have been possible without him. I also am grateful for all of my group members for readily going out of their way if I asked them for help with anything. I would also like to thank Dr. Ralph and Dr. Chang for taking time out to serve on my thesis reading committee.

Finally, I would like to thank my mother for all of the support that she has given me through the years. There are not enough words to express my gratitude. Without her guidance, I would not be where I am or who I am today. This thesis is mainly dedicated to you (and so that I can graduate). Thank you.

TABLE OF CONTENTS

LIST OF FIGURES

Page

SUMMARY

A novel approach to optical pulse shaping and arbitrary waveform generation (OAWG) using time-domain spectral shaping (TDSS) in negative and positive dispersion in commercial optical fibers has been proposed and evaluated. In order to study the pulse shaping capability of this OAWG system, mathematical analysis was used to determine expressions for the expected output waveform under certain assumptions. Then, Matlab code was developed to model the propagation of an optical signal through a fiber with arbitrary characteristics as well as optical modulation using an electro-optic modulator. The code was first benchmarked to several well-known theoretical systems to ensure that it produced accurate results, and then it was used to examine the ability of this novel OAWG approach to generate different waveforms under various conditions. The results of numerous simulations are presented and used to qualitatively examine the ability of this system to perform OAWG in a real-world setting.

Based on the results of simulations, mathematical modeling, as well as previous research in this area, it was determined that higher-order fiber dispersion could be a limitation to the time-bandwidth product and pulse shaping fidelity of this pulse shaping method. Additional dispersion compensation techniques were devised to help overcome these limitations such as the use of multiple dispersion-compensating fibers and spectral phase modulation. An OAWG system employing these techniques was also simulated using the developed Matlab code. Using these results, the possibility and feasibility of employing this system in various pulse shaping applications such as optical communications, are discussed and analyzed. Limitations of the system are also investigated, and methods to improve the system for future applications are suggested.

The thesis is organized as follows. Chapter 1 provides a brief discussion of the applications for pulse shaping and describes some of the potential advantages of using an

all-fiber OAWG system. Chapter 2 compares some of the different pulse shaping approaches currently being researched including the one presented in this thesis. Chapter 3 gives a theoretical investigation and some mathematical insight of the equations governing pulse shaping using optical fibers and electro-optic modulation. Chapter 4 shows simulation results obtained by Matlab simulation of the OAWG system, and Chapter 5 presents some experimental results. Finally, the thesis concludes with Chapter 6, which briefly looks at some of the main applications that can benefit from this pulse shaping method as well as its limitations, advantages, possible improvements and future utilization in pulse shaping applications.

INTRODUCTION

Motivation for arbitrary waveform generation

Pulse shaping and arbitrary waveform generation have been in great demand for a variety of engineering and scientific applications. In radar, signal processing, communications, and control applications, the ability to customize a signal is beneficial since an input signal can be optimized for better system performance as well as specified to simulate an arbitrary real-world signal. The focus on optical arbitrary waveform generation (OAWG) and pulse shaping in recent years has been due to the capability of using photonics techniques that have a greater potential to generate complex high-frequency waveforms than current electronic techniques that can currently only generate arbitrary signals up to 5GHz. [1] This results from the fact that these electronic techniques have to rely on electronic circuits to produce arbitrary waveforms, and these circuits suffer from inherent speed and bandwidth limitations.

The use of effective photonics techniques in pulse shaping and OAWG systems have been made possible mainly because of the development of low-cost turn-key high-powered femtosecond lasers. Femtosecond lasers currently serve as the best means of generating pulses of very short duration and hence high spectral bandwidth. At this time, lasers capable of generating down to six femtosecond or shorter pulses are commercially available. Using these femtosecond sources, a variety of pulse shaping techniques can be used to synthesize complicated ultrafast optical waveforms. The fact that waveforms of even shorter duration and increasing complexity can be created is very promising to and can be useful for a good number of fields such as those mentioned above as well as specific chemical and biological applications, nonlinear optics, imaging, control of molecular and atomic processes, quantum control, and spectroscopy. [2]

However, there can be different design constraints and required characteristics for an OAWG solution depending on the system for which it is going to be used. For instance, consider using pulse shaping to convert all incoming optical femtosecond pulses into a square pulse for improving the switching characteristics of a fiber nonlinear coupler[3] (for use as an optical switch) employed in a bulk optical receiver. In such an application, excellent control of the output features must be exercised to ensure that the waveform is as a close to a square pulse as possible, but the ability to reconfigure the pulse shaping apparatus is unnecessary since the same optical signal is desired. On the other hand, suppose pulse shaping is needed to generate short pulse optical packets at a gigabit per second data rate in a future high-speed optical network. [4] Reconfigurability (the speed at which the output waveform could be changed) would then become a huge issue, as optical packets would need to be updated at frequencies in the gigahertz range.

Techniques for pulse shaping and arbitrary waveform generation

Because of the wide range of areas that can benefit from arbitrary waveform generation technologies, there has been a huge amount of research to develop different femtosecond pulse shaping and OAWG techniques using femtosecond lasers. These techniques are usually Fourier-based and dependent on modulation of the broad spectrum of an ultrashort pulse, although alternative methods do exist. The most commonly used Fourier-based approach for pulse shaping uses a pair of diffraction grating and lens apparatuses and a spatial mask or a spatial light modulator (SLM) to perform parallel modulation on the spectrum of the pulse. [5] This system can allow for high resolution and excellent spectral phase and amplitude manipulation to generate very complex waveforms, but because of the slow response of materials used as a SLM, the refresh rate of the output waveform is limited to at the very most to 1 MHz. Due to the fact that it is a free-space arrangement, it requires alignment and would not be so easily incorporated

into fiber-optic systems (resulting from the difficulty in coupling the shaped waveform back into fiber) nor integrated onto a compact chip-scale device with waveguide elements. Also, increasing the pulse shaping complexity (the number of independent controllable features that can be placed in the output waveform) and time-bandwidth product (TBWP) would require a nontrivial increase in the physical size of the SLM, whereas would increasing the maximum temporal window would require an increase in the complexity and spatial resolution of the SLM. Some more recent proposed OAWG architectures have used arrayed waveguide gratings[6] combined with an array of modulators[7] to overcome the problems of free-space alignment, fiber coupling, and integration. However, the time-bandwidth product of a system employing these types of gratings still depends on the number of arrayed waveguide channels and affects the resolution of the spatial filter that performs the pulse shaping.

There are other OAWG techniques that utilize acousto-optic filters[8], tapped delay-line waveguide filters[9], or other linear filtering mechanisms. Acousto-optic filters can be programmable, have high resolution, and be reasonably compact, but there are limits on the spectral control and complexity. Tapped delay-line waveguide filters can also be programmable, but improved system complexity results in an increase in waveguide taps and phase shifters and requires phase stabilization for a higher number of delayed pulses.[2]

Fiber-based pulse shaping techniques

When considering OAWG and pulse shaping for the purposes of optical communications and networks, it is advantageous to use a technology that is compatible with fiber systems. For various optical communications applications, it also is beneficial to have an OAWG system that has a very fast waveform refresh rate (or reconfigurability) comparable to the anticipated data rates of future high-speed optical systems, has a high resolution and a high time-bandwidth product (TBWP), can be

compact, and use a simple scheme. This has precipitated the development of OAWG systems that use commercial optical fiber[10] or a chirped fiber Bragg grating (FBG) [11] as a dispersive element instead of a diffraction or arrayed waveguide grating. There are different variations of these types of systems, but in all of these systems, an optical signal with a broad spectrum (almost always a femtosecond pulse) is propagated through an optical fiber or a chirped FBG. The chromatic dispersion of the optical fiber or chirped FBG spreads the spectral components of the input signal in time. Pulse shaping or OAWG can then be achieved by serial modulation in the time domain to alter the spectrum of the pulse by applying an arbitrary RF (radio frequency) signal single electro-optic phase and/or amplitude modulator as opposed to parallel modulation in the spatial domain using an SLM. A grating pulse compressor[2] or a complementary chirped FBG or fiber[12] could recombine the modified spectral components generating the arbitrary waveform.

Since time-domain spectral shaping (TDSS) is used, the TBWP and resolution of the system depends on either the speed of the signal applied to the electro-optic modulator and the amount of chromatic dispersion in the fiber or FBG and does not affect the size or number of modulators used in the setup. As a result, the shaping complexity of the system is only affected by the dispersion of the fiber or FBG (which is also a function of the length of the fiber or FBG) and the modulation speed of the modulator, and thus the system can be made reasonably compact even when a large TBWP and high resolution is desired. A chirped FBG can provide a high amount of dispersion over a smaller length than a conventional optical fiber. However, fiber gratings are highly sensitive to temperature, their dispersion profiles cannot be altered, their reflected bands are not as wide and smooth as those of conventional fibers [11], and longer lengths of FBGs required for higher TBWPs are not as commercially available as silica fibers. For these reasons, OAWG using silica fibers commonly used in optical communications has some attractive properties.

Although the idea to use optical fiber as a pulse stretcher has been around for some time now[10], the utilization of complementary fiber as a pulse compressor for the purpose of TDSS has just been very recently proposed by Saperstein et al.[12] Advantages of this approach include the possibility of realizing high TBWPs without drastically increasing physical size, the use of only a single modulator for spectral modulation, compatibility with fiber systems, reconfigurability and high waveform refresh rate, polarization insensitivity, and use of cheap and commercially available components. In the proposed pulse shaping setup by Saperstein et al., an RF single-tone signal was applied to a Lithium Niobate electro-optic amplitude modulator to generate delayed satellite pulses. They noted that third-order and higher order chromatic dispersion was a limitation to the performance and achievable TBWP of their spectral shaping scheme. The research and analysis that will be presented in subsequent chapters of this paper will further examine and offer improvements for this TDSS approach as a pulse shaper and as a possible OAWG technology. The viability of using this technique in specific pulse shaping applications will also be determined.

CHAPTER 2

OPTICAL ARBITRARY WAVEFORM GENERATION TECHNOLOGIES

Introduction

There are a large number of different optical arbitrary waveform generation (OAWG) technologies being researched for different applications. This chapter gives a brief description and analysis of a select few of these different OAWG technologies and their capabilities to give an idea of the various methods used in pulse shaping. Then, finally OAWG using the proposed scheme of chromatic dispersion in silica fibers will be analyzed.

Metrics for pulse shaping systems

Due to the large number of pulse shaping applications and researched schemes for OAWG systems, there is a need to define characteristics specific to OAWG that are desired by a particular application and can be used to evaluate a particular OAWG architecture. These characteristics were mentioned in the previous chapter. In this section, each of these properties will be briefly discussed.

Temporal resolution

One important property for all OAWG technologies is the temporal resolution of the system. The recent interest in developing OAWG is principally because of their ability to produce ultrafast waveforms of very fine temporal resolution. The shortest achievable temporal duration or the temporal resolution for a pulse shaping schemes

usually is the pulse duration from the optical source and is not necessarily a function of the pulse shaping scheme itself. However, there are several OAWG schemes that can generate pulses of significantly shorter duration than that originating from the source. [2]

Maximum temporal window

The maximum temporal window is the duration over which significant temporal features in the output waveform can be changed. In most setups, this is related to the finest spectral feature that can be modified. Given a particular temporal resolution, the maximum temporal window is very important because if this window is not much larger than the temporal resolution, this limits the possible complexity of and the amount of temporal features that can be placed onto the output optical signal.

Pulse shaping complexity and time-bandwidth product

The pulse shaping complexity is the number of controllable independent temporal features that can be placed onto the output waveform. This is also usually the number of controllable independent spectral features that can be modified in the output waveform. Dividing the maximum temporal window by the minimum temporal resolution can closely approximate this number. The time-bandwidth product (TBWP) is another important property of a pulse shaping system, and it is closely related to the pulse shaping complexity. The TBWP of a pulse shaper is defined to be the multiplicative product of the modifiable spectral bandwidth and the temporal window of the output waveform. Since the modifiable spectral bandwidth is usually proportional to the minimum temporal resolution, then the TBWP is approximately proportional to the shaping complexity of the system. [5] These quantities are extremely important when considering the ability of an OAWG system to truly as a generator of an arbitrary waveform.

Phase and amplitude control

Whether the pulse shaping is performed by spectral modulation or directly altering the waveform temporally, precise control of the phase and/or amplitude of the output waveform is a very beneficial characteristic in OAWG. In certain applications like higher-order and dark soliton generation [2], molecular control, and spectroscopy, the phase of the output waveform is very important.[10] However, in dispersion compensation, the intensity of the output waveform is of principal concern whereas the phase can usually be ignored. Overall, excellent pulse shaping fidelity is achieved if the controllable features in a pulse shaping scheme can be well-manipulated in both amplitude and phase.

In Fourier-based OAWG techniques, this usually translates into the ability to apply the desired amplitude and phase modulation on the different spectral features of a pulse. For all OAWG technologies, this refers to the ability to make the temporal features of the output waveform as close as possible to a target waveform. Although the system complexity can serve as a gauge of the pulse shaping fidelity, the level at which the features of a waveform can be controlled is also important. For instance, consider a system that has a pulse complexity of 100,000 (implying that 100,000 distinct temporal features that can be controlled in the output waveform), but can only provide binary amplitude control for each of these features. Such a system would be impractical for generating a triangular pulse. This example shows that a certain level of amplitude and phase control may be needed in order to provide robust OAWG.

Reprogrammability and waveform refresh rate

Reprogrammability (or reconfigurability) refers to the ability of a pulse shaping method to change from one shaped waveform to another target waveform. This is obviously important in situations where the output needs to be changed. The time or speed at which it takes to reprogram the pulse shaper to produce a different waveform is referred to as the waveform refresh rate. The waveform refresh rate becomes an

important factor in applications where waveforms need to be updated in a very short time period.

Other considerations

Besides the above metrics, there are other considerations to be taken into account when looking at the feasibility of using a particular OAWG technology for a specific application. Some of these aspects include such things as size and overall compatibility within a system. For certain applications, a pulse shaping scheme does not need to excel at all of these metrics or may need to be judged on additional metrics; however, the metrics discussed above can be used to assess the pulse shaping capabilities of a particular system in the most general sense.

Different OAWG techniques

Pulse shaping using spatial light modulators

Most of the methods used for optical pulse shaping are Fourier-based techniques, meaning that these methods either select or filter out addressable spectral components of the initial optical pulse and use these components to synthesize a new waveform. [5] As mentioned in the previous chapter, the most popular of these pulse shaping techniques is the one presented by Weiner et al. [13] and is shown in Figure 2.1 below. There are numerous variations of this setup, but the principle behind each of these variations is the same. An initial optical pulse is spatially dispersed from a diffraction grating onto a Fourier plane where an SLM or spatial filter is located. As a result, the frequency components of the initial pulse are spread out spatially in a single dimension across the SLM. The SLM or spatial filter can then be made to alter the phase and/or amplitude of the different spectral elements in space. After the modified optical signal diffracts from another grating (or the same grating in some arrangements), the modified wavelength

components interfere with each other to generate an arbitrary waveform dependent on the spatial pattern of the SLM.

Pulse shaping apparatuses based on this concept require high-quality optical components and have strict alignment tolerances. However, if this is overlooked, then the performance of this system relies entirely on the properties of the SLM. If a fixed spatial mask designed with the use of microlithography techniques is used as an SLM, then the desired output waveform can be produced with excellent fidelity but reconfigurability of the waveform is impossible. If a programmable SLM is used, then there are mainly two different technologies that are considered as possible choices for the SLM. One type of SLM is a liquid crystal array, and another type of SLM is an acousto-optic modulator.

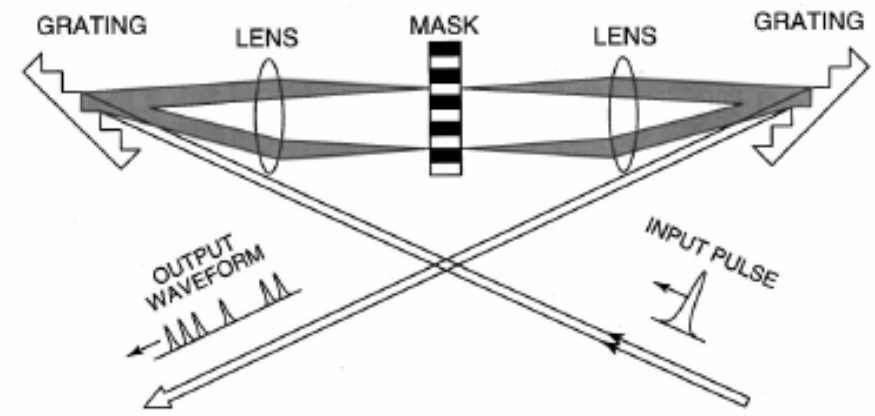

Figure 2.1: Schematic of a basic Fourier-based pulse shaping apparatus in a zero dispersion pulse compressor configuration.[2]

When an electronically addressable liquid crystal array is used for a spatial filter, electrodes are used to apply voltage to a nematic liquid crystal that can modify either the phase or amplitude of the light transmitted through the corresponding spatial pixel in the array. If a double liquid crystal SLM array is used, both optical phase and amplitude can be controlled for each spatial pixel. The number of electrodes addressing the spatial pixels within the crystal array places an upper limit on the pulse shaping complexity. Due to the nature of the crystal, the waveform refresh time of the system is limited to ~10ms.

When an acousto-optic modulator is used as an SLM, the spatial filtering is performed by driving an acousto-optic crystal with an arbitrary RF voltage signal. This signal is converted into an acoustic wave by the use of a transducer. This acoustic wave creates a diffraction pattern in the crystal for the incident dispersed light that modifies the spatially dispersed spectral elements. The waveform refresh time of this particular system is limited by the time it takes for an acoustic wave to propagate through the crystal, which can be on the order of microseconds. The pulse shaping complexity of this system is ultimately limited by the TBWP of the acousto-optic crystal which can be on the order of 1000, but other factors such as the properties of the crystal and the shaping apparatus around the crystal can make this number significantly less by about a factor of ten.

This pulse shaping arrangement using either of these programmable SLMs can generate a variety of arbitrary pulse shapes with a pulse shaping complexity of between 100 and 150. The reprogramming time for both SLMs is sufficient for many pulse shaping applications, and this technique provides excellent control of the amplitude and phase of a femtosecond laser spectrum. In the case of using a liquid crystal SLM, the pulse shaping fidelity can be negatively affected by pixellation effects (the fact that the spatial modulation is divided into spatial pixels) that generate temporal sidelobes in the output waveform. On the other hand, pulse shaping fidelity can be compromised by

acoustic nonlinearity and attenuation when using an acousto-optic modulator. In order to increase the complexity of this system for both SLMs, either the size or the spatial resolution of the SLM must be increased. But overall, this pulse shaping arrangement has been widely used in a number of applications for its ability to perform pulse shaping and produce a large number of high-resolution complex arbitrary waveforms. [5]

Use of Arrayed Waveguide Gratings

The use of arrayed waveguide gratings as an alternative to diffraction gratings (as mentioned in the system in the previous section) in a pulse shaping system has its own advantages. Using arrayed waveguide gratings as opposed to bulk gratings eliminates the requirements for alignment and high quality optical elements. This is a compact scheme that can easily be integrated into a fiber-optic system if so desired. Two possible implementations of arrayed waveguide gratings in an OAWG system are shown in Figure 2.2(a) and (b) below. In Figure 2.2(a) and 2.2(b), the arrayed waveguide grating can act as a wavelength demultiplexer to spatially separate the spectral elements of the initial signal or a multiplexer to recombine spectral elements from different waveguides into one output waveguide. In Figure 2.2(b) though, the same OAWG performs both functions, and the spatial filtering by the modulator array is electronically addressable.

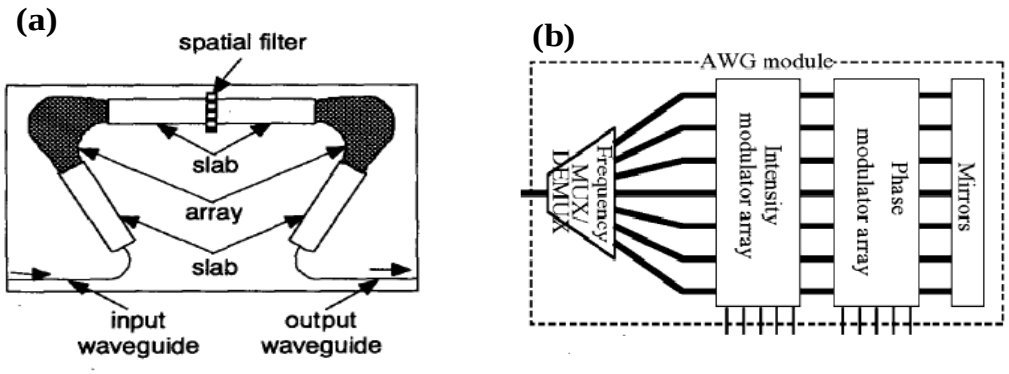

Figure 2.2: (a) Implementation of an arrayed waveguide grating pulse shaping system using a fixed spatial mask. [6] (b) Implementation of an arrayed waveguide grating OAWG with an electronically addressable modulator array. [7] In this implementation, the input signal enters from the left into the MUX/DEMUX and exits out the same MUX/DEMUX after reflection from the mirror.

The pulse shaping complexity of this technique is limited by the number of arrayed waveguides in the grating or the properties of the spatial filter. This number can be anywhere from about 50 to over 100 depending on these factors. Reconfigurability, phase and amplitude control, and the waveform refresh rate of this technique, similar to those of a diffraction grating-based SLM pulse shaper, are dependent on the properties of the spatial filter. The maximum time window for this pulse shaping technique can be quite large due to the high wavelength selectivity of an arrayed waveguide grating when considered as a bandpass filter. The time window for this technique can be in the nanosecond range and depends on the diffraction order (which is usually high since this has a direct effect on the spectral resolution of the spatial filter) and the number of waveguides used in the arrayed waveguide grating, whereas in the case of diffraction grating pulse shaper, the maximum time window can be from several to a hundred picoseconds. [6]

However, since each arrayed waveguide can be considered a periodic bandpass filter with bandpass center frequencies separated by a predefined free spectral range (FSR

or spectral window), this places an upper limit on the spectrum of the initial pulse. If the initial pulse spectrum exceeds the FSR of the arrayed waveguide grating, multiple spectral components separated by a frequency equal to the FSR would be present in each arrayed waveguide, and the pulse shaping fidelity would be degraded. The FSR is inversely proportional to a parameter known as the diffraction order that controls the temporal window and the modifiable spectral bandwidth. As a result of this, this pulse shaping technique is limited to shaping of picosecond pulses over a nanosecond time window. [14]

Acousto-optic filters

In looking at the previous scheme where an arrayed waveguide grating is used to separate the wavelengths of the initial pulse, it is seen that manipulation of multiple bandpass filters centered at different wavelengths can perform the same function. The operation of an acousto-optic filter is dependent on the ability of acoustic waves to change the polarization of an optical signal traveling through a birefringent crystal. These acoustic waves are generated by an RF signal driven into a transducer and can convert an optical signal from one polarization to another depending on a phase-matching condition. This phase matching condition is a factor of the frequency of the optical signal, the frequency of the acoustic wave, and the distance propagated by the optical signal in the crystal. In this way, the acoustic wave controls the diffraction of the optical signal from one polarization state to another. It can thus be shown that under suitable conditions the output optical waveform after propagating through the crystal is approximately proportional to the convolution of the input optical pulse and a time-scaled version of the RF signal driving the crystal.

Usually, an acousto-optic filter is a narrowband filter that can either remove or pass a narrow band of wavelengths of an optical signal depending on the frequency of the applied RF signal. If the RF signal contains a number of different frequencies, then

depending on the transmitted polarization state, this filter can pass and reject a good number of frequencies similar to the arrayed waveguide grating scheme mentioned above. Therefore, an acousto-optic tunable filter has many of the sought-after qualities of a pulse shaping system. It has a simple driving scheme similar the acousto-optic modulator SLM. Since it does not need to be used in an alignment-sensitive configuration with bulky diffraction gratings and lenses, the system can be made compact and compatible with waveguide devices and optical fibers. There are no limits on the temporal resolution of the system.

The temporal window of a system using a programmable acousto-optic filter is dependent on the length of the crystal. Commercial AOPDFs (acousto-optic programmable dispersive filters) can have a maximum temporal window of about 3ps. As a result, the time-bandwidth product is dependent on the length of the crystal and the input pulse duration. Higher TBWPs thus can be achieved by a shorter pulse duration that leads to higher temporal resolution and higher TBWP or a longer crystal that can increase the maximum temporal window. However, a longer crystal leads to a lower reprogrammability time because the time to refresh a shaped waveform depends on the time it takes for an acoustic wave to propagate across the length of the crystal. Control of the shaped waveform can be limited by acoustic nonlinearities and attenuation such as in the case of an acousto-optic modulator, whereas specifically sharp spectral features of the output waveform are severely limited by temporal windowing in the system. This is the inverse situation of the case where pixellation effects produce temporal sidelobes in the output waveform of the liquid crystal SLM pulse shaper. [15]

Fiber-based time-domain spectral shaping

The demand for OAWG at very high rates, shaping complexity, and temporal resolution that can be made compact without affecting the TBWP has motivated research in the area of time-domain spectral shaping (TDSS). TDSS is analogous to the technique

using SLM pulse shapers, but there are very important differences. Figure 2.3 below show a general scheme for TDSS. In such a scheme, modulation is performed in the time-domain as opposed to spatially using an SLM. The dispersive element is either an optical fiber or a fiber grating whose chromatic dispersion provides a way to spread out the frequencies of the initial pulse in time.

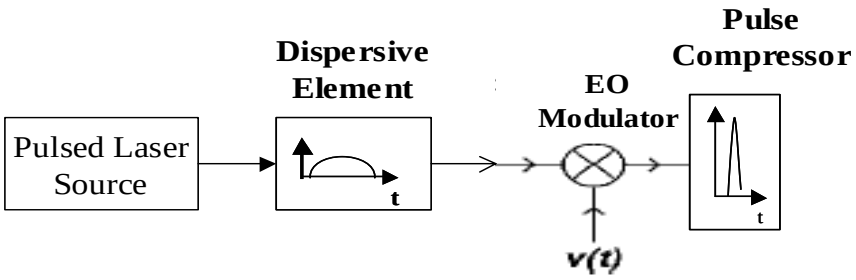

Figure 2.3: Schematic for time-domain spectral shaping. An optical pulse is propagated through a dispersive element that disperses the spectral elements of the pulse in time. An electro-optic (EO) modulator modulates the pulse spectrum, and a pulse compressor recombines the modulated spectral elements.

Chirped fiber Bragg gratings

A fiber Bragg grating is a periodic variation of the refractive index along the core of an optical fiber. This grating then reflects light at the Bragg frequency. If a chirped Bragg grating is used, then the grating becomes a dispersive device since each reflected frequency has a different group delay or propagation time along the grating. Apodization of the chirped FBG results in a smoother reflected spectrum and dispersion profile. Since the dispersion depends on the design of the grating, chirped FBGs can be designed to provide a large amount of chromatic dispersion over a few meters of length. Thus, a

system using FBGs as dispersive elements and pulse compressors can be made extremely compact. [16]

One very recent implementation[17] of a pulse shaper using FBGs is described below and shown in Figure 2.4. Although this implementation does not fit the general scheme described above in Figure 2.3, the pulse shaping is still controlled by an electrical signal and the operation of pulse expansion and compression is still a result of chromatic temporal dispersion. Under conditions where no pulse shaping is performed, an initial pulse is temporally dispersed and reflected by the first FBG, goes through two circulators, and is routed to a compressing FBG which recompresses the pulse. However, when an electrical signal is applied to an on-chip micro-electro-mechanical system (MEMS) array, the array induces strain on a FBG located between arrays of MEMS actuators. This alters the refractive index profile of this FBG used for pulse compression. As a result, the output waveform is dependent on and can be shaped according to the applied signal into the MEMS array.

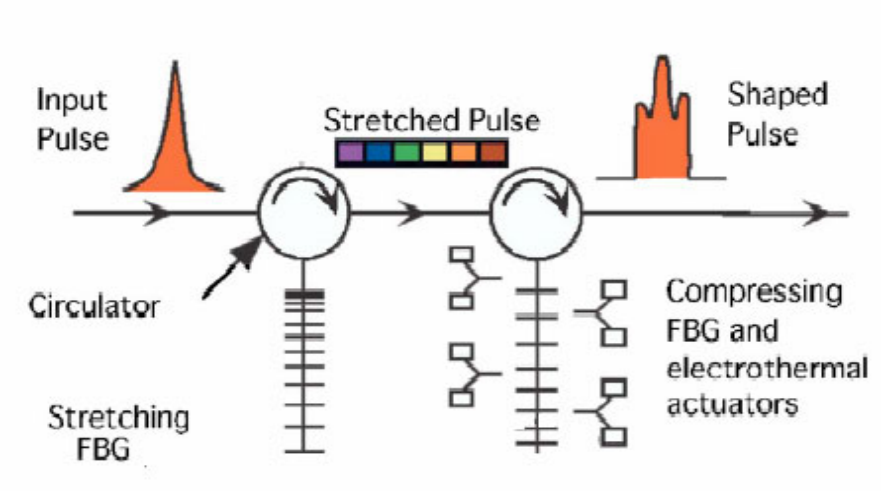

Figure 2.4: A FBG implementation of a pulse shaper. An electronically and thermally controlled FBG pulse compressor shapes the pulse in this setup. [17]

Although the length of the FBG used in the demonstrated system was small and therefore the maximum time window and even temporal resolution were not great, this system shows the ability and flexibility of fiber-MEMS integrated devices and a possible future compact integrated pulse shaping scheme. This technique may be extended to longer FBGs to improve the pulse shaping complexity.

A more conventional approach for the use of chirped FBGs in a TDSS scheme is to use chirped FBGs as both a pulse shaper and compressor in the general scheme illustrated in Figure 2.3. When the dispersions of the pulse shaper and compressor are equal and opposite, this scheme can provide pulse shaping capabilities with great resolution. The advantage of using chirped FBGs as a pulse stretcher and compressor is the ability to tailor the dispersion such that the chromatic dispersion is large and the higher-order dispersion is small over a short length of fiber. The disadvantages are high temperature sensitivity, relatively narrow and non-uniform reflected spectrum in longer FBGs[11], and the need for circulators due to the reflective nature of FBGs.

Optical fibers

The alternative to using chirped FBGs is to use optical fibers, usually silica fibers. An illustration of this technique that will be further discussed later is shown in Figure 2.5. Chromatic dispersion in silica fibers is a combination of waveguide and material dispersion. The waveguide dispersion is due to the waveguiding properties of the core and cladding of a fiber and can be tailored by the refractive index profile of the fiber. The dispersion of a fiber is usually given as a Taylor expansion about the center wavelength or frequency of an optical signal whose second-, third-, and fourth-order dispersion parameters are enough to describe the propagation of an optical signal through fiber, and in most cases second- and third-order dispersion coefficients are enough. When propagating a pulse through a fiber, chromatic dispersion temporally spreads out

the frequencies of the pulse provided the length of the fiber is long enough. A fiber with opposing dispersion characteristics can be used to provide pulse compression. [18] Advantages of this technique are that its components are cheap and readily commercially available, the total dispersion is easy to adjust, it can easily be incorporated in fiber systems, the dispersed spectrum is wide and smooth, and fiber does not take up very much space. Disadvantages are that very long lengths of fiber or very ultrashort pulses are usually required to provide a good temporal window and higher-order dispersion can be a factor in pulse compression when using ultrashort pulses.

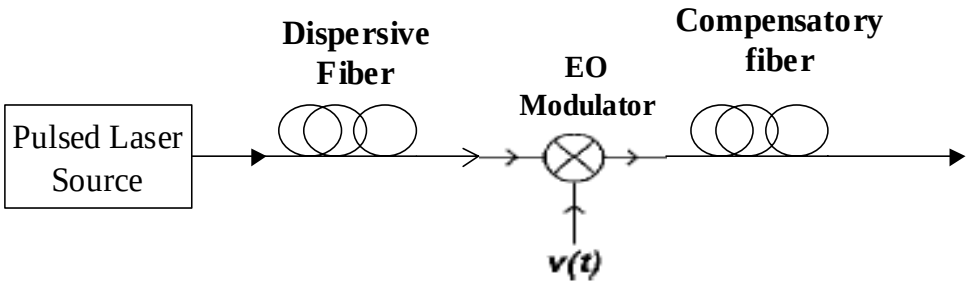

Figure 2.5: TDSS using dispersive and dispersion-compensating fibers.

Overall evaluation of TDSS

Time-domain spectral shaping can provide nice temporal resolution and waveform refresh rate comparable to the pulse repetition rate. Since spectral modulation is not done spatially, maximum temporal windows do not increase the size of the overall system significantly and systems can therefore be made reasonably compact. Components used in pulse shaping are usually cheap, and the systems do not require precise alignment or high-quality optical elements and can be easily incorporated into

fiber-based systems. Spectral phase and amplitude modulation can be provided by the use of an electro-optic phase and/or amplitude modulator.

However, since the reprogrammability time is dependent on the laser repetition rate, a faster reprogrammability time restricts the temporal window since spectral modulation is done temporally. The temporal window is also dependent on the RF waveform driven into the electro-optic (EO) modulator and the bandwidth of the EO modulator since the smallest resolvable spectral feature, which in this case is accessed by the modulating waveform, also determines the temporal window. These limits combine to place a restriction on the TBWP of the system, so there can be a tradeoff between TBWP and the waveform refresh rate. Finally, due to system design, there is an inherent chirp in the output waveform that can be significant over the duration of the time window, which places a restriction on phase control of the output waveform. Overall, TDSS can be a very useful, reasonably compact, and cost-effective pulse shaping and OAWG technique in situations where waveforms need to be updated continuously or to provide high potential TBWPs and pulse shaping complexity when a slower update rate can be used.

CHAPTER 3

THEORY

Introduction

For the purpose of simulation and to provide a framework to predict the operation of an OAWG system using dispersive optical fibers, theory must be developed and analyzed. With this theoretical background, it can be seen under what conditions the desired output waveform can be generated from the system. So, in this chapter, we explore the effects of fiber dispersion and modulation on a pulse.

Fiber propagation

The equation that approximately describes the propagation of an optical signal through fiber is the nonlinear Schrödinger equation (NLSE) and is given below in Equation 3.1.

$$\frac{\partial A(z,t)}{\partial z} = \overbrace{-\frac{\alpha}{2}A(z,t)}^{Absorption} - \overbrace{\underbrace{\frac{i}{2}\beta_2\frac{\partial^2 A}{\partial t^2}}_{GVD} + \underbrace{\frac{1}{6}\beta_3\frac{\partial^3 A}{\partial t^3}}_{3OD} + \underbrace{\frac{i}{24}\beta_4\frac{\partial^4 A}{\partial t^4}}_{4OD}}^{Dispersion} + \overbrace{i\gamma\underbrace{|A|^2 A}_{SPM}}^{Nonlinearity}, \qquad (3.1)$$

where the slowly-varying envelope approximation is used and it is assumed that the nonlinear response is instantaneous. A(z, t) is the complex envelope of the electric field amplitude of the optical signal at a retarded time (a temporal frame of reference moving with the group velocity of the pulse), t, and after propagating distance, z, and α, β_2, β_3, β_4, and γ are parameters of the medium in which the pulse is propagating. Specifically, β_2, β_3, and β_4 are the second-, third-, and fourth-order dispersion coefficients of the medium

respectively, while α is the loss parameter of the medium, and γ is the nonlinear coefficient. The terms above denoted absorption and nonlinearity (SPM – self phase modulation) are considered separately from the terms above denoted group velocity dispersion (GVD – also 2OD or second-order dispersion), third-order dispersion (3OD), and fourth-order dispersion (4OD). [18] If Raman scattering and a delayed nonlinear response are considered, the above nonlinear Schrödinger equation becomes the propagation equation (3.2) below.

$$\frac{\partial A(z,t)}{\partial z} = \overbrace{-\frac{\alpha}{2}A(z,t)}^{Absorption} - \overbrace{\underbrace{\frac{i}{2}\beta_2\frac{\partial^2 A}{\partial t^2}}_{GVD} + \underbrace{\frac{1}{6}\beta_3\frac{\partial^3 A}{\partial t^3}}_{3OD} + \underbrace{\frac{i}{24}\beta_4\frac{\partial^4 A}{\partial t^4}}_{4OD}}^{Dispersion} + i\gamma\left(1+\frac{i}{\omega_0}\frac{\partial}{\partial t}\right)\overbrace{\left(A(z,t)\int_0^\infty R(t')\left|A(z,t-t')\right|^2 dt'\right)}^{Nonlinearity}$$

(3.2)

In the above propagation equation (3.2), ω_0 is the center carrier frequency of the optical pulse, and R(t) is the Raman response function accurately modeled by the following equations:

$$R(t) = (1-f_R)\delta(t) + f_R h_R(t), \qquad (3.3)$$

$$h_R(t) = \frac{\tau_1^{\,2}+\tau_2^{\,2}}{\tau_1\tau_2^{\,2}}\exp(-t/\tau_2)\sin(t/\tau_1), \qquad (3.4)$$

where commonly used values for silica fiber are f_R = 0.18, τ_1 = 12.2fs, and τ_2 = 32fs. Depending on the pulsewidth of the input optical pulse (for pulsewidths greater than 50fs), this delayed nonlinear response and Raman response can usually be neglected and the NLSE (3.1) can be used. [19]

Equation 3.5 below can be used to approximate the NLSE (3.1) under suitable conditions and for the purposes of computer modeling and simulation. These conditions

result when the loss of the medium and the instantaneous signal power are negligible and when the pulse is of significant duration. In such a situation, the pulse propagation through the fiber is referred to as being in the linear regime. As a result, Equations 3.6 and 3.7 can be used to analyze the equation in the Fourier domain to come up with an expression to describe the spectrum of the output waveform in Equation 3.8. In these equations, ω is taken to be the frequency relative to the center frequency of the optical signal.

$$\frac{\partial A(z,t)}{\partial z}+\frac{i}{2}\beta_2\frac{\partial^2 A}{\partial t^2}-\frac{1}{6}\beta_3\frac{\partial^3 A}{\partial t^3}-\frac{i}{24}\beta_4\frac{\partial^4 A}{\partial t^4}=0 \qquad (3.5)$$

$$\tilde{A}(z,\varpi)=\int_{-\infty}^{\infty}A(z,t)e^{i\varpi t}dt \qquad (3.6)$$

$$\frac{\partial \tilde{A}(z,\varpi)}{\partial z}-\frac{i}{2}\beta_2\varpi^2\tilde{A}(z,\varpi)-\frac{i}{6}\beta_3\varpi^3\tilde{A}(z,\varpi)-\frac{i}{24}\beta_4\varpi^4\tilde{A}(z,\varpi)=0 \qquad (3.7)$$

$$\tilde{A}(z,\varpi)=\tilde{A}(0,\varpi)\exp(\frac{i\beta_2\varpi^2}{2}z+\frac{i\beta_3\varpi^3}{6}z+\frac{i\beta_4\varpi^4}{24}z) \qquad (3.8)$$

In the case in where the input pulse is a Gaussian pulse and the effects of β_3 and β_4 are just about negligible, there are analytical equations that describe the propagation of such a pulse over a certain length. These equations are given below.

$$\tilde{A}(z,\varpi)=A_0\sqrt{2\pi T_0^{\,2}}\exp(\frac{-T_0^{\,2}\varpi^2}{2}+\frac{i\beta_2\varpi^2}{2}z) \qquad (3.9)$$

$$A(z,t)=\frac{A_0 T_0}{\sqrt{T_0^{\,2}-i\beta_2 z}}\exp(\frac{-t^2}{2(T_0^{\,2}-i\beta_2 z)}) \qquad (3.10)$$

$$\frac{|T_z|}{T_0} = \sqrt{1+\left(\frac{\beta_2 z}{T_0^{\,2}}\right)^2} \qquad (3.11)$$

In the equations above, T_0 and T_z refer to the Gaussian intensity pulsewidths (half-width at 1/e point) of the pulse envelope after a propagation distance 0 and z respectively. [18]

It can be seen from the above equation (3.11) that the pulsewidth broadening at a distance, z, is dependent on the initial pulsewidth, T_0, and the second-order dispersion coefficient, β_2. This prompts the use of figures of merit that convey the length over which dispersive effects are very conspicuous. In a purely lossless linear dispersive medium, there are several characteristic typical z-length scales. L_D is the characteristic dispersive length ($T_0^2/|\beta_2|$). On the other hand, L_D' ($T_0^3/|\beta_3|$) is the length scale over which the effects of β_3 are highly visible. Usually, in fibers with non-zero β_2, the effect of β_3 is negligible since β_2 is usually much larger than β_3; however in second-order dispersion compensated systems, the effects of β_3 and β_4 are very critical and needs to be considered. [19]

Pulse shaping analysis

So, in looking at the scheme shown in above in Figure 2.5, there are two things that result in pulse shaping: the dispersion in the fibers and the modulator. So, assume the input signal has a frequency bandwidth of approximately $0.44/T_0$ [5] and assume that the power is low enough so that Equation 3.8 can be used. If these assumptions are made, the input into the electro-optic modulator, $b(z_1, t)$, after the input pulse envelope, $b(0, t)$ has propagated a distance, z_1, in the first dispersive fiber medium can be expressed using the following relations (3.12) and (3.13). In the below and subsequent relations, β_{ij} refers to the i^{th} dispersion coefficient of the j^{th} fiber medium, and ω and u are variables corresponding to the deviation from the center frequency of the input pulse.

$$\tilde{B}(z_1,u) = \tilde{B}(0,u)\exp(\frac{i\beta_{21}u^2}{2}z_1 + \frac{i\beta_{31}u^3}{6}z_1 + \frac{i\beta_{41}u^4}{24}z_1) \quad (3.12)$$

$$b(z_1,t) = \frac{1}{2\pi}\int_{-\infty}^{\infty}\tilde{B}(z_1,u)e^{-iut}dt \quad (3.13)$$

After the modulator, a signal, m(t), with spectrum, M(ω) (obtained by Equation 3.6), is applied to the dispersed spectrum, b(z_1, t), of b(0, t). The output of the modulator, D(t), and its corresponding spectrum D(ω) can be described Equations 3.14 and 3.15. Equation 3.14 is the result of multiplication in the time-domain, whereas Equation 3.15 is the result after convolution in the frequency domain. After the modulator, the output signal, c(t), and its spectrum, C(ω), after the modulated signal propagates a distance, z_2, in a compensatory second fiber medium is given by Equations 3.16 and 3.17.

$$D(t) = \frac{1}{2\pi}m(t)\int_{-\infty}^{\infty}\tilde{B}(0,u)\exp(\frac{i\beta_{21}u^2}{2}z_1 + \frac{i\beta_{31}u^3}{6}z_1 + \frac{i\beta_{41}u^4}{24}z_1)e^{-iut}du \quad (3.14)$$

$$\tilde{D}(\omega) = \int_{-\infty}^{\infty}\tilde{B}(0,\omega-u)\tilde{M}(u)\exp(\frac{i\beta_{21}(\omega-u)^2}{2}z_1 + \frac{i\beta_{31}(\omega-u)^3}{6}z_1 + \frac{i\beta_{41}(\omega-u)^4}{24}z_1)du$$

(3.15)

$$\tilde{C}(\omega) = \int_{-\infty}^{\infty}\tilde{B}(0,\omega-u)\tilde{M}(u)\exp(\frac{i(\beta_{21}(\omega-u)^2 z_1 + \beta_{22}\omega^2 z_2)}{2} + \frac{i(\beta_{31}(\omega-u)^3 z_1 + \beta_{32}\omega^3 z_2)}{6})$$

$$\exp(\frac{i(\beta_{41}(\omega-u)^4 z_1 + \beta_{42}\omega^4 z_2)}{24})du \quad (3.16)$$

$$c(t) = \int_{-\infty}^{\infty}\int_{-\infty}^{\infty}\tilde{B}(0,\omega-u)\tilde{M}(u)\exp(\frac{i(\beta_{21}(\omega-u)^2 z_1 + \beta_{22}\omega^2 z_2)}{2} + \frac{i(\beta_{31}(\omega-u)^3 z_1 + \beta_{32}\omega^3 z_2)}{6})$$

$$\frac{1}{2\pi}\exp(\frac{i(\beta_{41}(\omega-u)^4 z_1 + \beta_{42}\omega^4 z_2)}{24})e^{-i\omega t}du \times d\omega \quad (3.17)$$

For simplicity, consider the ideal case when third- and fourth-order dispersion terms are negligible, and second-order dispersion is compensated for in both fiber media. In such a case, $\beta_{21}z_1 = -\beta_{22}z_2$, and Equation 3.17 becomes Equation 3.18 below. Assuming b(0, t) is an ultrashort pulse of duration, T_0, and vanishes quickly outside of T_0, then provided $\beta_{21}z_1 >> T_0$, the last term of the equality in Equation 3.18 can be approximated by Equation 3.19.

$$c(t) = \frac{1}{2\pi}\int_{-\infty}^{\infty}\int_{-\infty}^{\infty}\tilde{B}(0,\omega-u)\,\tilde{M}(u)\exp(i\beta_{21}z_1\frac{u^2}{2})\exp(-i\omega(\beta_{21}z_1u+t))d\omega\times du$$

$$= \int_{-\infty}^{\infty} b(0,\beta_{21}z_1u+t)\exp(-iu(\beta_{21}z_1u+t))\,\tilde{M}(u)\exp(i\beta_{21}z_1\frac{u^2}{2})du$$

$$= \frac{1}{\beta_{21}z_1}\int_{-\infty}^{\infty} b(0,x)\,\tilde{M}\left(\frac{x-t}{\beta_{21}z_1}\right)\exp(i\frac{t^2-x^2}{2\beta_{21}z_1})dx \qquad (3.18)$$

$$c(t) \approx \frac{1}{\beta_{21}z_1}\exp(i\frac{t^2}{2\beta_{21}z_1})\int_{-\infty}^{\infty} b(0,x)\,\tilde{M}\left(\frac{x-t}{\beta_{21}z_1}\right)dx \qquad (3.19)$$

In (3.19), the output can be recognized as the convolution of the input pulse, b(0,t), with the spectrum of $m(\beta_{21}z_1t)$ multiplied by a quadratic phase term. As a result, it can be said that the act of second-order dispersion places a frequency component, ω, of the input pulse envelope at a temporal location, $\omega/\beta_{21}z_1$. The modulating waveform, m(t), then modulates these frequency components in time. Now, considering third-order dispersion to be appreciable and second-order dispersion to still be compensated, (3.18) becomes (3.20).

$$c(t) = \frac{1}{2\pi}\int_{-\infty}^{\infty}\tilde{M}(u)\exp\left(i(\beta_{21}\frac{u^2}{2}-\beta_{31}\frac{u^3}{6})z_1\right)\bullet\int_{-\infty}^{\infty}\tilde{B}(0,\omega-u)\exp\left(\frac{-i\beta_{31}u\omega^2z_1}{2}\right)$$

$$\exp\left(-i\omega(\beta_{21}uz_1 + t - \frac{\beta_{31}u^2 z_1}{2})\right)\exp(i\frac{(\beta_{31}z_1 + \beta_{32}z_2)}{6}\omega^3)d\omega \times du \quad (3.20)$$

Now, to get an idea of the implications of this formula, consider the situation where m(t) is a complex exponential of frequency deviation, ω_0 (or actual angular frequency, ω_0-ω_c), and M(ω) is a unit impulse at the frequency, -ω_0. This is considered in great detail by Saperstein et al. [12] The output complex pulse envelope of this system can then be written as Equation 3.21.

$$c(t) = \exp\left(i(\beta_{21}\frac{\omega_0^{\ 2}}{2} + \beta_{31}\frac{\omega_0^{\ 3}}{6})z_1\right)\exp(i\omega_0 t)\times$$

$$\left\{b(0, t - \beta_{21}\omega_0 z_1 - \frac{\beta_{31}\omega_0^{\ 2}z_1}{2}) \otimes \exp\left(\frac{-it^2}{2\beta_{31}z_1\omega_0}\right) \otimes FT\left(\exp(i\frac{(\beta_{31}z_1 + \beta_{32}z_2)}{6}\omega^3)\right)\right\}$$

(3.21)

Here, $\otimes$ is the convolution operator, and FT() is the Fourier transform operator given by Equation 3.13. Ideally, in light of examining (3.19), the expected output in a situation without second-order dispersion should be a time-shifted version of the input pulse, known as a satellite pulse, by the amount of $\omega_0\beta_{21}z_1$, a frequency-shifted version of the pulse by the amount of ω_0, multiplied by an appropriate quadratic phase term. However, due to third-order dispersion, (3.21) shows that there is an additional cubic phase term, an additional time shift of $\omega_0^2\beta_{31}z_1/2$, and a convolution with a quadratic phase term and a third-order dispersion term.

It can be shown that the convolution with the quadratic phase term broadens the time-shifted input pulse by an amount approximately proportional to $\omega_0\beta_{31}z_1$, and the third-order dispersion term can be responsible for conspicuous asymmetric third-order dispersion distortion of the shifted pulse. The third-order dispersion term can be

eliminated provided that the residual third-order dispersion is negligible in the two complementary fiber media. These two convolutions provide an extra limitation for the realizable TBWP of an optical pulse shaping system using optical fibers, although the last convolution can be neglected by matching third-order dispersion in the two fiber media. Also, the multiplication of the quadratic and cubic phase terms provides some extra complexity when trying to manipulate the phase of the output waveform. When fourth-order dispersion is significant, it is easy to show that Equation 3.21 becomes 3.22. However, since the third-order dispersion coefficient, β_3, of a fiber is usually a good deal higher in magnitude than the fourth-order dispersion coefficient, β_4, if the modulation frequency, ω_0 is not extremely high (which is limited by the applied electronic signal frequency into the EO modulator), only the third-order and fourth-order dispersion Fourier transform (FT) terms are significantly affected by the fourth-order dispersion coefficient.

$$c(t) = \exp\left(i(\beta_{21}\frac{{\omega_0}^2}{2} + \beta_{31}\frac{{\omega_0}^3}{6} + \beta_{41}\frac{{\omega_0}^4}{24})z_1 \right)\exp(i\omega_0 t)\times$$

$$\left\{ b(0, t - \beta_{21}\omega_0 z_1 - \frac{\beta_{31}{\omega_0}^2 z_1}{2} - \frac{\beta_{41}{\omega_0}^3 z_1}{6}) \otimes \exp\left(\frac{-it^2}{2(\beta_{31}z_1\omega_0 + \frac{\beta_{41}z_1\omega_0^2}{2})} \right) \otimes \right.$$

$$\left. FT\left(\exp(i\frac{(\beta_{31}z_1 + \beta_{32}z_2 + \beta_{41}z_1\omega_0)}{6}\omega^3) \right) \otimes FT\left(\exp(i\frac{(\beta_{41}z_1 + \beta_{42}z_2)}{24}\omega^4) \right) \right\} \qquad (3.22)$$

Limitations for pulse shaping

Considering (3.21) and (3.22), when m(t) is a complex exponential and M(ω) is a unit impulse function, the output shaped waveform for this fiber pulse shaper configuration is the convolution of the spectrum of m(t) and distorted phase-shifted time-

shifted versions of the input signal. Neglecting the effects of third- and fourth-order dispersion on the time shift, the time shift, T_S, corresponding to a complex exponential input into an ideal modulator is equal to $\omega_0\beta_{21}z_1$. Now, assuming third- and fourth-order dispersion compensation in both fiber media, a Gaussian envelope with pulsewidth, T_0 (intensity half-width at 1/e point), as an input, and ignoring the effect of fourth-order dispersion on pulse broadening, it can be shown (with the help of Equations 3.9-3.11 and 3.21 or in [12]) that the time shift corresponding to a 3dB decrease in the peak power of the input pulse (or equivalently a broadened satellite pulse of twice the initial pulsewidth), T_D, is equal to $\sqrt{3}\,T_0^2\beta_{21}/\beta_{31}$. An illustration of this is shown in Figure 3.1. The frequency, ω_{3dB}, that corresponds to such a time shift is equal to $\sqrt{3}\,T_0^2/(\beta_{31}z_1)$, and it is safe to say that modulation frequencies above this frequency would result in temporal features, at temporal locations far away from the center of the shaped pulse, that deviate appreciably from the ideal situation given by Equation 3.19.

Therefore, if the drive frequency into the modulator is limited to frequencies lower than this frequency, then dividing twice the time shift, T_D, either the broadened or initial pulsewidth, gives an expression for the approximate potential pulse shaping complexity, η_{app}. This number, η_{app}, is between $\sqrt{3}\,T_0|\beta_{21}/\beta_{31}|$ and $2\sqrt{3}\,T_0|\beta_{21}/\beta_{31}|$. For commercial fibers and a 100fs Gaussian pulse, this number can be between 30 and 60. Increasing η_{app} either requires an increase in the ratio of second- to third-order dispersion or an increase in T_0.

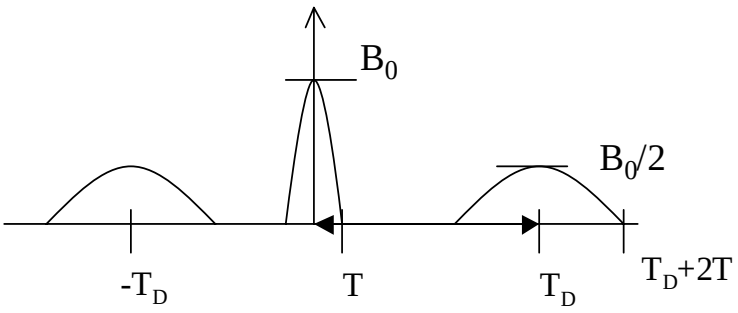

Figure 3.1: Illustration of intensity of broadened time-shifted satellite pulse envelope

This suggests that this system cannot realize high potential shaping complexities or TBWPs as initially thought with regular commercial fibers unless the ratio of second-order to third-order dispersion is increased. Also, over longer lengths of fiber, it is necessary to ensure that the second- and third- order dispersions are compensated in both fiber media precisely or else additional dispersion effects will be present that will further decrease the temporal resolution and TBWP of the system. A method to ensure that higher-order dispersion is compensated in the two complementary fiber media is described later. Now, suppose that commercial fibers are used in the OAWG system so that the ratio of second- to third-order dispersion is fixed, but T_0 is increased to increase the potential TBWP. One, this will limit the temporal resolution and make the smallest temporal feature in the shaped waveform increase in duration. Two, in order to keep ω_{3dB} fixed, a quadratic increase in the length of the first fiber medium, z_1, is required. This will increase the size of the system.

Now assume that the minimum time between (maximum repetition rate of) each pulse is T_{rep}, the initial pulse still has a Gaussian envelope with pulsewidth, T_0, and that the pulse undergoes linear propagation through a length, z_1, through the first fiber medium. Provided that $z_1 >> T_0^2/|\beta_{21}|$, the pulsewidth of the signal before the modulator will be approximately $|\beta_{21}|z_1/T_0$. This places a limitation on either the repetition rate (or

waveform refresh rate) of the desired shaped waveform or the amount of spectral features that can be placed on the output waveform. For example, if m(t) has a limited bandwidth with no significant frequency components above f_{max}, then the minimum period is $1/f_{max}$, and the number of temporal pixels can be given by $f_{max}T_{rep}$. So, given a desired repetition rate of 128MHz and a maximum modulating frequency of 10GHz, then the maximum number of temporal pixels is 78. To achieve this with a 300fs Gaussian pulse with a fiber with β_2 equal to 150ps^2/km, the length of fiber needs to be 15.625km.

Now, if an optical source with a fixed pulse repetition rate is used, and independent pulse shaping is to be performed on each pulse, then it is required that $T_{rep} > |\beta_{21}|z_1/T_0$. This is shown in Figure 3.2. As a result, a limit on the maximum number of temporal pixels, N_{tp}, is given by $|f_{max}\beta_{21}z_1/T_0|$. Considering that f_{max} can be at most 5GHz for commercial electronic arbitrary waveform generators and 40 Gigabit/second (Gbps) for commercial pattern generators [20], using standard SMF (single mode fiber) that has β_2 equal to about -20ps^2/km and a laser that generates 100fs Gaussian pulses requires N_{tp} km of SMF to have a maximum of N_{tp} to $8N_{tp}$ pixels. This means that 4km of SMF can generate 32 temporal pixels with a 40Gbps pattern generator. Ideally, it would be beneficial to generate more pixels with a shorter length of fiber.

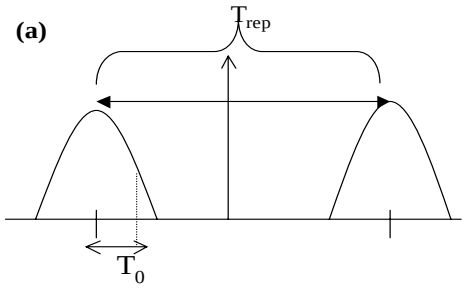

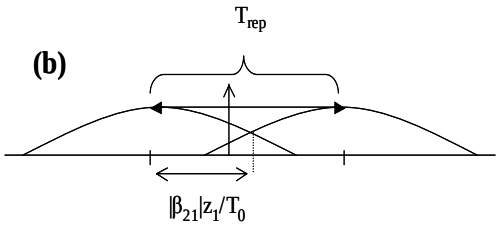

Figure 3.2: (a) Input pulse train into first fiber medium to be shaped is separated by the repetition period. (b) Broadened pulses starting to overlap before going through the optical modulator. Independent pulse modulation must be performed on non-overlapping parts of the pulse

Nonlinearity

Up to this point, it has been assumed that the power of the initial signal was low enough so that the nonlinearity and absorption terms in the NLSE (3.1) and the propagation equation (3.2) can be ignored. Now, in the case where the dispersion terms can be ignored, the NLSE can be significantly reduced to Equation 3.23 and can be solved explicitly in Equation 3.24. Equations 3.23 and 3.24 are important since nonlinearity and absorption cannot be simplified in the Fourier domain as in (3.5)-(3.8) and need to be analyzed separately from dispersion terms. It can be seen that nonlinear SPM (self-phase modulation; specifically the nonlinear term in the NLSE) tends to positively chirp a signal in time as it propagates a distance, z, since γ is positive. Looking back at the Equation 3.8, it can be seen that second-order dispersion imparts a positive time chirp if β_2 is positive and negative time chirp if β_2 is negative. It is also well known that SPM in fiber due to high-powered signals can generate a broader signal spectrum.[19] Taking these facts into account, if a fiber with positive β_2 is used to propagate a high-powered pulse, the combined positive chirp due to second-order and SPM effects can spread the pulse spectrum further out in time than when nonlinear effects are absent.

$$\frac{\partial A(z,t)}{\partial z} = -\frac{\alpha}{2} A(z,t) + i\gamma |A|^2 A \qquad (3.23)$$

$$A(z,t) = A(0,t)\exp(-\frac{\alpha z}{2} + i\gamma |A(0,t)|^2 \frac{(1-\exp(-\alpha z))}{\alpha}) \qquad (3.24)$$

This would allow lower modulating frequencies to be used without sacrificing the number of temporal pixels and using longer lengths of fiber. However, nonlinearity effects would degrade the temporal resolution since the smallest temporal feature in the output waveform would be broadened by the nonlinearity of the first fiber medium. But if the length of the complementary fiber medium is chosen correctly, nonlinearity can be used to possibly to improve the temporal resolution. Also, if high-powered signals were propagated in a fiber medium with negative β_2, this would result in what is known as soliton propagation. Solitons are stable solutions to the NLSE and can be described as pulses that propagate in a fiber, break up over a certain distance, and return back to the original shape after a distance known as the soliton period. Soliton propagation could be beneficial in an OAWG arrangement, but such a scheme is not discussed here. A full mathematical treatment on how specifically SPM can improve the pulse shaping capabilities of this OAWG system is not given, but it should be noted that SPM may be useful in improving the TBWP and decreasing the length of fiber needed.

Modulator analysis

The final component to the OAWG system that has yet to be considered is the modulator. The modulator ideally can be seen as a device that multiplies the input optical signal by a complex arbitrary signal m(t). In an electro-optic (EO) modulator, this modulating signal is generated by an electrical signal that modulates the optical phase or amplitude of the input optical signal. The general principle of operation is that applying a voltage differential across an EO crystal creates a change in the index of refraction causing a phase shift proportional to the voltage differential. This principle alone can be

used for an EO phase modulator, while using a Mach-Zehnder interferometer configuration of an EO phase modulator makes an EO amplitude modulator.[21] Combining both of these components can generate any complex arbitrary modulating signal m(t) provided that $|m(t)| < 1$ and m(t) contains frequencies within the modulator driver bandwidth and the modulation bandwidth of the crystal. As the optical signal enters the EO crystal used in the amplitude or phase modulator, a voltage signal, v(t), is applied across the crystal and serially provides amplitude or phase modulation to the optical signal.

However, there are modulator characteristics that must be taken into account when using an EO crystal as an optical phase or amplitude modulator. The characteristics of the optical modulator that should be taken into account are the on-off ratio, risetime, and variation of V_π as a function of wavelength (which can be very observable due to the broad spectrum of the optical pulse to be modulated). The effect of the risetime of a modulating signal limited by either the bandwidth of the Lithium Niobate electro-optic modulator or the bandwidth of the electrical signal generator can be modeled by the following equation (3.25).

$$v_1(t) = \int_0^\infty v_{in}(t-\tau) e^{-\frac{\tau(\ln(9))}{t_r}} d\tau \qquad (3.25)$$

In Equation 3.25, $v_1(t)$ is the effective input voltage into the modulator as a function of time, $v_{in}(t)$ is the applied drive voltage to the modulator, and t_r is the risetime of the modulator defined as the time needed for the voltage to go from 10% to 90% of its maximum value.

The equations describing the operation of the electro-optic amplitude and phase modulator are given below:

$$E_{out}(t) = E_{in}(t) \times \left[0.5 \exp\left(\frac{j\pi v_1(t)}{V_\pi(\lambda)} \right) + \frac{\gamma_m}{2} \right] \quad \text{amplitude modulation,} \qquad (3.26)$$

$$E_{out}(t) = E_{in}(t) \times \exp\left(\frac{j\pi v_1(t)}{V_\pi(\lambda)} \right) \quad \text{phase modulation,} \qquad (3.27)$$

where $v_1(t)$ is the effective input voltage into the modulator used to modulate the optical signal, γ_m is a scaling factor (between 0 for a very poor device and 1 for an ideal device) to account for a nonideal extinction (on-off) ratio, and V_π is a parameter dependent on the modulator as well as the wavelength, λ, of the optical signal. The optical power switching (off to on) ratio of the modulator can be easily determined and is $(1-\gamma_m)^2/(1+\gamma_m)^2$. It can be seen that amplitude modulation cannot be performed without some level of phase modulation. The only voltages that do not produce significant phase modulation are voltages in an amplitude modulator are the voltages very close to zero and V_π. The wavelength dependence of V_π is approximated by the following equations.

$$R = \left. \frac{dV_\pi}{d\lambda} \right|_{\lambda_0} \Big/ \frac{V_{\pi 0}}{\lambda_0} \qquad (3.28)$$

$$V_\pi(\lambda) = \frac{RV_{\pi 0}}{\lambda_0} \Delta\lambda + V_{\pi 0} \qquad (3.29)$$

R and $V_{\pi 0}$ are parameters of the modulator, while λ_0 and $\Delta\lambda$ are the center wavelength and deviation from the center wavelength, respectively, of the optical signal[22]. If λ does not vary much over the duration of the optical signal, then V_π is well approximated by $V_{\pi 0}$. Since a broadband short-duration optical signal is desired in this particular OAWG application, V_π can vary significantly over the duration of the optical signal. This will have an effect on the modulation of the optical signal when compared to ideal amplitude or phase modulation.

Overall OAWG implementation considerations

Dispersion Compensation

So looking at the theory for modulation and dispersion for pulse shaping in optical fibers, nonlinearity, dispersion compensation, and modulation are very important factors of an all-fiber OAWG system. When using commercial fibers, it is very difficult to use two fibers that are completely compensated for second- and third-order dispersion since this requires that β_2/β_3 is the same for both fibers. Since residual third-order dispersion can impair the temporal resolution of a fiber TDSS system over long lengths of fiber, it is very advantageous to come up with a scheme to reduce or negate residual third-order dispersion over the length of the system.

Employing a scheme that is usually used for dispersion compensation[23], we can devise a way to almost guarantee that second- and third-order dispersion will be compensated in an OAWG system using conventional SMF (single mode fibers) and DCF (dispersion compensating fibers) fibers. If three fibers are used, and the lengths of the three fibers can be chosen to satisfy (3.30) and (3.31) below, then simultaneously second- and third-order dispersion will be compensated for over the lengths of the three fibers. In the equations below, z_i is the propagation length of the optical signal over the i^{th} fiber. So, if a fiber medium is composed of multiple fibers, then the total effective j^{th} order dispersion quantity, $\beta_j z$, is given by Equation 3.32 below. Here, z is the length and β_j is the effective j^{th} order dispersion coefficient of the fiber medium.

$$\beta_{21} z_1 + \beta_{22} z_2 + \beta_{23} z_3 = 0 \qquad (3.30)$$

$$\beta_{31} z_1 + \beta_{32} z_2 + \beta_{32} z_3 = 0 \qquad (3.31)$$

$$\beta_j z = \sum_i \beta_{ji} z_i \qquad (3.32)$$

Essentially, Equation 3.32 can be used to compensate any order dispersion in any fiber medium provided the correct amount of fibers. However the ability to simultaneously correct higher orders of dispersion is more complicated, necessitating control of fiber lengths of a greater number of fibers. Also, since length cannot be negative, this technique requires the right dispersion characteristics for each fiber to give a sensible and valid solution for the required lengths of each fiber.

Ideally, this technique could be used to generate a fiber medium and a complementary fiber medium that each has high total second-order dispersion and low third-order dispersion to significantly improve the potential TBWP of the system. However, such a technique with commercial fibers would require very long lengths of fiber to provide enough chromatic dispersion so that a bandwidth-limited modulator can provide a high N_{tp}. This technique however is very suitable in eliminating residual 3OD in our pulse shaping system.

Nonlinearity

Fiber nonlinearity is usually avoided because it can produce irreversible broadening effects and cannot be easily described quantitatively in the presence of high dispersion. Also, when higher powers are used in anomalously dispersive fibers (fibers with negative β_2), this can form soliton propagation limiting pulse dispersion or compression. However, the ability of nonlinearity to generate a broader pulse spectrum and capability of nonlinearity to be used to compress a pulse beyond its original pulse width can be useful in an OAWG scheme. Overall, if higher powers were to be used in a fiber OAWG system, it would be beneficial to use normally dispersive fibers (fibers with positive β_2) as the dispersive medium since SPM effects would enhance the dispersion and further broaden the usable spectrum for modulation, increasing N_{tp}. Such an OAWG implementation is shown below in Figure 3.3 as well as a three-fiber implementation that

can be used to simplify second- and third-order compensation in the dispersive and compressive fiber media.

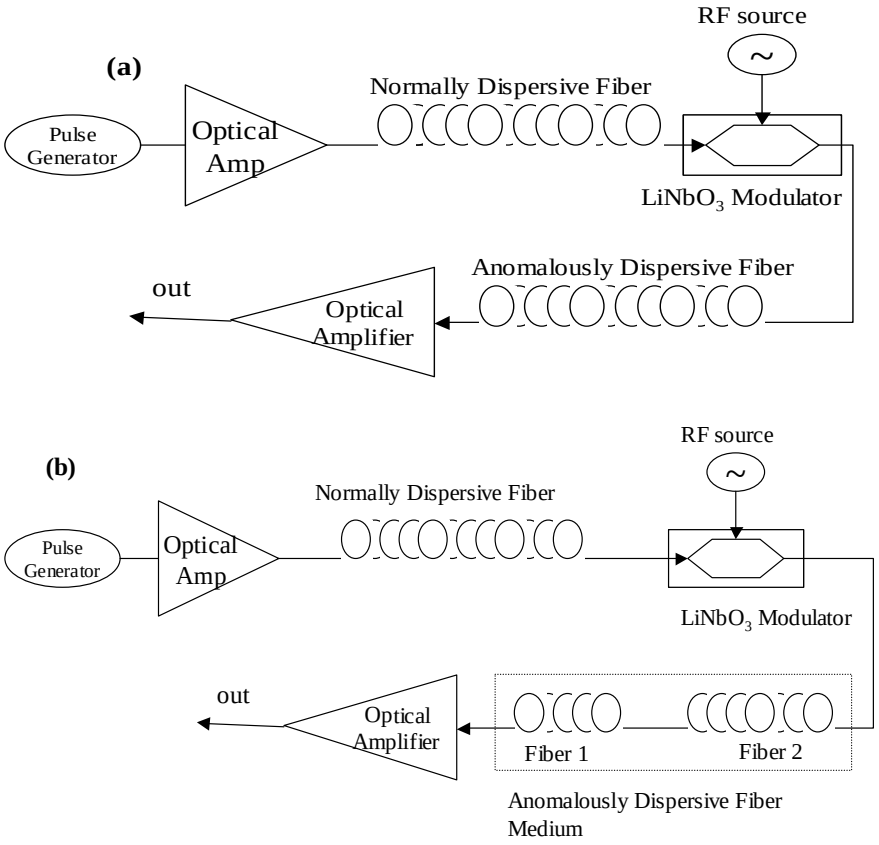

Figure 3.3: (a) Two-fiber implementation of an OAWG using a DCF fiber as the first medium and a SMF fiber as the second medium. (b) Three-fiber implementation of a DCF fiber as the dispersive first medium and 2 SMF fibers as the compressive second medium.

Modulation

An amplitude and/or phase modulator can be used to generate a modulating signal to serially modulate the spectrum of the initial optical pulse in the OAWG system. The amplitude modulator has the advantage of being able to completely attenuate a given

frequency component or pass desired spectral elements, giving it an excellent ability to tailor the spectrum of the output waveform. However, in using an EO amplitude modulator for pulse shaping, phase modulation is inherently performed (see Equation 3.26). Also, amplitude modulation can significantly decrease the power of the output waveform and make it extremely difficult to detect and measure the output signal. This is because amplitude modulation cannot increase the power of any spectral components, but it can definitely attenuate spectral components. This result alone means that if an amplitude modulator attenuates more frequencies, lesser power will be available to the output shaped signal.

Phase modulation, on the other hand, ideally conserves optical power (if one neglects inherent loss through the modulator) since no frequency components are attenuated in the process. Also, it can be performed independently from amplitude modulation and easily be used for dispersion compensation. However, it is limited in its pulse shaping capabilities because the phase modulator passes all frequency components of the initial signal.

The best situation is to use amplitude and phase modulation together to have the ability to provide arbitrary phase and amplitude modulation to the pulse spectrum. This would allow for extra degrees of freedom in generating shaped waveforms. However, such a situation would still have the disadvantage of power being lost in the attenuation of optical frequencies. A future enhancement to the proposed all-fiber OAWG system is to use a phase modulator to perform third-order dispersion compensation after a dispersive fiber medium before applying a phase and/or amplitude modulating signal to the dispersed optical pulse. Third-order dispersion compensation in this way can improve the TBWP of the overall pulse shaping system. A possible OAWG implementation using this compensation scheme is presented in Figure 3.4.

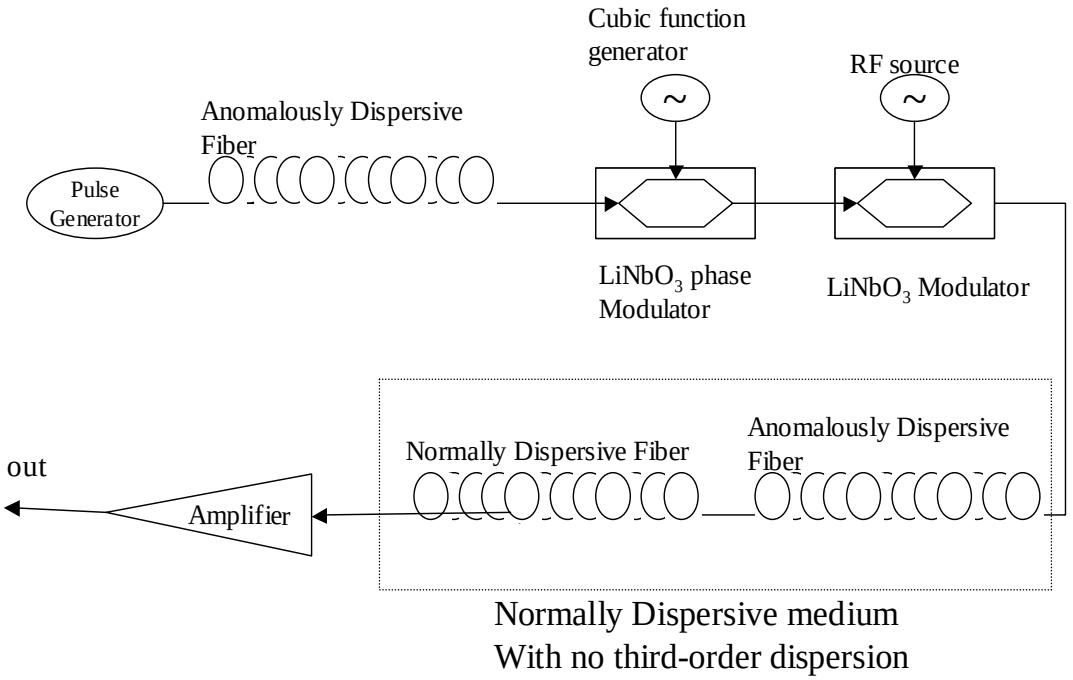

Figure 3.4: Schematic of an all-fiber OAWG system using a Lithium Niobate phase modulator driven by cubic voltage signal in time for 3OD compensation. The compressive fiber medium uses a normally dispersive fiber and a slightly anomalously dispersive fiber to provide large 20D with negligible 3OD.

Arbitrary waveform generation

When looking specifically at this TDSS fiber OAWG setup as a means to perform arbitrary waveform generation, there are several key factors discussed above in evaluating the ability of a given OAWG system to generate a complex waveform. Arbitrary waveform generation is performed in the system when the EO modulator imparts arbitrary phase or amplitude modulation to a particular slice of frequencies, which in a TDSS setup corresponds to a particular temporal pixel or period of time within the dispersed (or chirped) optical pulse. The maximum number of temporal pixels, N_{tp}, in a system can essentially determine how many different waveforms can be generated or

how many spectral features can be modified, and this depends on the initial pulsewidth of the optical source, the dispersion of the fibers (i.e. the lengths and second-order dispersion coefficients), and the modulation bandwidth or speed. On the other hand, the approximate potential pulse shaping complexity, η_{app}, is an estimate of the number of independent and distinct controllable spectral or temporal features that can be placed on the output waveform and depends on the initial pulsewidth of the optical source and the second- and third-order dispersion characteristics of the fibers.

The number of amplitude levels of the drive signal into the EO modulator can also be a key consideration in using TDSS for arbitrary waveform generation. A drive signal capable of providing any level of voltage during a given temporal pixel or period of time would be the ideal situation. However, electrically generated waveforms may be limited in this capacity especially at higher modulation speeds. So, a tradeoff in using a modulator driver may be between employing a slower electronic arbitrary waveform generator with a large number of amplitude levels and using a faster electronic pattern generator that can only generate a limited number of amplitude levels. A slower electronic arbitrary waveform generator can address a smaller number of spectral components but apply a higher number of amplitude or phase (depending on the type of modulation) weights to each temporal pixel or spectral components. On the other hand, a faster binary pattern generator can address more spectral components but can only provide each group of wavelengths with two possible amplitude or phase weights. Using a limited-bandwidth drive signal would result in the shaped pulse having a short temporal duration (looking at the implications of Equation 3.19); while using only a binary drive signal would generate output waveforms whose spectral elements can have only two values.

Assuming that a 40Gb/s binary pattern generator and a 200fs Gaussian output from a femtosecond optical source (with low enough power to ensure approximately linear propagation) are to be used for OAWG, the maximum number of temporal pixels

and the approximate potential pulse shaping complexity can be looked at with respect to the dispersion characteristics of the dispersive medium and their lengths. Figures 3.5 and 3.6 illustrate the maximum number of temporal pixels and the minimum and maximum approximate potential pulse shaping complexity as a function of the length of a dispersive fiber. The fiber characteristics used for the dispersive medium (pulse stretching) were based on those of Corning SMF-28 fiber (β_2 = -21.6321ps^2/km and β_3 = 0.1284 ps^3/km) for Figure 3.5 and those of EWBDK-DCF fiber (β_2 = 152.9479 ps^2/km and β_3 = -0.9533 ps^3/km) for Figure 3.6. As stated before, using pulses with higher peak powers in a normally dispersive fiber could possibly increase the number of temporal pixels, but only linear propagation is considered in this case.

In Figure 3.5, it can be seen that in order to achieve the minimum approximate pulse shaping complexity of 58 (or equivalently have N_{tp} equal η_{app}) in this OAWG setup, about 13.5km of SMF-28 needs to be used. Consequently, about 27km of SMF-28 needs to be used to achieve the maximum approximate pulse shaping complexity of 117. On the other hand, in Figure 3.6, it can be seen that in order to achieve the minimum approximate pulse shaping complexity of 56, about 1.8km of DCF needs to be used. Consequently, about 3.6km DCF needs to be used to achieve the maximum approximate pulse shaping complexity of 111. The huge difference between the lengths of the two fibers is obviously due to their difference in second-order dispersion coefficients. Now, using an 8-level 5GHz electronic arbitrary waveform generator as the modulator driver instead of a 40Gbps binary pattern generator would increase the length of fiber eightfold; however, each of these temporal pixels or (equivalently) spectral components could have eight different modulation levels for significantly added flexibility in generating arbitrary waveforms.

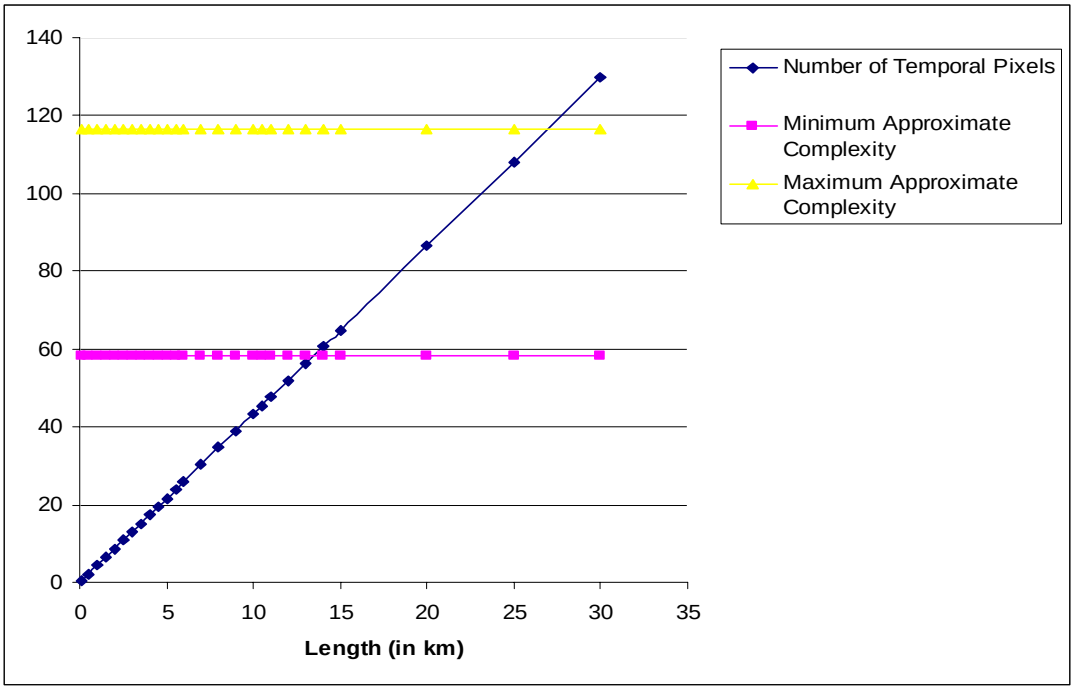

Figure 3.5: Maximum number of temporal pixels and minimum and maximum approximate pulse shaping complexities versus length of dispersive medium for SMF-28 fiber and 40GHz modulator.

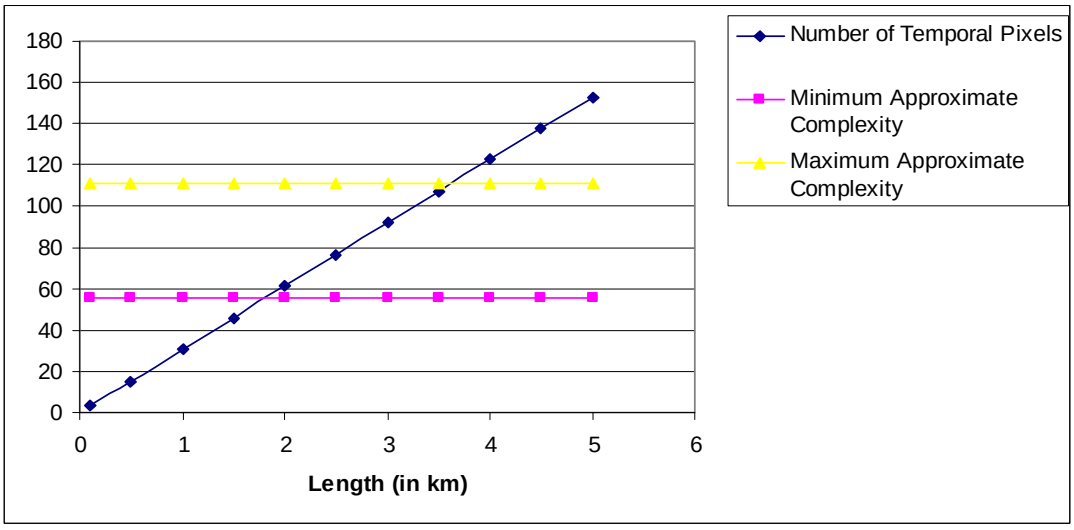

Figure 3.6: Maximum number of temporal pixels and minimum and maximum approximate pulse shaping complexities versus length of dispersive medium for EWBDK-DCF fiber and 40GHz modulator.

Although higher total dispersion (either by using longer lengths of fiber or fiber with high β_2) in the pulse stretcher section of the OAWG system has the desirable advantage of giving the fiber TDSS pulse shaper more temporal pixels, this also places a limit on the repetition rate of independently shaped output waveforms. Figure 3.7 shows how the maximum repetition rate of independently shaped output waveforms is affected by the length of the dispersive medium assuming that DCF fiber (β_2 = 152.9479 ps^2/km and β_3 = -0.9533 ps^3/km) is used as a pulse stretcher. This is assuming that a 200fs Gaussian pulse is the initial optical signal and the pulse power is low enough so that propagation is approximately linear. The maximum repetition rate is about 1.3GHz when 1km of DCF is used, about 870MHz when 2km of DCF is used and about 260MHz when 5km of DCF is used. At these frequencies for the respective DCF lengths, the broadened and dispersed Gaussian pulses only overlap outside of their half-widths at 1/e intensity point. Despite the significant decrease in the maximum rep rate over longer lengths of fiber, these waveform refresh rates are still higher than those achievable by SLMs in a traditional grating pulse shaper.

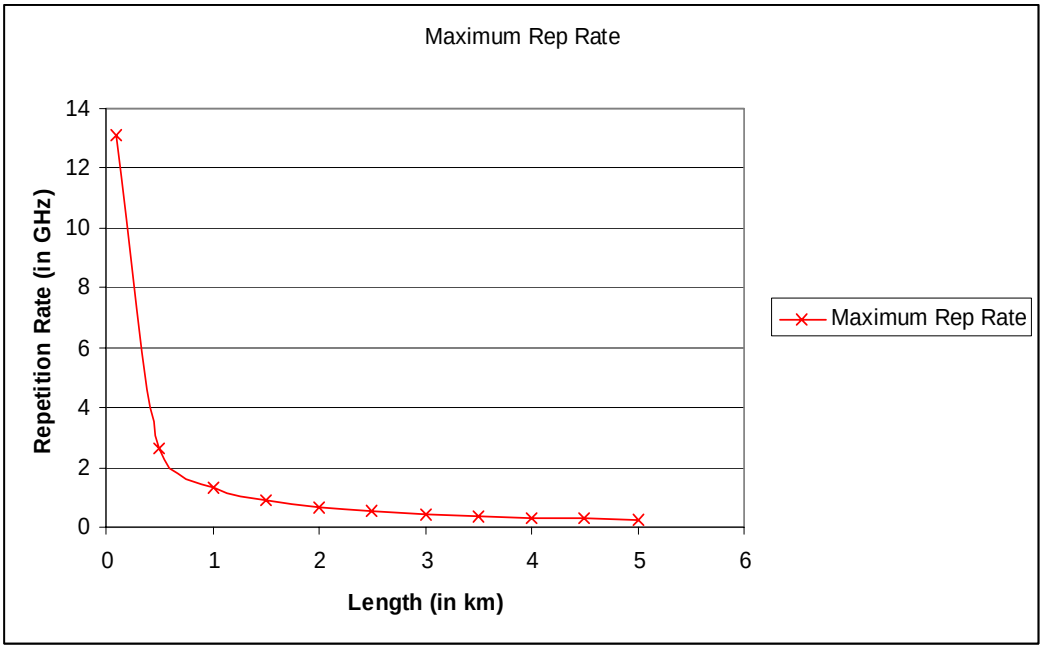

Figure 3.7: Maximum repetition rate versus length of dispersive medium for EWBDK-DCF fiber and 200fs input Gaussian pulse.

To show the effect of modulation bandwidth and pulsewidth on N_{tp} and η_{app}, an OAWG setup with 2km of DCF fiber used as a pulse stretcher (β_2 = 152.9479 ps^2/km and β_3 = -0.9533 ps^3/km) and two complementary SMF fibers used for pulse compression (2OD and 3OD compensation) can be examined. Figure 3.8 shows how N_{tp} varies with modulation bandwidth, assuming that the system is used with an optical source that produces 200fs Gaussian pulses. Figure 3.9 shows how both N_{tp} and η_{app} vary with the input Gaussian pulsewidth, assuming that a 40GHz modulator is used. The approximate potential shaping complexity increases with the pulsewidth of the initial optical signal, but increasingly longer lengths of fiber are needed in order to achieve a comparable maximum number of temporal pixels. Figure 3.8 shows that an increase in optical modulation bandwidth can improve the number of temporal pixels greatly.

Of course, the optical modulation bandwidth is limited by the electronics used to drive the modulator as well as the modulator itself, and if it could be increased without limit, OAWG could easily be performed by simple and direct optical modulation. Currently, the bandwidth of a $LiNbO_3$ modulator can be designed to be 100GHz or higher.[24] This means that the maximum approximate potential pulse shaping complexity of 110 can be exceeded by the maximum number of temporal pixels when 2km of the DCF fiber is used with a 200fs Gaussian optical pulse in the OAWG system if the modulator is driven with signals above 70GHz. In such a situation, the OAWG system is then limited by third-order dispersion effects and not modulation speed.

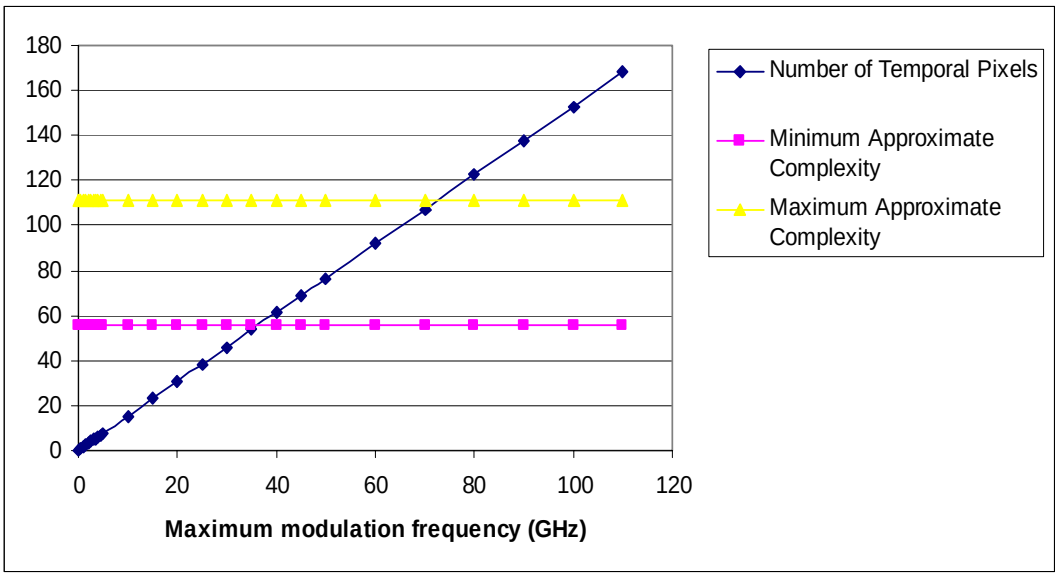

Figure 3.8: Maximum number of temporal pixels and minimum and maximum approximate pulse shaping complexities versus modulation bandwidth for 2km of DCF fiber.

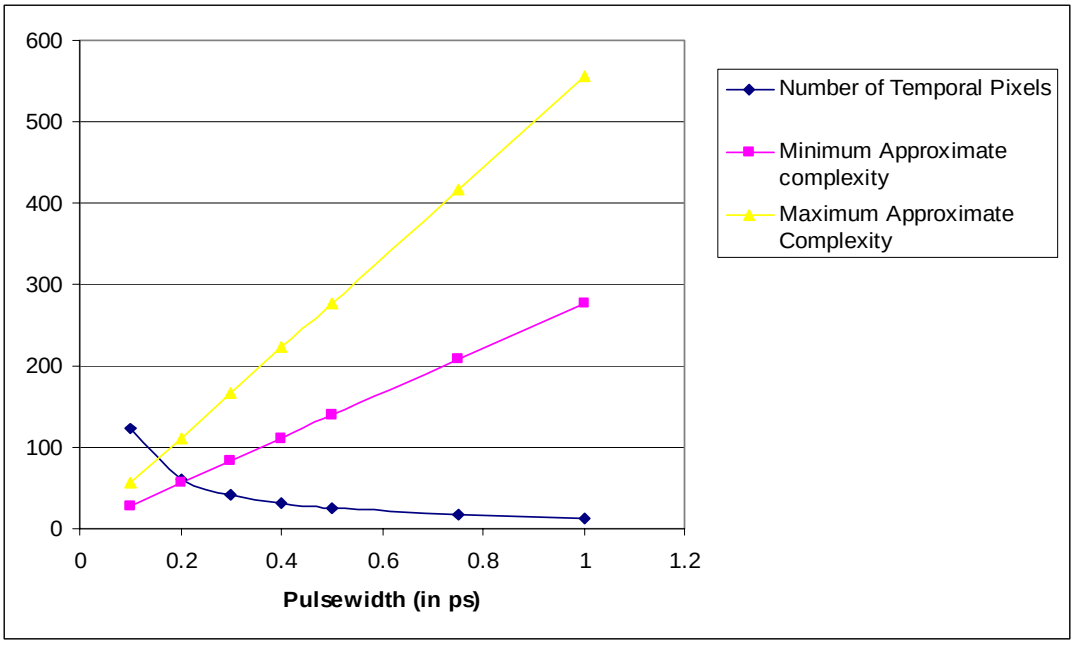

Figure 3.9: Maximum number of temporal pixels and minimum and maximum approximate pulse shaping complexities versus initial Gaussian pulsewidth for 2km of DCF fiber.

CHAPTER 4

COMPUTER MODELING AND SIMULATIONS

Introduction

In considering the theory of the previous chapter in propagating an optical signal through a fiber, it is impossible to determine analytical expressions for the output signal using the NLSE or propagation equation if the input signal has an arbitrary shape. Only, under specific conditions and assumptions with specific input signals can an expression be derived for the output signal. Adding a modulator between two fiber media can even make it harder to predict exactly what the output waveform should like. Therefore, before constructing the OAWG system, it would be extremely beneficial to model the entire system to be able to simulate how it would operate under a variety of conditions and with different input optical signals. This includes being able to simulate an arbitrary signal propagating through a fiber with given dispersion, loss, and nonlinear characteristics and being modulated with a nonideal Lithium Niobate modulator. This chapter gives the details of the modeling and simulation that was done (mostly using Matlab) in order to test the performance of the proposed OAWG system using dispersive fibers.

Modeling of fiber propagation

Fiber dispersion in the absence of absorption and nonlinearity is very easily modeled since it can be viewed as multiplication in the Fourier domain looking at Equation 3.8. Using an FFT (Fast Fourier Transform) of the input optical pulse envelope and an IFFT (inverse Fast Fourier Transform) of the spectrum of the dispersed pulse

envelope in Matlab, a simulation of a pulse propagating through a strictly dispersive fiber can be performed very quickly. Matlab code was written to model this phenomenon for an arbitrary optical pulse envelope and a fiber with arbitrary β_2, β_3, and β_4. Several input pulses were propagated through standard SMF fiber and compared against several benchmarks. The graphs comparing the simulated output with the benchmarks can be found in Appendix A.

When a pulse is propagating through in a fiber with nontrivial nonlinear and absorption characteristics, the above code would not be practical in predicting the output. This is shown in Figure 4.1 below where higher-powered pulses experience higher SPM effects, and their outputs deviate from the lower-powered pulse that experiences negligible SPM effects. A highly accurate and useful tool in the modeling of nonlinear fiber propagation is the split-step Fourier method. The split-step Fourier technique is a well-known method to tackle the nonlinearity and dispersion in the nonlinear Schrödinger equation. The basic formalism consists of a half step of dispersion, followed by a half step of nonlinearity. In the half step of nonlinearity, Equation 3.23 or 3.24 can be used to find the output pulse in the absence of dispersion.

Since the nonlinearity is dependent on the intensity, an iterative nonlinear solver is used. An accurate method to estimate the z-step size is determined by considering the typical length scales in the simulation, e.g. the dispersive length scale L_D ($T_0^2/|\beta_2|$) and the nonlinear length scale L_N ($1/\gamma P_0$, where P_0 is the peak power of the input pulse). Since the nonlinear length scale is power dependent, at very high powers, a small z-step has to be considered to accurately model the nonlinearity. Using small z-steps makes the split-step Fourier technique simulate nonlinear propagation with less error, but it increases the number of FFTs that need to be taken over a given distance and the time to run a simulation as a result. [19] Keeping this in mind, code was written to implement the split-step Fourier technique to numerically solve the NLSE and propagation equation and give a simulated output for pulse propagation through a fiber with given dispersive, loss, and

nonlinear characteristics. The original program written to simulate dispersion was used in the dispersion step of the split-step Fourier technique, while additional Matlab code was used to model the nonlinearity for the nonlinear step. More benchmarking exercises were simulated to verify that the code was running accurately and producing correct and expected outputs. Plots of the output of the split-step Fourier code can be found in Appendix A.

As mentioned before, the Fourier split-step method can be very accurate in simulating pulse propagation in fibers provided that the z-step size is well under L_N. Figure 4.2 compares outputs obtained by simulations with different step-sizes when using the Fourier split-step method to propagate an initial Gaussian pulse through two complementary fibers. However, over the course of propagation through a length of fiber, the peak power can vary and hence longer step sizes can be taken if the peak power decreases. It would be useful for the propagation program to be able to determine the longest step to take in a given split-step iteration without sacrificing too much accuracy. To optimize the propagation code using the split-step method and decrease computation time, variable length step-sizes were used similar to the approach demonstrated by Sinkin et al.[25]

In this modified Fourier split-step implementation, relative error is calculated between the solution of a split-step iteration taken with one coarse z-step and that of two sequential split-step iterations taken with half of the coarse z-step. If the relative error is below a desired level, then a suitable combination of the coarse-step solution and the finer-step solution is used as the output pulse after the z-step. For the next iteration, the length step is increased. However, if the relative error is above a desired level, then the solutions are discarded, the z-step size is decreased, and the process is repeated. Using this modification, the propagation program can determine the right step-size to use for the split-step method and simulate pulse dispersion and compression with greatly reduced computation time and increased accuracy. Figure 4.3 below illustrates the improvement

in the performance of the split-step Fourier technique as a result of using variable step-sizes.

Next, a program was written to use the split-step Fourier technique to simulate the pulse dispersion and compression of a 71fs (half-width intensity 1/e point) Gaussian pulse after propagating through specified commercial DCF and SMF fibers achieving approximately 4000X (4000 times) pulse expansion. In writing the code to do pulse dispersion and compression using 2OD compensation in a given SMF and a DCF fiber, it became apparent that in achieving 4000X pulse expansion on a 71fs pulse, third-order dispersion becomes very conspicuous after pulse compression. This is because the length of fiber over which dispersion and compression occurs traverses a good number of third-order dispersal lengths (L_D'). Therefore, additional code was written to do pulse dispersion and compression over four different types of commercial fiber (two anomalously and two normally dispersive fibers) as opposed to only two complementary fibers in order to do both second- and third-order dispersion compensation.

Only three fibers are sufficient to accomplish this, but the use of four different types of fiber allows for more flexibility in choosing the lengths of each type of fiber. So, when given two lengths for the two normally dispersive fibers with arbitrary dispersion coefficients, the program can automatically find the necessary lengths of the anomalously dispersive fibers so that 2OD and 3OD compensation is realized. As a result, if the input pulse goes through the entire OAWG system without modulation, the output can more closely resemble the input. An illustration of this fact is shown in Figure 4.4 below.

In order to sufficiently sample the initial, dispersed, and recompressed pulse in a fixed time window, a large number of sample points were required, lengthening the amount of computation time to perform a FFT and IFFT and significantly increasing the amount of time to run the overall code. Thus, in coding the propagation program, it became advantageous to implement a variable time window during simulation to

significantly cut down the computation time. The time window algorithm used in our propagation program is described below, and a similar variable time window algorithm can be found in a paper by Shen et al. [26]

Initially, a certain number of samples in a specified time window were used to sample the initial pulse. As the pulse began to broaden, if the edge of the pulse was within –150dB of the peak power, then the number of samples and the width of the time window were doubled provided that the time window was not too large. The maximum number of samples was limited to 262, 145. If the sampled signal intensity is less than –150dB relative to the peak power in the first and last quarters of the time window during pulse compression, then the time window was halved and the samples in the first and last quarters of the time window were removed. The amount of computation time saved by this variable time window algorithm in simulating 4000X pulse expansion and compression can be a little less than half the amount of time it takes to run a fixed time window simulation. A comparison of the outputs of a fixed time window simulation and a variable time window simulation is shown below in Figures 4.5 and 4.6.

Fiber propagation simulations

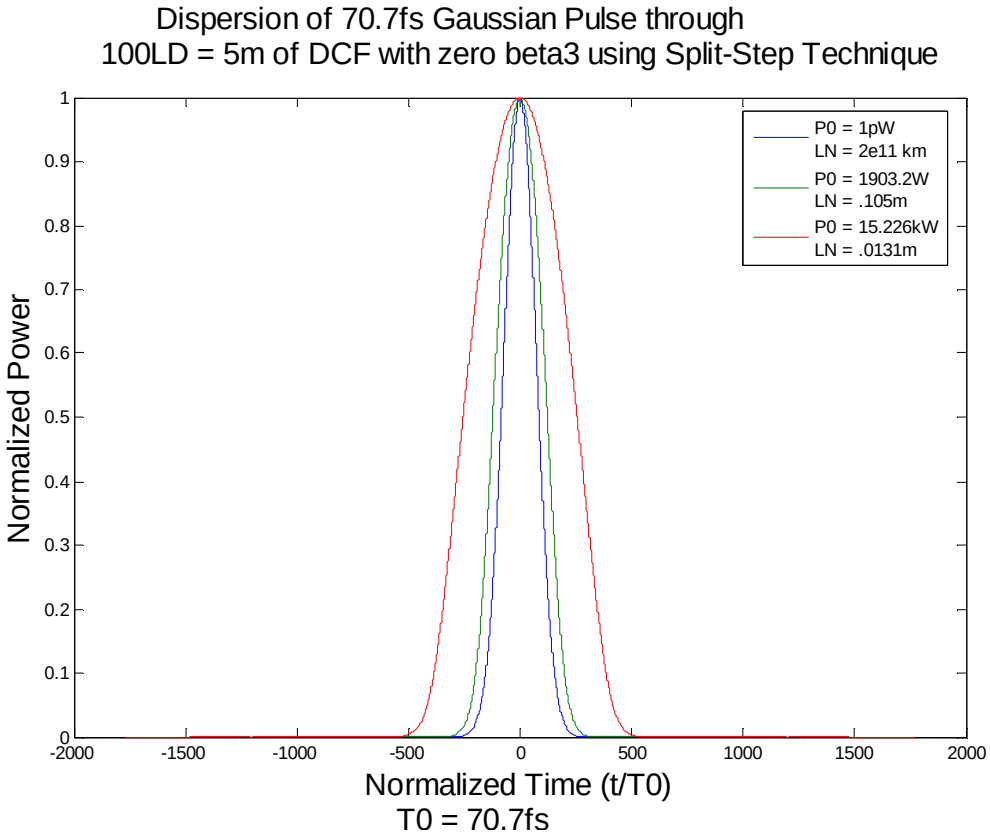

Figure 4.1: Demonstration of the effect of nonlinearity on the output after the propagation of a 70.7fs Gaussian pulse through 5m of DCF using split-step technique. Here P0 denotes peak power, LD denotes 2OD length scale and LN denotes nonlinear length.

In Figure 4.1, the higher-powered Gaussian pulses experience more broadening, while the Gaussian pulse of peak power 1pW experiences a negligible nonlinear effect on its pulsewidth and undergoes the least amount of broadening. The initial pulse into the DCF was a 70.7fs Gaussian pulse. The power in the graph is normalized to the peak power. The characteristics of the DCF fiber that was used are $\beta_2 = -101.97$ ps^2/km, $\beta_3 = 0$ ps^3/km, $\beta_4 = 0$ ps^4/km, $\alpha = 0.55$dB/km, $\gamma = 5$W^{-1}/km, $\lambda_0 = 1550$ nm.

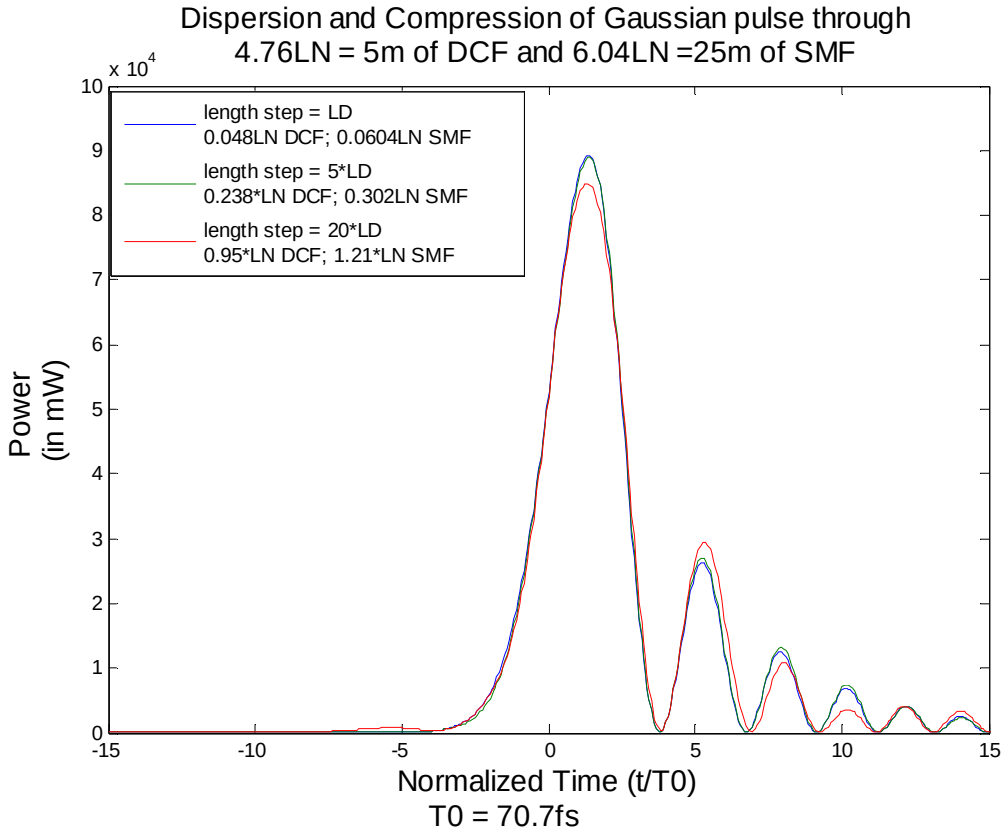

Figure 4.2: Dispersion and compression of 70.7fs 190.32W peak power Gaussian pulse after 5m of DCF and 25m of SMF using the split-step technique with various fixed length steps.

The simulation shown in Figure 4.2 was run to observe the significance of the size of the length step using the split-step technique. In this case, the SMF and DCF fibers have opposing total second-order dispersion, but third-order dispersion is not completely compensated as seen by the cubic phase distortion of the output pulse. The assumed characteristic values for the SMF fiber were β_2 = -20.3931 ps^2/km, β_3 = 0.1282ps^3/km, β_4 = 0 ps^4/km, α = 0.22dB/km, γ = 1.27W^{-1}/km, and λ_0 = 1550 nm. The assumed characteristic values for the DCF fiber were β_2 = -101.97 ps^2/km, β_3 = 0 ps^3/km, β_4 = 0 ps^4/km, α = 0.55dB/km, γ = 5W^{-1}/km, λ = 1550 nm. It can be seen that not too much accuracy is lost by increasing the step size from $0.06L_N$ (where $L_N = 1/\gamma P_0$) to $0.3L_N$ in

the SMF. However, a more noticeable amount of error is visible in increasing the step size from $0.3L_N$ to $1.21L_N$ in the SMF.

It is safe to assume from this that as long as the length step stays well enough below L_N, the solution obtained from simulation is fairly accurate. A heuristic argument to explain this assumption is that if the length step is sufficiently less than L_N, then the length step could be accurately simulated by its dispersive properties, which do not require a split-step technique, but mainly a simple Fourier and inverse Fourier transform. Using this result, given a length of SMF and DCF fiber, some approximate limits on the length step can be determined in the use of the split-step technique to simulate pulse compression and dispersion.

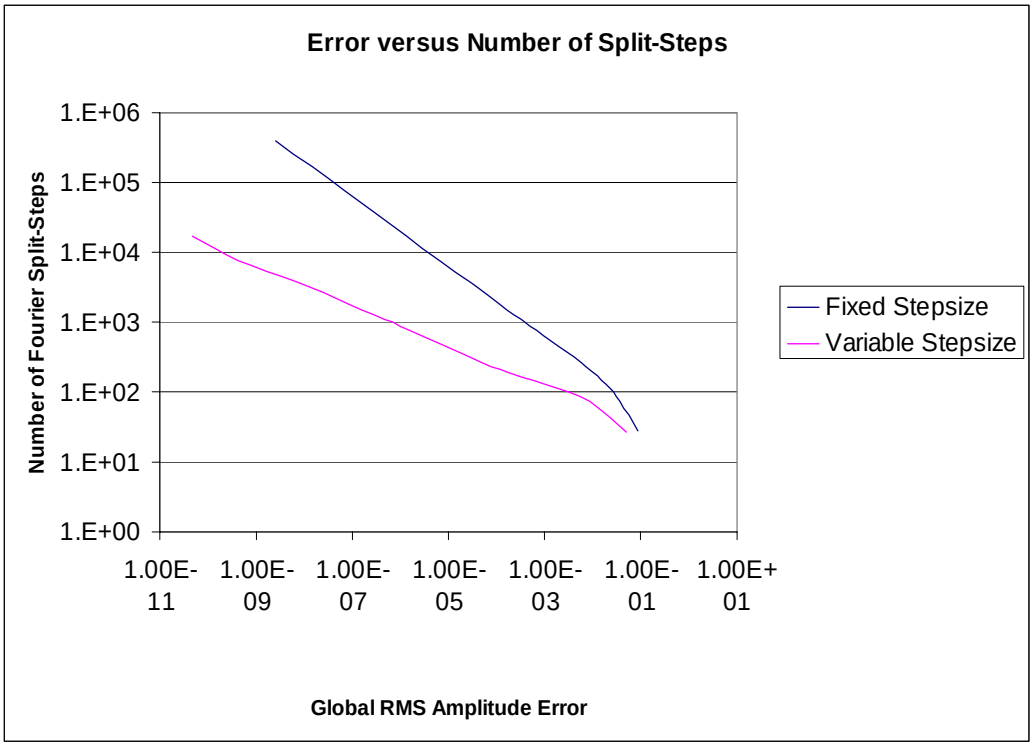

Figure 4.3: Plot showing the number of split-steps versus global RMS amplitude error for simulations using fixed and variable step-sizes. The number of split-steps is approximately proportional to the computation time.

Figure 4.3 shows a plot of the number of Fourier split-steps (each split-step requiring 3 FFTs and 3 inverse FFTs) versus the global error in RMS amplitude (square root of the instantaneous pulse power) for a dispersion and compression simulation using a 1550nm, 70.7fs-pulsewidth, 100W peak power Gaussian input pulse. The length of initial DCF fiber (β_2 = -101.97 ps^2/km, β_3 = -0.3366 ps^3/km, β_4 = 0 ps^4/km, α = 0.55dB/km, $\gamma = 5W^{-1}$/km, λ_0 = 1550 nm) was 10m, and the length of the subsequent SMF fiber (β_2 = -20.3931 ps^2/km, β_3 = 0.1282ps^3/km, β_4 = -3.6068e-4 ps^4/km, α = 0.22dB/km, $\gamma = 1.27W^{-1}$/km, and λ_0 = 1550 nm) was 50m. It is easily seen from the Figure 4.3 that for the same global error, using the program that takes variable split-step Fourier step-sizes can decrease the number of Fourier split-steps by one to two orders of magnitude less, provided the required global error is less than 1e-3 (10^{-3}). When the global error exceeds 0.1 to 1 percent, not too much benefit is gained in using variable step-sizes over fixed step-sizes.

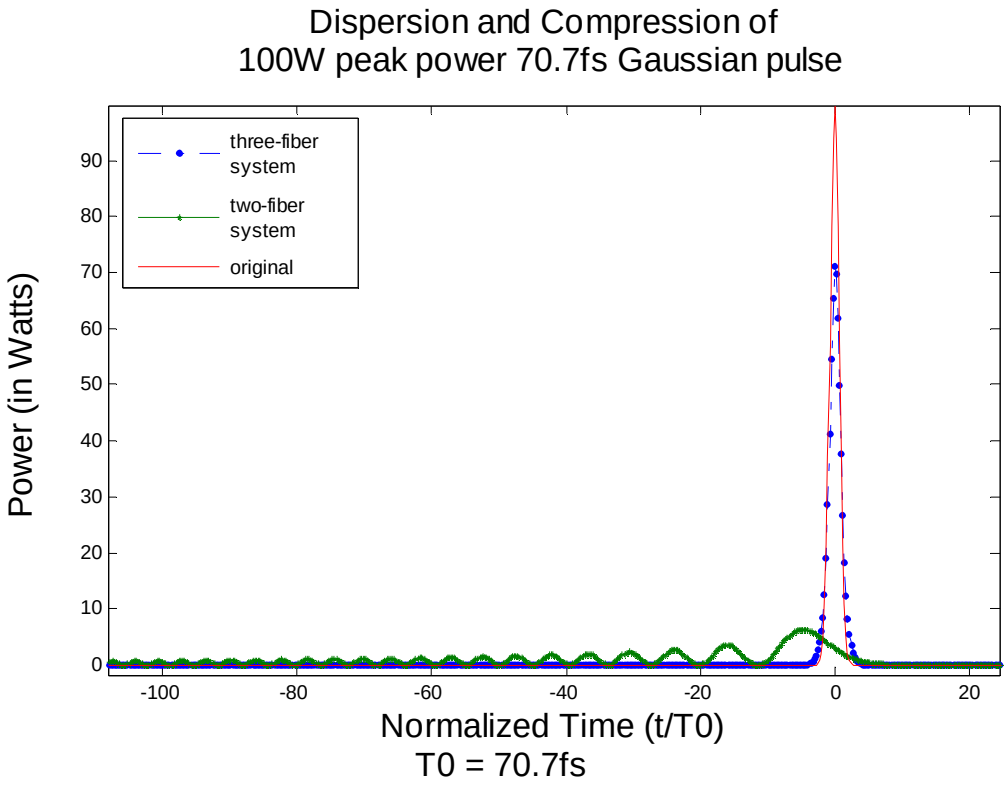

Figure 4.4: Propagation of 100W peak power 70.7fs Gaussian pulse through 4400L_D of DCF and subsequent recompression through either a complementary length of SMF (two-fiber system) or a complementary medium of 2 different SMFs (three-fiber system).

Figure 4.4 shows the difference obtained when using three fibers to do both second- and third-order dispersion compensation as opposed to using two fibers to do only second-order dispersion compensation. The original 70.7fs 100W Gaussian pulse is compared to the output of the three-fiber system and the output of the two-fiber system. The three fibers that were used were a DCF fiber (β_2 = 121.0838 ps^2/km, β_3 = -1.2023 ps^3/km, β_4 = 3.463e-3 ps^4/km, α = 0.5938dB/km, γ = 7.3W^{-1}/km), an SMF fiber (β_2 = -21.6321ps^2/km, β_3 = 0.1284 ps^3/km, β_4 = -3.6068e-4 ps^4/km, α = 0.22dB/km, γ = 1.073W^{-1}/km), and a second SMF fiber (β_2 = -5.6081 ps^2/km, β_3 = 0.0791 ps^3/km, β_4 = -2.37e-4 ps^4/km, α = 0.22dB/km, γ = 1.793W^{-1}/km). The three-fiber system used 181.7m of the DCF fiber, 519.6m of the first SMF fiber, and 1.9188km of the second SMF fiber, while

the two-fiber system used 181.7m of the DCF fiber, 1.017km of the first SMF fiber, and 0m of the second SMF fiber. Figure 4.4 shows how helpful a three-fiber system can be in performing second- and third-order dispersion compensation with three fibers that have arbitrary β_2 and β_3 and the importance of third-order dispersion compensation. The difference between the output of the three-fiber system and the input signal can be attributed to the nonlinearity and loss of the three fibers and the high peak power of the input.

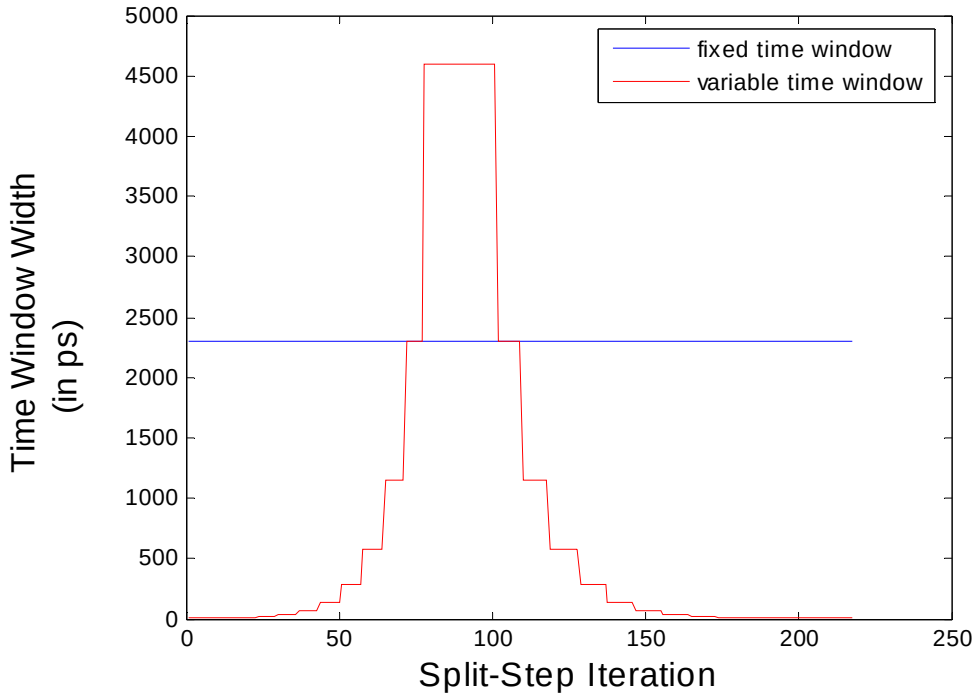

Figure 4.5: Plot of time window width versus split-step iteration for fixed time window and variable time window simulations. The time window width is proportional to the number of samples used to sample the pulse at a particular distance along the fiber.

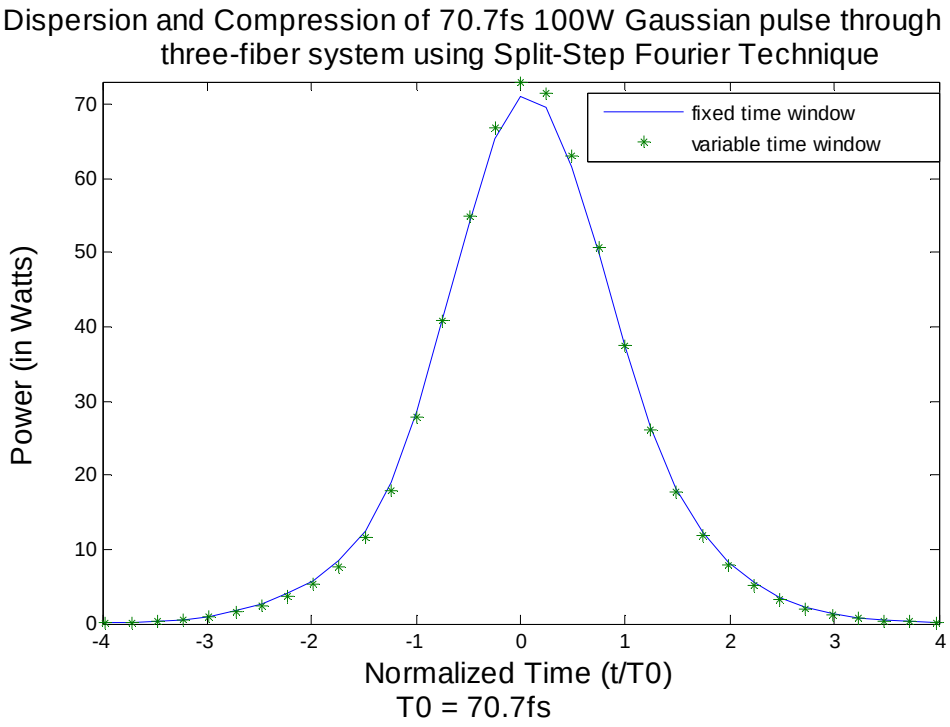

Figure 4.6: Plot of output pulse after propagation through a 2OD- and 3OD-compensated three-fiber system for fixed time window and variable time window simulations.

Pulse expansion and compression was simulated in the propagation of a 100W 70.7fs Gaussian pulse through a three-fiber system with second- and third-order dispersion compensation in order to test the performance of the variable time window simulation code relative to the fixed time window simulation code in terms of speed of simulation and error in simulation. Plots of the width of the variable time window are shown in Figure 4.5. The three fibers that were used in simulation were a DCF fiber (β_2 = 121.0838 ps^2/km, β_3 = -1.2023 ps^3/km, β_4 = 3.463e-3 ps^4/km, α = 0.5938dB/km, γ = 7.3W^{-1}/km), an SMF fiber (β_2 = -21.6321ps^2/km, β_3 = 0.1284 ps^3/km, β_4 = -3.6068e-4 ps^4/km, α = 0.22dB/km, γ = 1.073W^{-1}/km), and a second SMF fiber (β_2 = -5.6081 ps^2/km, β_3 = 0.0791 ps^3/km, β_4 = -2.37e-4 ps^4/km, α = 0.22dB/km, γ = 1.793W^{-1}/km). The lengths of each fiber were 181.7m of the DCF fiber, 519.6m of the first SMF fiber, and

1.9188km of the second SMF fiber. The output waveforms for both the fixed time window and variable time window simulations are shown in Figure 4.6.

The RMS amplitude (square root of pulse power) error between the two simulation outputs (fixed time window and variable time window) was found to be 2.07%, which is relatively small. The amount of computation time of the variable time window simulation was a little less than half the amount of computation time of the fixed time window simulation. This reduction in computation time is a great improvement considering that depending on the simulation, the fixed time window simulation could take between 1 and 4 hours of computation time. Also, looking at Figure 4.6, the difference in output waveforms is not that much, so the decrease in computation time may be a benefit that greatly outweighs the possible error created by using a variable time window.

Modeling and simulation with modulation

After modeling fiber propagation and benchmarking the code used to simulate fiber propagation, code was written to model the entire OAWG system including the modulator. In order to verify the pulse shaping capabilities of the OAWG system under ideal conditions (linear propagation, no higher-order dispersion and ideal modulation), a benchmark modulating waveform was used on a dispersed pulse in order to obtain a desired shaped output signal. Figure 4.7 shows the modulating waveform and the modulated dispersed Gaussian pulse. The dispersed Gaussian pulse was obtained after propagating a 100W 70.7fs Gaussian pulse through 1km of SMF fiber (β_2 = -21.6321 ps^2/km) with no nonlinearities and no higher-order dispersion. The modulating waveform can be considered as a 106.1Gb/s binary phase-only filter of 44 temporal pixels (0 or pi) and 414.75ps in duration over the center of the dispersed Gaussian pulse. Over this duration, the Gaussian pulse can be considered as being approximately flat.

The rest of the Gaussian pulse can be thought of as being modulated with a binary amplitude-only filter (0 or 1) that completely attenuates the part of the dispersed Gaussian pulse not being modulated by the phase-only filter. In this sense, the modulating waveform may be modeled as cascaded binary phase-only and amplitude-only filters. The resulting output after compression through a complementary length of DCF fiber, with no nonlinearity or higher order dispersion, is shown in Figure 4.8. This is in good agreement with the expected output of a similar OAWG system using the same binary phase-only filter. [27]

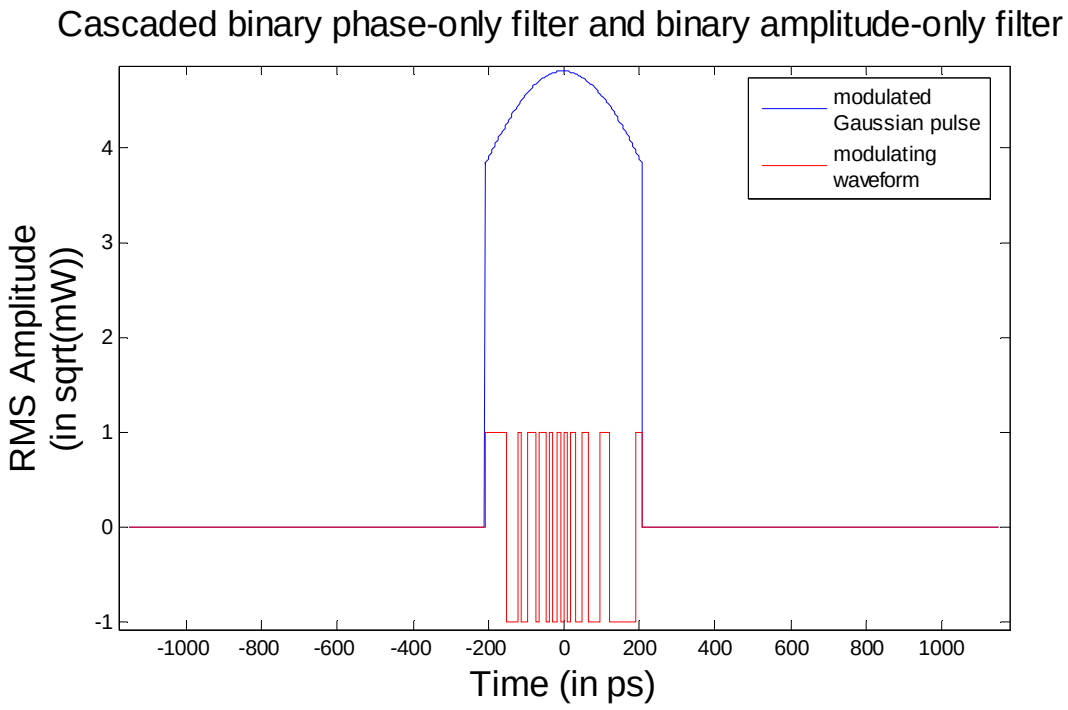

Figure 4.7: RMS amplitude (square root of power) of modulated dispersed Gaussian and the modulating waveform. The modulating waveform takes three values 1, 0, and –1.

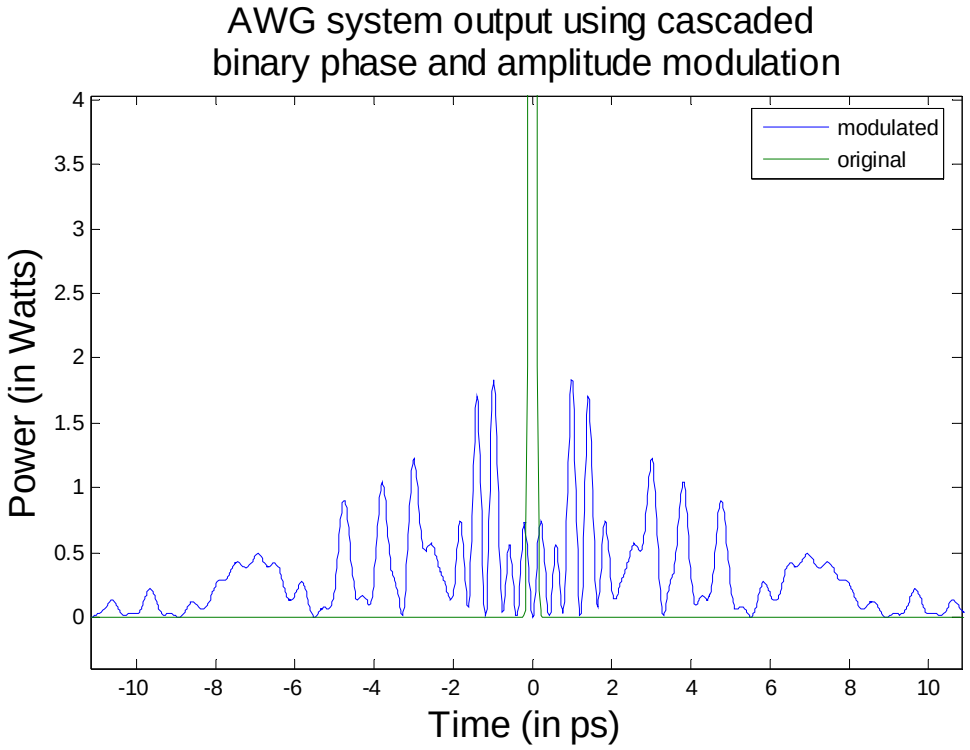

Figure 4.8: Output of OAWG system after recompression of the modulated dispersed original pulse.

We now examine our OAWG system in a more practical setting using fibers with realistic dispersive and nonlinear characteristics. Figure 4.9 demonstrates the benefit of using a three-fiber system over a two-fiber system to do second- and third-order dispersion compensation in an OAWG setup. An initial 100W peak power 70.7fs Gaussian pulse was propagated through 141.434m of DCF fiber (β_2 = 152.9479 ps^2/km, β_3 = -0.9533ps^3/km, β_4 = 2.515e-3 ps^4/km, α = 0.4286dB/km, γ = 5.212W^{-1}/km), modulated with the waveform shown in Figure 4.7, propagated through 963.6m of one SMF fiber (β_2 = -21.6321ps^2/km, β_3 = 0.1284 ps^3/km, β_4 = -3.6068e-4 ps^4/km, α = 0.22dB/km, γ = 1.073W^{-1}/km), and 140.5m of a second SMF fiber (β_2 = -5.6081 ps^2/km, β_3 = 0.0791 ps^3/km, β_4 = -2.37e-4 ps^4/km, α = 0.22dB/km, γ = 1.793W^{-1}/km). The length

of the DCF fiber was chosen to give the same pulse broadening of that of 1 km of the first SMF fiber. This is so that ideally the generated waveform should match that of the Figure 4.8. However, as a result of third-order dispersion, the output waveform is slightly different from the output shown in Figure 4.8. As indicated by Equation 3.21, the third-order dispersion has a greater effect on temporal features farther away from the middle of the temporal window.

Another simulation was run using a two-fiber system that provides the same second-order dispersion compensation as the three-fiber system; however, the 3OD was left uncompensated. The two fibers that were used were a DCF fiber (β_2 = 121.0838 ps^2/km, β_3 = -1.2023 ps^3/km, β_4 = 3.463e-3 ps^4/km, α = 0.5938dB/km, γ = 7.3W^{-1}/km) and an SMF fiber (β_2 = -21.6321ps^2/km, β_3 = 0.1284 ps^3/km, β_4 = -3.6068e-4 ps^4/km, α = 0.22dB/km, γ = 1.073W^{-1}/km). The two-fiber system used 181.7m of the DCF fiber and 1.017km of the first SMF fiber. Both the three- and two-fiber systems were compared to a linear system with no third- or fourth- order dispersion. The results are shown in Figure 4.9. Because of the residual 3OD, there is a great amount of discrepancy between the output in the ideal linear case and the output of the uncompensated 3OD two-fiber system.

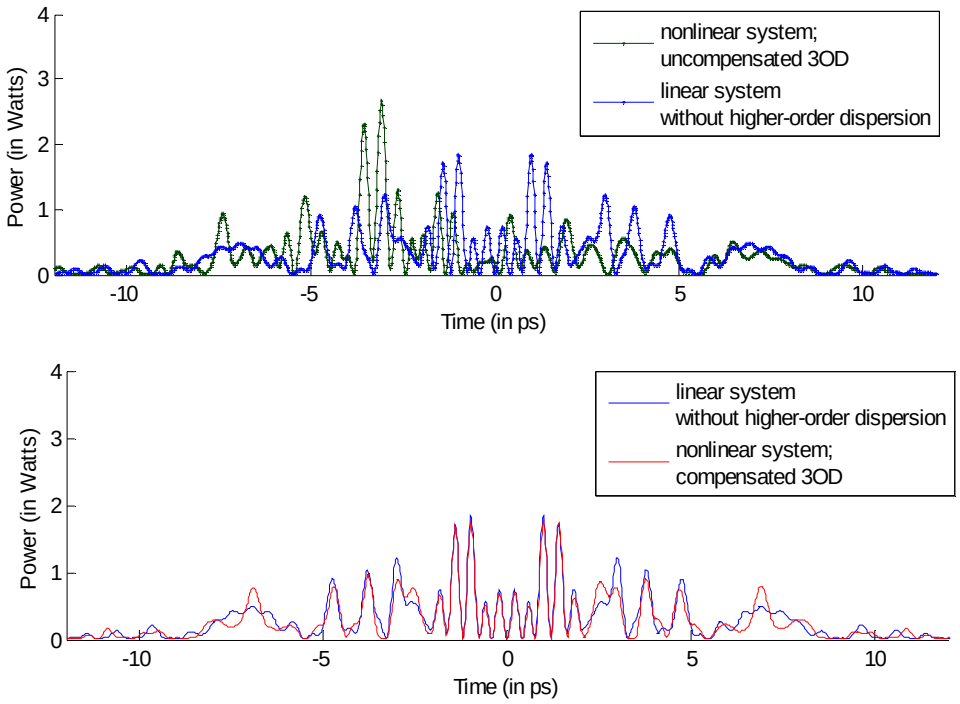

Figure 4.9: Top plot compares the simulated outputs of an OAWG system using linear fibers without 3OD and using nonlinear fibers with uncompensated 3OD. Bottom plot compares the simulated outputs of an OAWG system using linear fibers without 3OD and using nonlinear fibers with compensated 3OD.

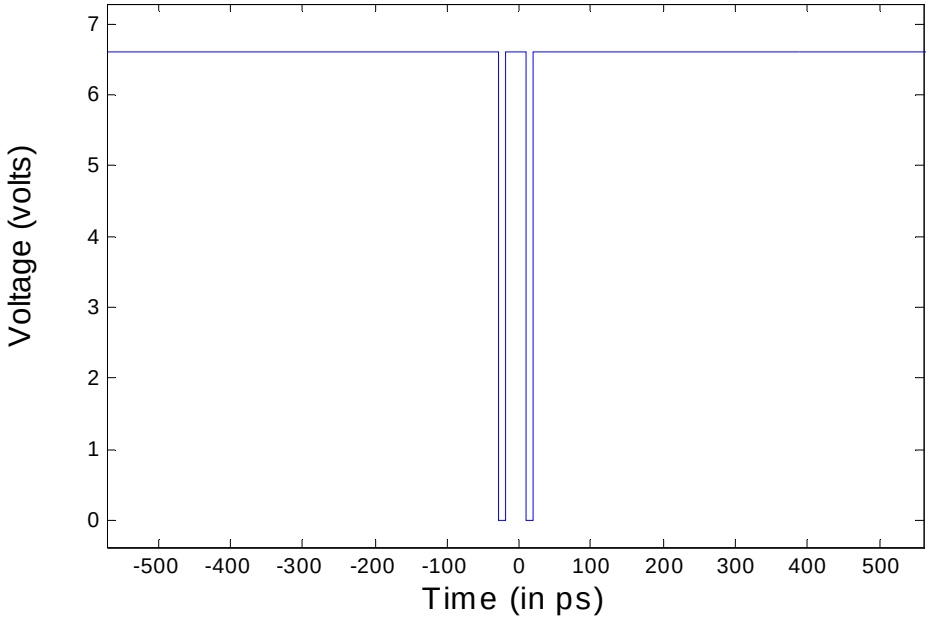

Figure 4.10: Applied voltage to a $LiNbO_3$ amplitude modulator with $V_{\pi 0}$ = 6.6V.

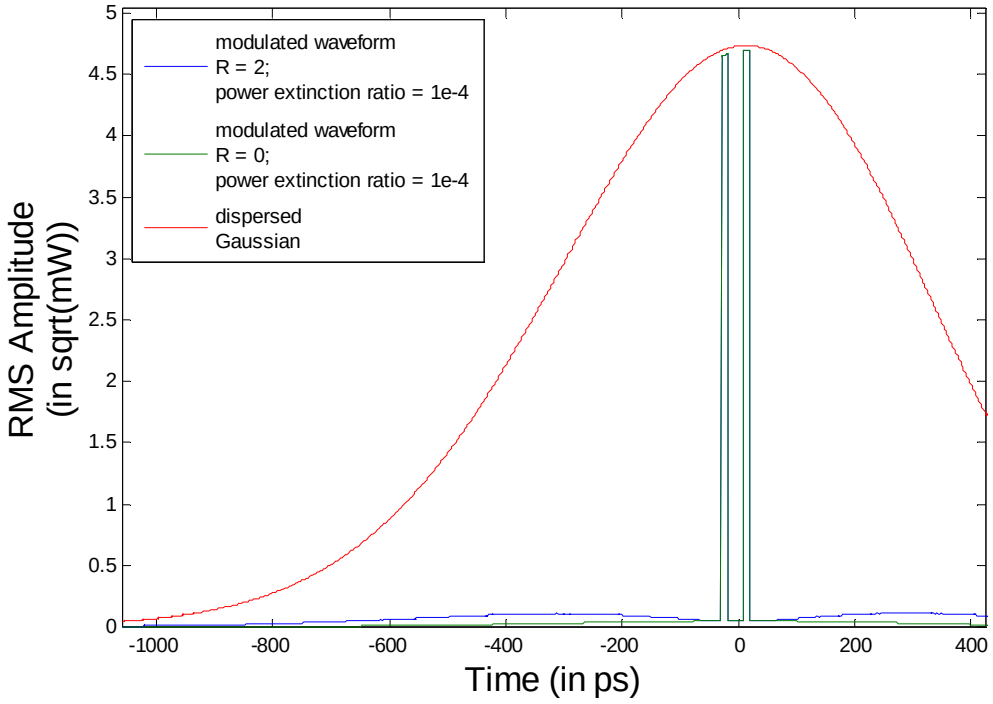

Figure 4.11: Propagation of 70.7fs 100W Gaussian pulse through 4326.4L_D of DCF. Modulated optical signal after amplitude modulation with a modulator with R = 0 and a modulator with R = 2.

In order to demonstrate both the pulse shaping capabilities of the three-fiber OAWG system and show the effects of a nonideal modulator, a simulation was run involving an ideal Lithium Niobate ($LiNbO_3$) amplitude modulator (with no risetime effects, ideal on-off ratio, and constant $V_\pi(\lambda)$), an amplitude modulator with a power extinction ratio of -40dB and constant V_π of 6.6V, and an amplitude modulator with a power extinction ratio of -40dB and R = 2 (see Eq. 3.28 and Eq. 3.29). The R-value for a $LiNbO_3$ is usually 2 for a wavelength of 1550nm. The fibers used in this simulation are 141.434m of a DCF fiber (β_2 = 152.9479 ps^2/km, β_3 = -0.9533ps^3/km, β_4 = 2.515e-3 ps^4/km, α = 0.4286dB/km, γ = 5.212W^{-1}/km), 963.6m of a SMF fiber (β_2 = -21.6321ps^2/km, β_3 = 0.1284 ps^3/km, β_4 = -3.6068e-4 ps^4/km, α = 0.22dB/km, γ = 1.073W^{-}

^{1}/km), and 140.5m of a second SMF fiber (β_2 = -5.6081 ps^2/km, β_3 = 0.0791 ps^3/km, β_4 = -2.37e-4 ps^4/km, α = 0.22dB/km, γ = 1.793W^{-1}/km). The lengths of these fibers ensured second- and third-order dispersion compensation. The amplitude modulation was accomplished by doing simple on-off modulation at 106.1Gb/s with 244 pixels (2300ps in duration or 9.43ps/pixel). Only two of the 244 pixels (the 120th and 124th pixels) are nonzero. With amplitude modulation using an EO modulator, this corresponds to applying 0V during these pixels and a voltage of V_π for all other times. Figure 4.10 shows the applied voltage while Figure 4.11 shows the dispersed Gaussian pulse before undergoing modulation and after being modulated for nonideal modulation with R = 0 and R = 2. The output waveforms after compression of the modulated Gaussian pulse for the ideal and nonideal modulation cases are given in Figure 4.12.

To verify that the ideal output in Figure 4.12 is what should be expected, the modulating and output waveforms will be briefly examined. The modulating waveform can be approximated by two delta functions located at about 18.85ps away from the center of the dispersed pulse. Using the result from Equation 3.19, this corresponds to an approximate output frequency of $\Delta\omega = \Delta t/(\beta_2 z_1)$. Therefore, the output shown in Figure 4.12 should be a cosine-squared function, having spectral components equal to $2\Delta\omega$ and a period of $\pi/\Delta\omega$ = 3.6ps. This is consistent with Figure 4.12; however, the envelope of this cosine-squared output can be attributed to the fact that the modulating waveform is actually closer to two square pulses than two delta functions.

The difference between output waveforms with different modulator characteristics can be seen in Figure 4.12. The outputs for all three cases are very similar except for at the center of the time window. In the case where R is equal to zero and the power extinction ratio is –40dB, there is a dip in the output at the center of the generated waveform. For the case when R is 2, the output develops a large dip and a large peak at the center of the waveform. In both nonideal modulation cases, the deviation from the ideal modulation OAWG output at the center of the time window is a result of the

nonideal switching ratio. The undiminished energy contained in the time pixels of a modulated dispersed Gaussian pulse when the applied voltage is $V_{\pi 0}$ (or V_{π}) shows up as large distortions at the center of the output waveform. These distortions appear large since the ideal output waveform has a very weak peak power relative to the peak power of the input optical signal. For the nonzero R case, the distortions are larger due to the variation of V_{π} over the dispersed wavelengths of the broadened pulse resulting in more undiminished energy at higher frequencies (relative to the center frequency). The input optical signal was a 100W 70.7fs Gaussian pulse.

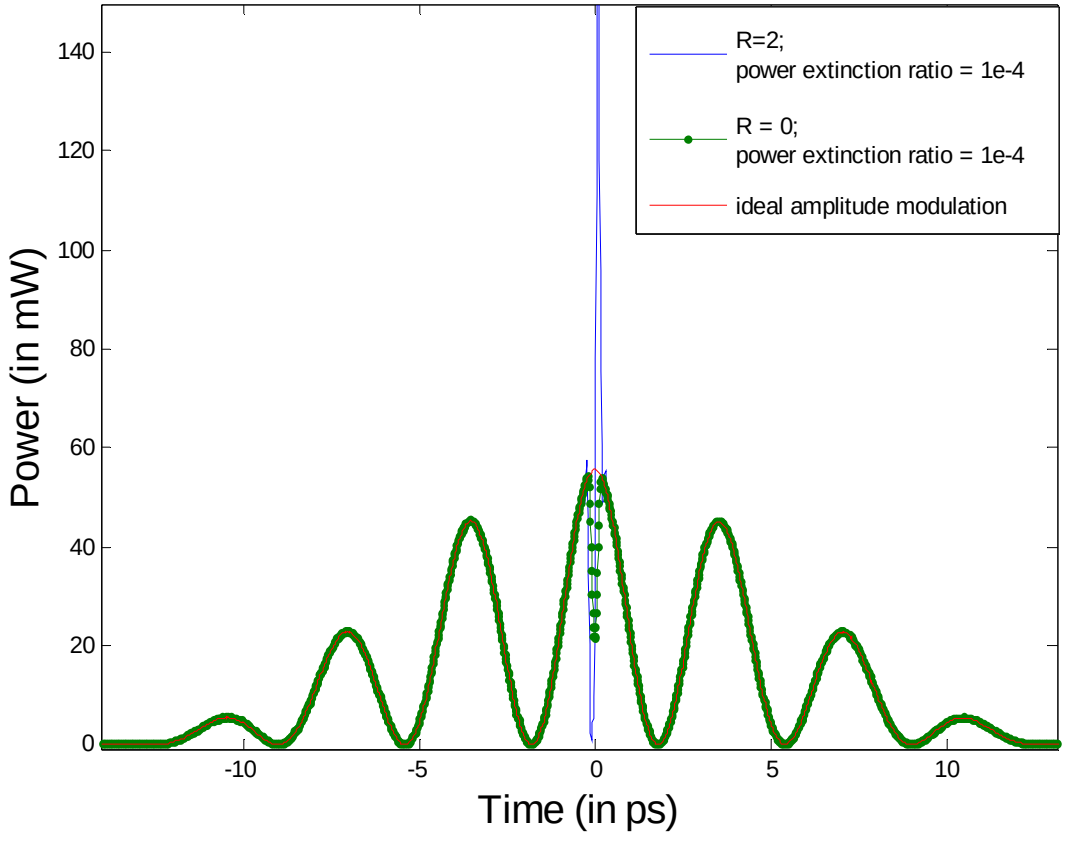

Figure 4.12: Output of OAWG system after binary amplitude modulation with different modulator characteristics.

In order to see the effect of a limited modulation bandwidth, a 1mW soliton (hyperbolic secant) pulse of 200fs duration (0.5673 times the soliton full-width half maximum) was sent through an OAWG system. The initial soliton was propagated through 440m of a DCF fiber (β_2 = 152.9479 ps^2/km, β_3 = -0.9533 ps^3/km, β_4 = 2.515e-3 ps^4/km, α = 0.4286dB/km, γ = 5.212W^{-1}/km) and modulated by an ideal amplitude modulator driven by a binary signal. The binary amplitude modulation was a 20-bit pattern (11011010101010011000) applied across the center of the dispersed soliton using bitrates of 10, 40, and 188.7Gb/s. The rest of the dispersed soliton was completely attenuated. The dispersed soliton and the amplitude modulating waveforms for the different modulating bitrates are shown in Figures 4.13, 4.14, and 4.15.

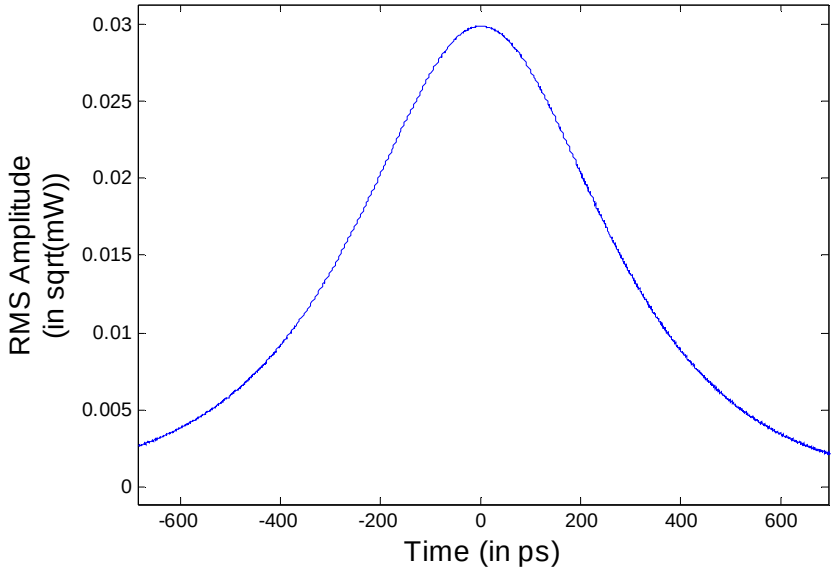

Figure 4.13: Dispersed 1mW peak power 200fs soliton pulse after 440m of DCF

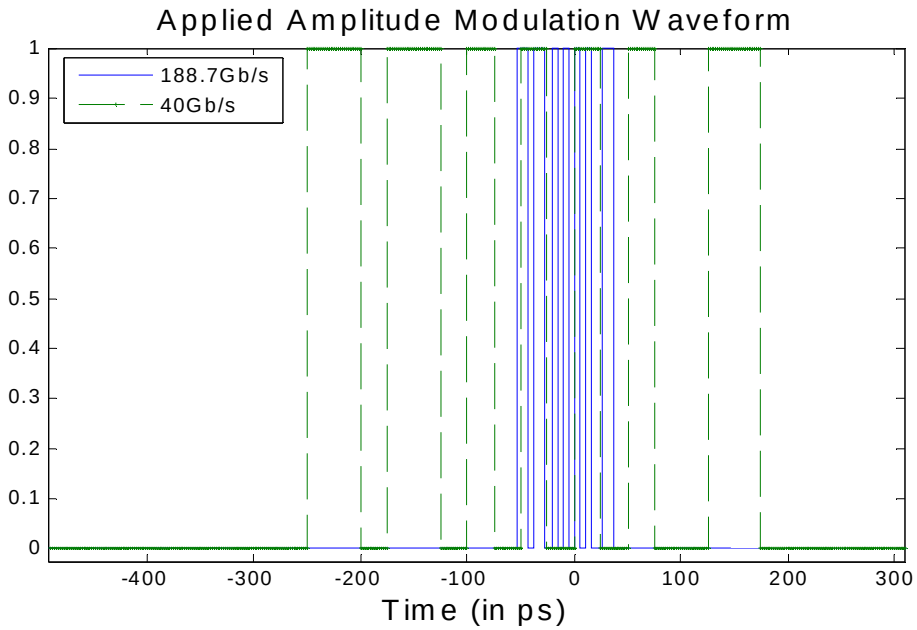

Figure 4.14: Amplitude modulating waveforms for a 20-bit pattern of 188.7Gb/s and 40Gb/s centered over the center of the dispersed pulse.

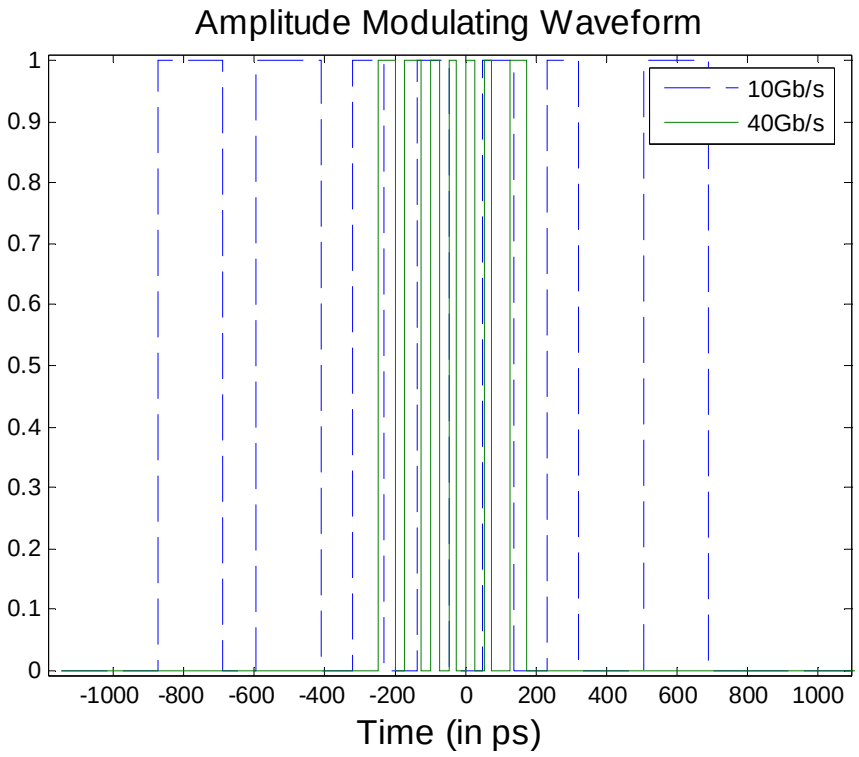

Figure 4.15: Amplitude modulating waveforms for a 20-bit pattern of 40Gb/s and 10Gb/s centered across the center of the dispersed pulse.

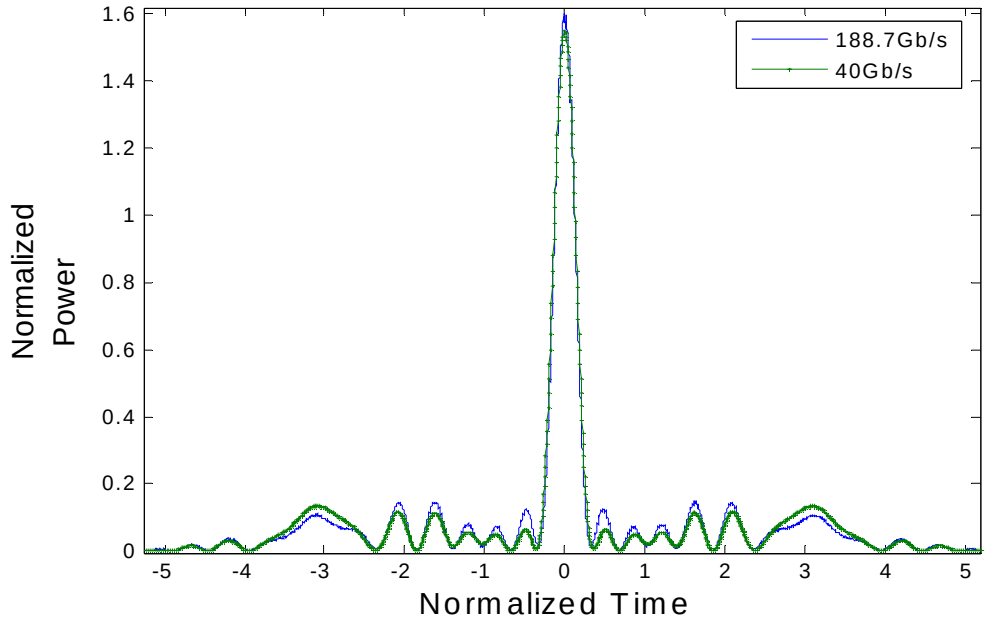

Figure 4.16: Normalized OAWG output for 188.7Gb/s and 40Gb/s modulation

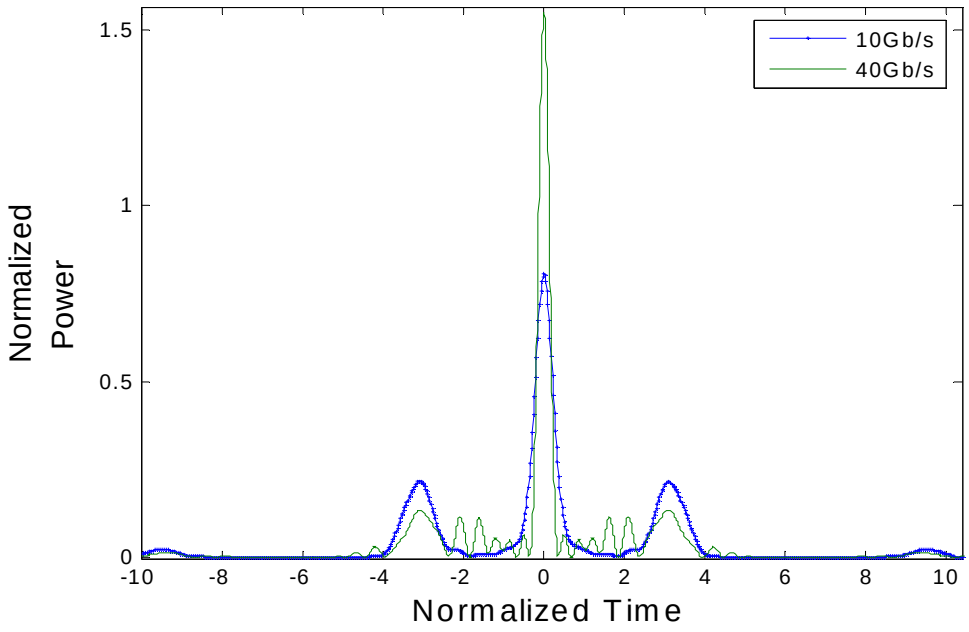

Figure 4.17: Normalized OAWG output for 10Gb/s and 40Gb/s modulation

After modulation, the modulated pulse was recompressed after propagating through 2.998km of one SMF fiber (β_2 = -21.6321ps^2/km, β_3 = 0.1284 ps^3/km, β_4 = -3.6068e-4 ps^4/km, α = 0.22dB/km, γ = 1.313W^{-1}/km) and 427m of a second SMF fiber (β_2 = -5.7355 ps^2/km, β_3 = 0.0809 ps^3/km, β_4 = -2.4286e-4 ps^4/km, α = 0.22dB/km, γ = 2.445W^{-1}/km). The outputs for the different modulation bitrates are shown in Figures 4.16 and 4.17. The time axis is normalized by the spectral resolution (time per bit or pixel divided by $\beta_{2,DCF}z_{DCF}$), while the power is normalized so that the integral of the output over normalized time is one. This normalization allows for the comparison of the quality of shaped outputs using time-dilated or time-compressed versions of the same modulating waveform. The outputs in Figure 4.16 are similar because in both cases, the modulation is performed on the portion of the dispersed optical pulse that is relatively flat and above the –3dB point. This also means that the passed (non-attenuated) spectral elements are so close to the center frequency that the output waveform has slowly varying temporal features when compared to the initial pulse (which is a measure of the smallest temporal feature).

However, in Figure 4.17, the waveform generated by 10Gb/s modulation is significantly different than its 40Gb/s counterpart. In the 10Gb/s case, the amplitude modulation has nonzero elements that experience attenuation due to the dispersed pulse envelope. This means that the higher spectral elements that are further deviated from the center wavelength are attenuated, and the smaller temporal features in the output waveform are blurred due to convolution with the initial soliton pulse. In looking at this from the perspective of the normalized time output shown in Figure 4.17, the initial soliton pulse has a broader pulsewidth over normalized time as the modulation bitrate decreases. So, the minimum temporal feature over normalized time increases in duration

as the bitrate decreases leading to the severe blurring of the output waveform in the 10Gb/s case.

To study the effects of nonideal amplitude modulation, a 70.7fs 100W Gaussian pulse was propagated through 141.434m of a DCF fiber (β_2 = 152.9479 ps^2/km, β_3 = -0.9533 ps^3/km, β_4 = 2.515e-3 ps^4/km, α = 0.4286dB/km, γ = 5.212W^{-1}/km). An amplitude modulating waveform was applied over the center of the dispersed Gaussian pulse. The input voltage is shown in Figure 4.18 and was a 10Gb/s binary digital waveform (0 or $V_{\pi 0}$) of 23 time pixels (2300ps in total duration). For the nonideal EO modulator, R was equal to 2, the power switching ratio was 1e-4, and the risetime of the modulating waveform was 40ps. A voltage of $V_{\pi 0}$ (equal to 6.6V) was applied on the odd time pixels of the dispersed pulse, while no voltage was applied on the even time pixels of the dispersed pulse. After the dispersed 100W 70.7fs Gaussian pulse was modulated with the amplitude modulating waveforms shown in Figure 4.19, the modulated pulse was propagated through 963.6m of one SMF fiber (β_2 = -21.6321ps^2/km, β_3 = 0.1284 ps^3/km, β_4 = -3.6068e-4 ps^4/km, α = 0.22dB/km, γ = 1.313W^{-1}/km) and 137.269m of a second SMF fiber (β_2 = -5.7355 ps^2/km, β_3 = 0.0809 ps^3/km, β_4 = -2.4286e-4 ps^4/km, α = 0.22dB/km, γ = 2.445W^{-1}/km). The OAWG system outputs are shown in Figure 4.20.

Looking at the OAWG outputs in Figure 4.20, the increasing attenuation of the satellite pulses is due to the nonzero risetime of the nonideal modulation. The risetime is an indication of the lowpass filtering effect of a noticeable modulation bandwidth. As a result, higher modulation frequencies in the desired modulating waveform face higher attenuation and as a result satellite pulses further away from the center of the time window face higher attenuation.

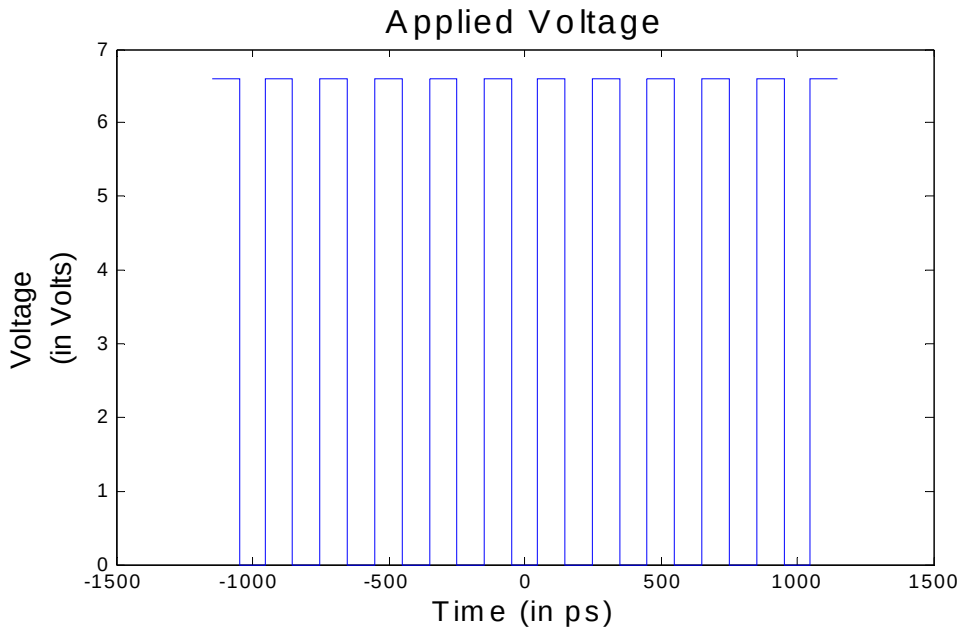

Figure 4.18: Twenty-three-bit 10Gb/s voltage signal for amplitude modulation.

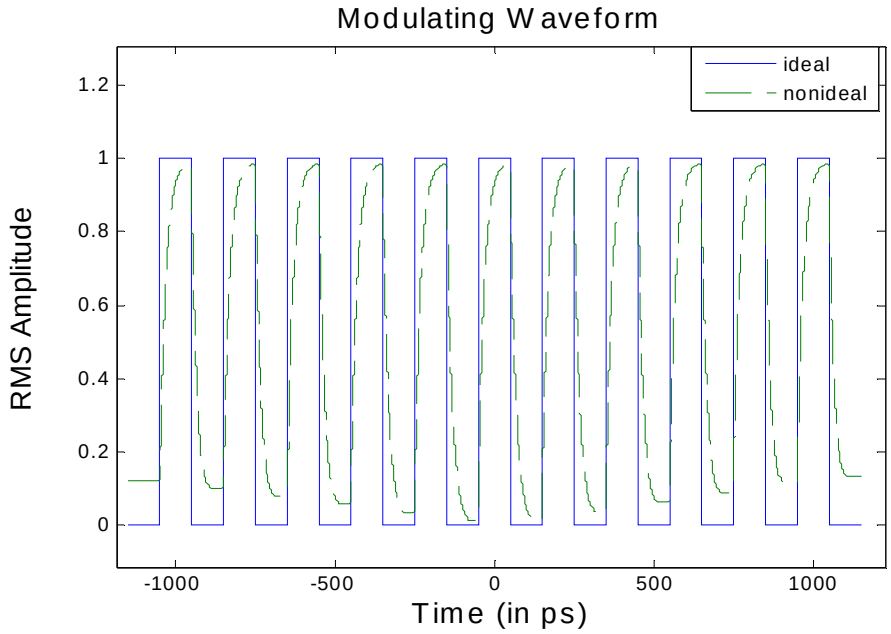

Figure 4.19: Ten Gb/s amplitude modulating waveforms for an ideal modulation and nonideal modulation with a risetime of 40ps, R = 2, and power switching ratio of 10^{-4}.

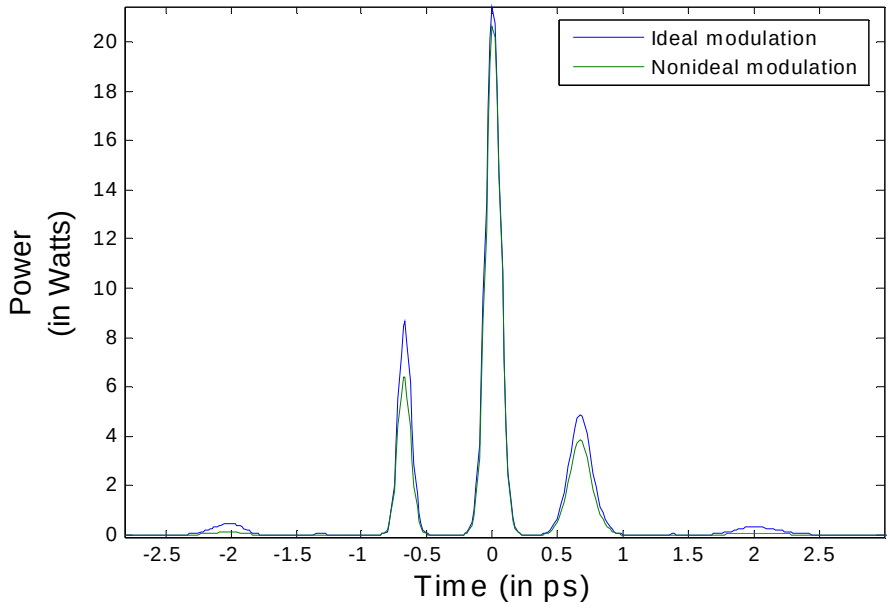

Figure 4.20: Comparison of OAWG outputs using ideal modulation and nonideal modulation with a risetime of 40ps, R = 2, and power switching ratio of 10^{-4}.

To consider the effects of nonideal phase modulation, the case where the modulating waveform is a complex exponential or applies linear phase to the optical signal can be studied. This case was already studied mathematically and can be summarized by Equations 3.19, 3.21, or 3.22 depending on the strength of the third- and fourth-order dispersion coefficients of the fibers. However, the variation of V_π and the modulation bandwidth can alter the relationships in Equation 3.19, 3.21, and 3.22. So, a simulation was run where voltage was applied to change the phase of a dispersed optical soliton 24.19rads/ns using a phase modulator. A 100mW peak power, 200fs soliton was propagated through 440m of a DCF fiber (β_2 = 152.9479 ps^2/km, β_3 = -0.9533 ps^3/km, β_4 = 2.515e-3 ps^4/km, α = 0.4286dB/km, γ = 5.212W^{-1}/km) and modulated with a phase

modulator with different modulation bandwidths. The applied voltage is shown in Figure 4.21, and the phase modulating waveforms are shown in Figure 4.22 and 4.23.

In the ideal modulation case, the risetime was 0ps and R = 0. In the nonideal modulation cases in Figure 4.22, the risetime was 10ps, R = 2, and there were only seven available voltage levels for the modulator driver: 0V, $\pm V_\pi/3$, $\pm 2V_\pi/3$, and $\pm V_\pi$. These voltages corresponded to six phases: 0, $\pm\pi/3$, $\pm 2\pi/3$, and $\pm\pi$ radians. The risetime affected the transition to these phases. The two different nonideal modulators had drive speeds of 8.7GHz and 17.4GHz. In the nonideal modulation case in Figure 4.23, the risetime was 30ps and R = 0. After modulation, the modulated signals in all cases were propagated through 2.998km of one SMF fiber (β_2 = -21.6321ps^2/km, β_3 = 0.1284 ps^3/km, β_4 = -3.6068e-4 ps^4/km, α = 0.22dB/km, γ = 1.582W^{-1}/km) and 437.1m of a second SMF fiber (β_2 = -5.6081 ps^2/km, β_3 = 0.07908 ps^3/km, β_4 = -2.3735e-4 ps^4/km, α = 0.22dB/km, γ = 2.4947W^{-1}/km).

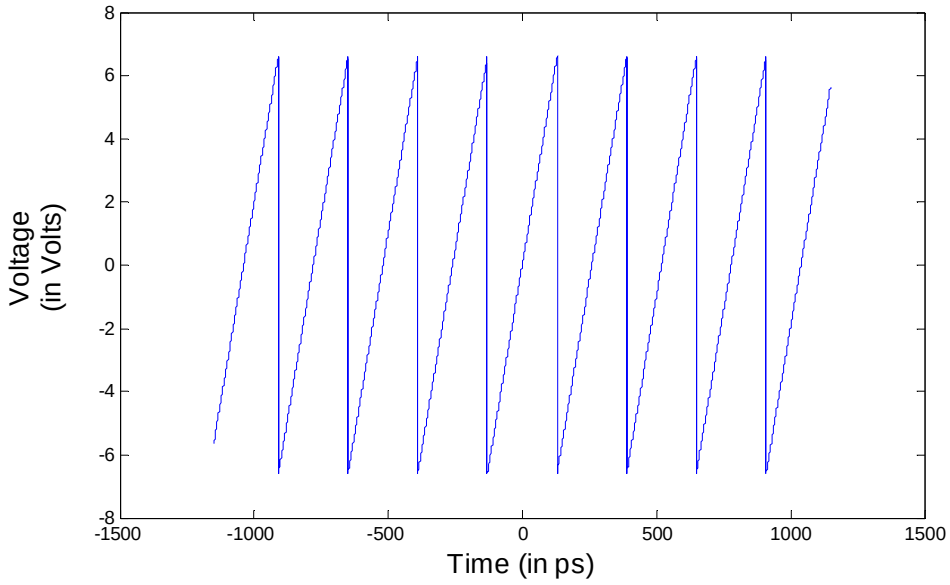

Figure 4.21: Applied voltage to a $LiNbO_3$ phase modulator with $V_{\pi 0}$ = 6.6V to achieve linear phase modulation modulo 2π.

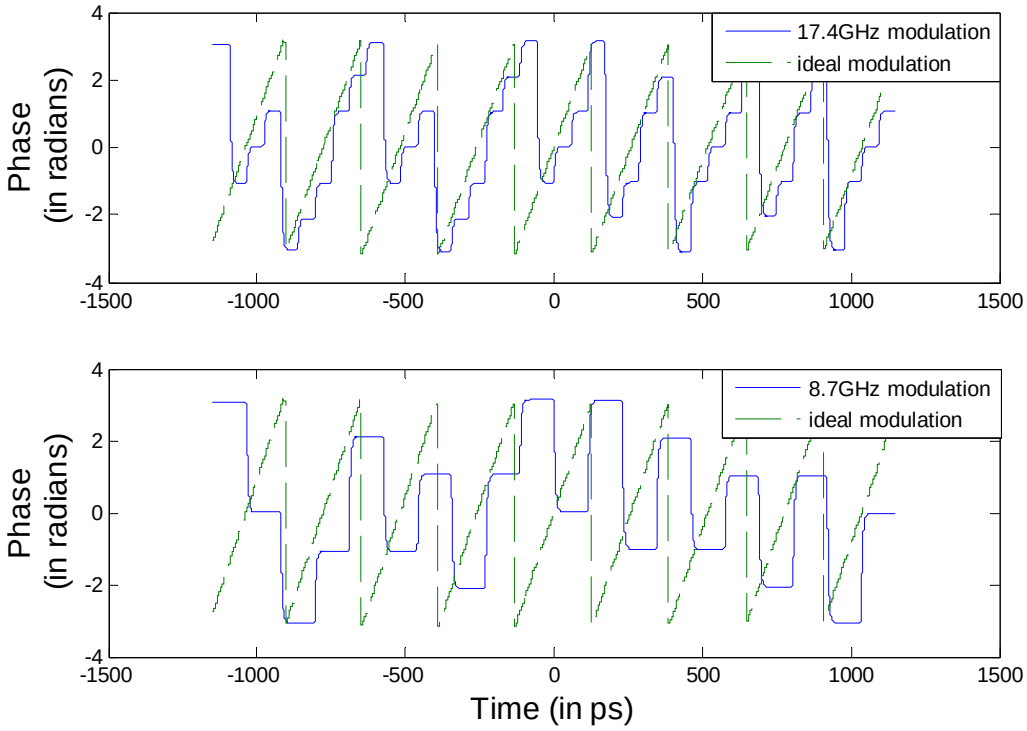

Figure 4.22: Ideal linear phase modulating waveform with no risetime and corresponding 17.4GHz (top) and 8.7GHz (bottom) 7-level phase modulating waveforms with 10ps risetime.

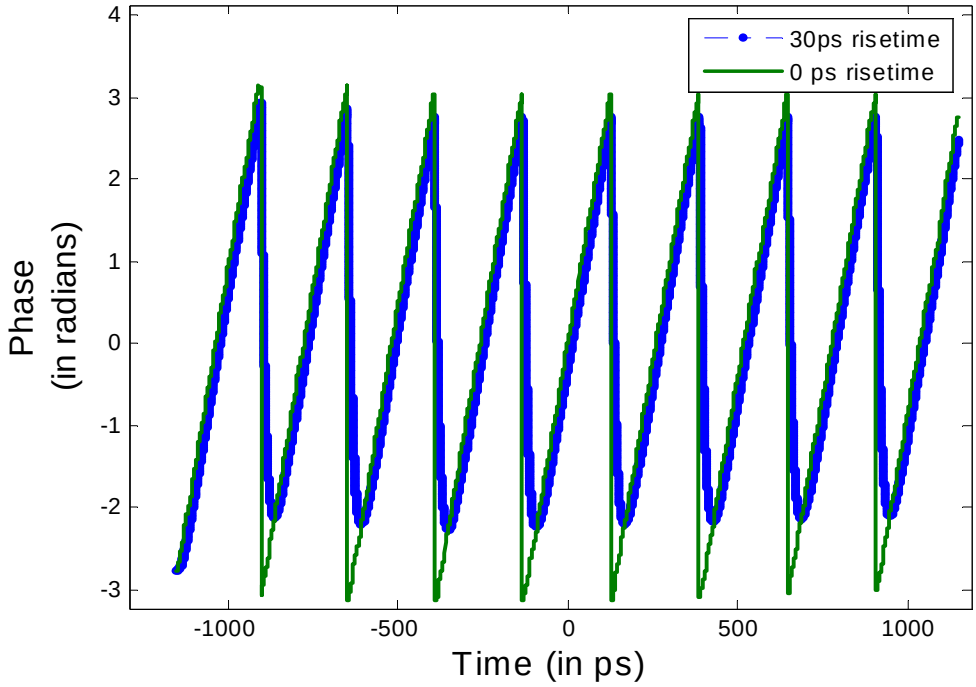

Figure 4.23: Linear phase modulating waveforms with 0ps and 30ps risetimes.

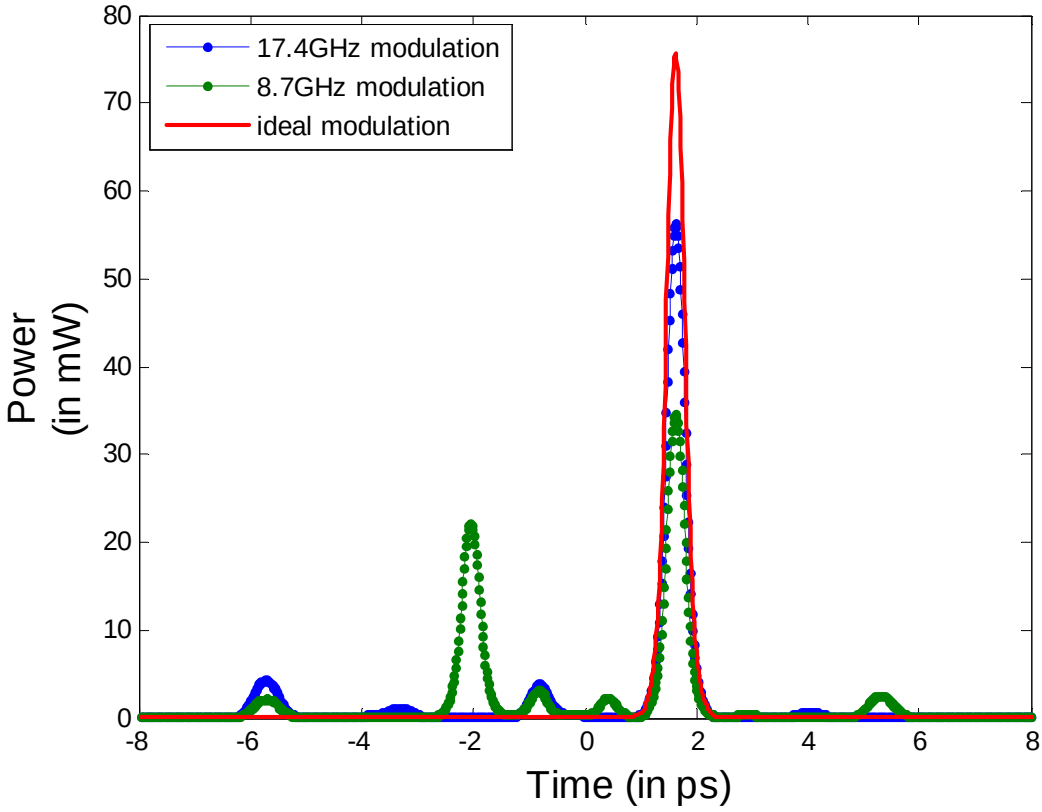

Figure 4.24: OAWG system outputs with linear phase modulation of a dispersed 200fs 100mW soliton-shaped (hyperbolic secant) pulse. A 7-level phase modulator with 10ps risetime was used in the nonideal phase modulation cases.

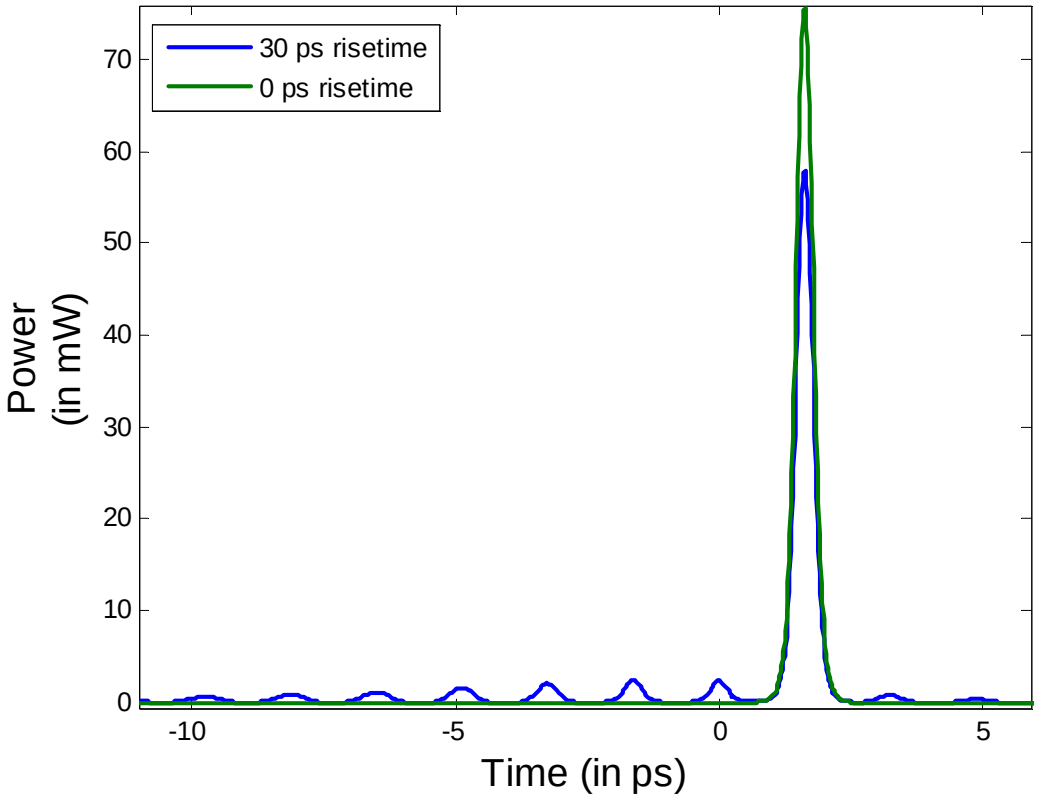

Figure 4.25: OAWG system outputs with phase modulation of a dispersed 200fs 100mW soliton-shaped (hyperbolic secant) pulse.

Using the results of Equation 3.19, it can be shown that the expected output waveform after phase modulation of 24.19rads/ns is the input pulse shifted over to the right 1.63ps. The OAWG outputs corresponding to the ideal and nonideal modulation cases are shown in Figures 4.24 and 4.25. As a result of a combination of temporal pixellation effects and limitations to the voltage levels, the nonideal phase modulation causes energy from the ideal shifted pulse to be transferred to temporal sidelobes. When looking at Figure 4.22, in the case of the 8.7GHz modulation, the modulation is so slow that the modulating waveform appears to have significant spectral content at around half its frequency (4.35GHz). This explains the shifted pulse at about 2ps, which is close to

the expected shifted pulse at 4.35GHz of 1.84ps. At a modulation frequency of 17.4GHz, the deviation from the ideal case is much less pronounced but still observable. In Figure 4.25, the effect of risetime seems to transfer a little bit of energy from the expected time-shifted pulse to a train of pulses separated by the time shift of 1.63ps. Figures 4.24 and 4.25 show the importance of the risetime, the modulation bandwidth and amplitude leveling, and the R parameter on the modulation capabilities of an EO modulator and pulse shaping quality of this OAWG system.

Simulation using phase modulation for third-order dispersion compensation

A method that could be used in improving the TBWP and potential pulse shaping complexity of our system is to perform cubic phase compensation and phase modulation in the middle of pulse dispersion and compression. This was mentioned before and an illustration of a possible implementation can be seen in Figure 3.4. If a fiber similar to TrueWave RS SMF fiber, which has a very low β_2 and high β_3/β_2, is used, then this implementation can be realized with reasonable lengths of fiber. So, a simulation was run to show the possible improvement that this technique could have. Again, a 100mW 200fs soliton was the input pulse. In the case where the OAWG system had no 3OD or higher-order dispersion, the soliton was propagated through 440m of a DCF fiber (β_2 = 152.9479 ps^2/km, β_3 = 0 ps^3/km, β_4 = 0 ps^4/km, α = 0.4286dB/km, γ = 5.212W^{-1}/km). Otherwise, the DCF fiber had β_3 = -0.9533 ps^3/km and β_4 = 2.515e-3 ps^4/km. The dispersed soliton outputs after the DCF fiber without 3OD and with 3OD are shown in the top half of Figure 4.26.

After propagating through a DCF fiber, an ideal phase modulating waveform (zero risetime and constant V_π) was applied over the center of the dispersed soliton. The ideal modulating waveform is shown in the bottom half of Figure 4.26 and was an 86.96Gb/s binary digital waveform (0 or $V_{\pi 0}$) of 200 time pixels (2300ps in total

duration). A voltage of $V_{\pi 0}$ (equal to 6.6V) was applied on the odd time pixels of the dispersed pulse, while no voltage was applied on the even time pixels of the dispersed pulse. After modulation, the pulse was propagated through 2.998km of an SMF fiber (β_2 = -21.6321ps^2/km, β_3 = 0.1284 ps^3/km, β_4 = -3.6068e-4 ps^4/km, α = 0.22dB/km, γ = 1.313W^{-1}/km), and 427 of a second SMF fiber (β_2 = -5.7355 ps^2/km, β_3 = 0.0809 ps^3/km, β_4 = -2.4286e-4 ps^4/km, α = 0.22dB/km, γ = 2.445W^{-1}/km) in the case where the OAWG system had 3OD. In the case where the OAWG system was assumed to have no higher 3OD, the third- and fourth- order dispersion coefficients of each SMF fiber were set to zero. The second SMF fiber was modeled off of TrueWave RS SMF fiber, whose 2OD and 3OD characteristics make it a possible choice for compensating the 3OD in a DCF and maintaining a good amount of 2OD.

The OAWG system outputs for the cases where the fibers had nonzero 3OD and neglected 3OD are shown in Figures 4.28 and 4.29. In Figure 4.28, only the OAWG output for the case where the fibers had nonzero 3OD is shown. The broadening of satellite pulse further away from the center of the time window is slightly observable. A plot showing higher temporal resolution is given in Figure 4.29. Figure 4.29 shows the effect of 3OD on the broadening of satellite pulses as opposed to the case where the OAWG system contains fibers without 3OD. This illustrates the degradation of TBWP due to the presence of 3OD. These broadened satellite pulses are also harder to detect due to the decrease in peak power. In order to see the improvement of using phase modulation to do third-order dispersion compensation, the initial soliton was dispersed through 3.111km of SMF (β_2 = -21.6321ps^2/km, β_3 = 0.1284 ps^3/km, β_4 = -3.6068e-4 ps^4/km, α = 0.22dB/km, γ = 1.313W^{-1}/km). This length of this particular SMF provides the same 2OD as 440m of the DCF fiber.

Cubic phase modulation to eliminate the 3OD of the first SMF was provided using the modulation waveforms shown in Figure 4.27. The top half of Figure 4.27 shows the ideal modulation waveform, while the bottom plot shows nonideal modulation

with a 55.65GHz electronic arbitrary waveform generator (can update voltage levels in about 18ps) with 5ps risetime and a $LiNbO_3$ modulator with R = 2. The cubic phase modulation can be determined by considering that fiber 3OD introduces a cubic phase modulation of its own on the frequency components of the initial pulse. By assuming that a frequency component (relative to the center frequency), ω, of the initial pulse is located at a temporal location, $\beta_2 \omega z$, from the center of the pulse, 3OD can be seen as having the effect given in Equation 4.1.

$$\tilde{B}(\varpi) = \tilde{B}_2(\varpi)\exp(\frac{i\beta_3\varpi^3}{6}z) \approx \tilde{B}_2(\varpi)\exp\left(\frac{i\beta_3\left(\frac{t}{\beta_2 z}\right)^3}{6}z\right) = \tilde{B}_2(\varpi)\exp\left(\frac{i\beta_3 t^3}{6\beta_2{}^3 z^2}\right)$$

(4.1)

Here, B(ω) and $B_2(\omega)$ are the spectra of the dispersed pulse and the dispersed pulse neglecting 3OD effects, respectively, and z is the length of the initial SMF fiber with 2OD and 3OD parameters, β_2 and β_3. In (4.1), t is the retarded time in the reference frame of the dispersed pulse. Using a cubic modulation that offsets the exponential term in (4.1) will approximately negate the effect of the 3OD in the first fiber.

After applying this cubic phase modulation, the ideally modulated signal was modulated by the ideal modulating waveform shown in Figure 4.26, and the signal that underwent nonideal cubic phase modulation was modulated by the nonideal modulating waveform also shown in Figure 4.26. After the second modulation, the signals were sent through 788.4m of the DCF fiber (β_2 = 152.9479 ps^2/km, β_3 = -0.9533 ps^3/km, β_4 = 2.515e-3 ps^4/km, α = 0.4286dB/km, γ = 5.212W^{-1}/km) and 9.29km of the second SMF fiber based on TrueWave RS SMF. The OAWG output due to ideal modulation is shown in Figures 4.29-4.31, while the OAWG output due nonideal modulation is shown in

Figures 4.30 and 4.31. In Figure 4.29, the improvement in the shaped output by using cubic phase modulation for 3OD compensation is definitely observed. There is no observable broadening in the output satellite pulses, and the only difference between it and the ideal situation with 3OD completely absent is the attenuation of the satellite pulses. Almost all of this attenuation is caused by the loss of going through the extra length of the second SMF fiber. Over such a length of fiber, fiber loss becomes increasingly apparent. The deviations seen between the nonideal and the ideal modulation cases in Figures 4.30 and 4.31 can be attributed largely to the effect of the risetime on the phase modulating waveform seen in Figure 4.26.

The risetime and hence the modulation bandwidth causes increasing attenuation in the output satellite pulses located farther from the center of the time window. Also, it takes away energy from the expected satellite pulses to form an undesired pulse train. One of the pulses from this pulse train can be clearly seen in the rightmost figure in Figure 4.31. This unwanted pulse at $t = 0$ has one-third of the peak power of the output waveform. This shows that clearly the modulation bandwidth and risetime can pose some problems in trying to generate an arbitrary waveform. Also, in terms of being able to use this cubic phase modulation technique to improve the TBWP, the main problems are the significant increase in fiber length, which in itself is creates a size issue but also may result in 4OD being a problem, and the increased fiber loss due to longer lengths of fiber. If these problems can be addressed, an OAWG system using commercial fibers can realize large TBWPs and pulse complexities in a highly reconfigurable environment.

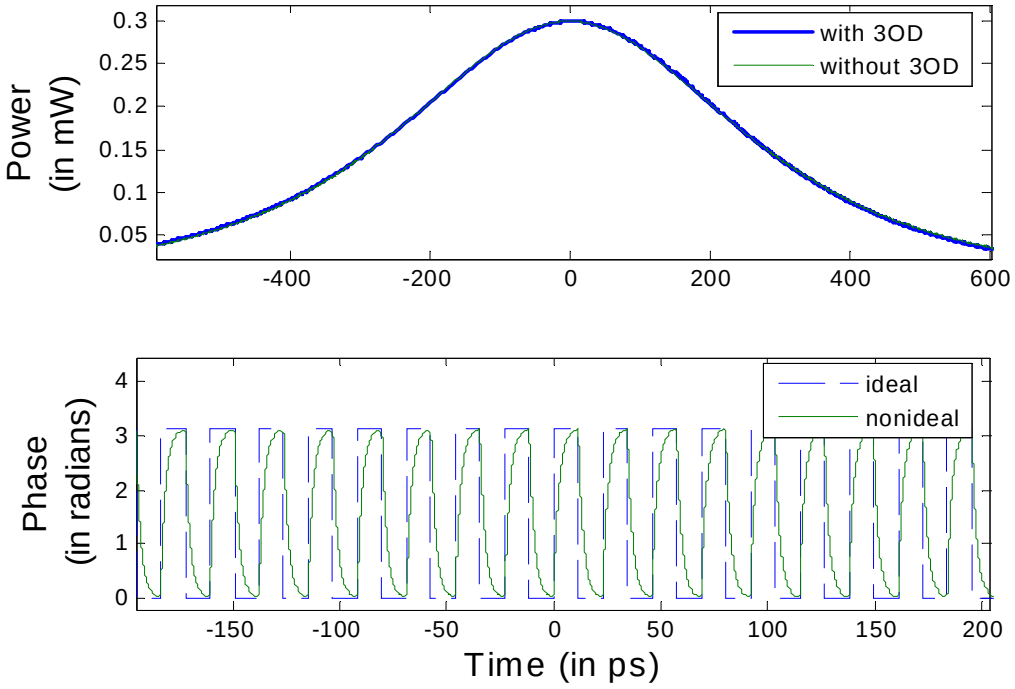

Figure 4.26: Top plot shows the very similar intensity profiles of a dispersed soliton through a dispersive fiber with 3OD and without 3OD. The bottom plot compares the phase modulating waveform of ideal modulation and that of nonideal modulation of 5ps risetime and R = 2.

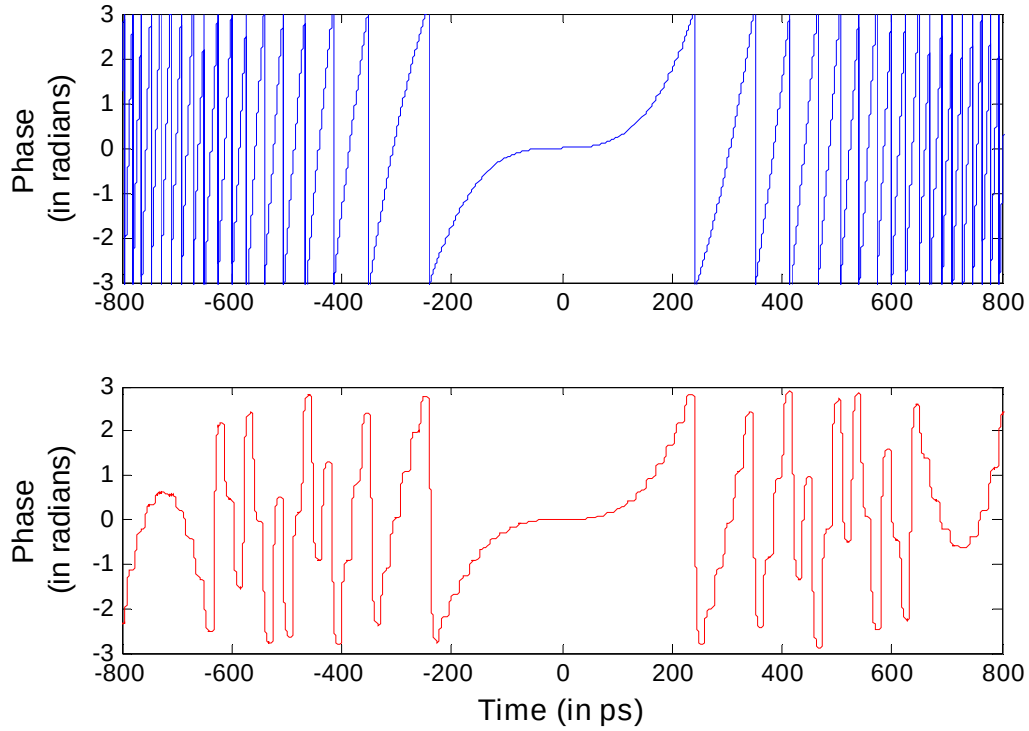

Figure 4.27: Phase modulating waveforms for 3OD compensation. Top plot shows the ideal modulating waveform. Bottom plot shows the modulating waveform generated by a voltage waveform limited to 55.65GHz, 5ps risetime, and a $LiNbO_3$ modulator with R = 2.

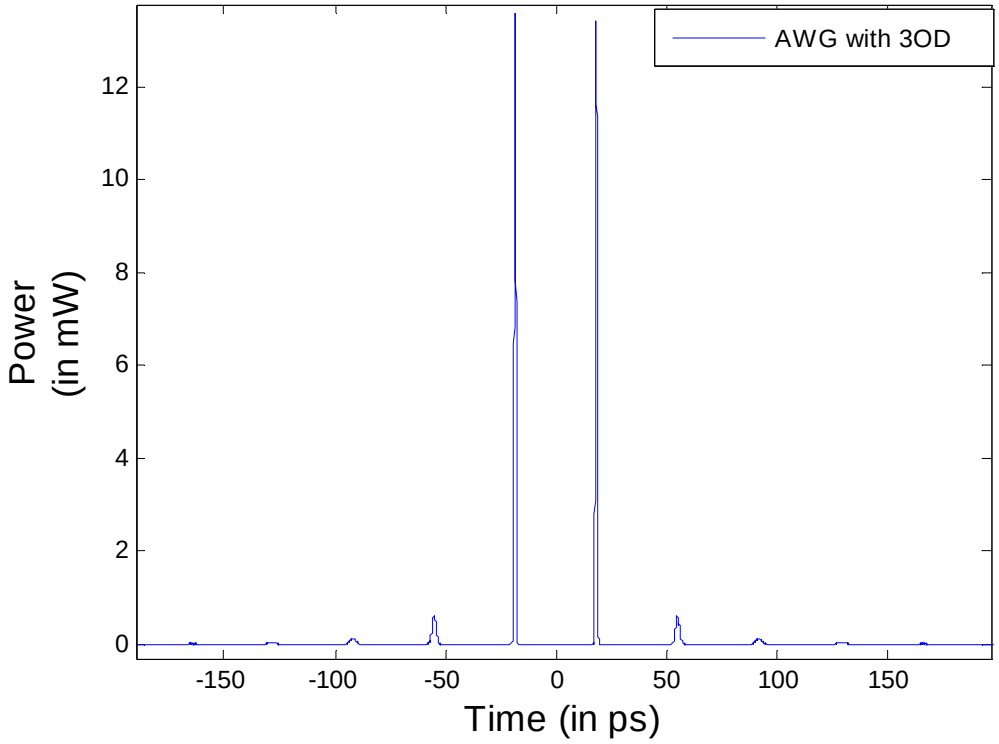

Figure 4.28: Shaped waveform after propagating through OAWG system with higher-order dispersion

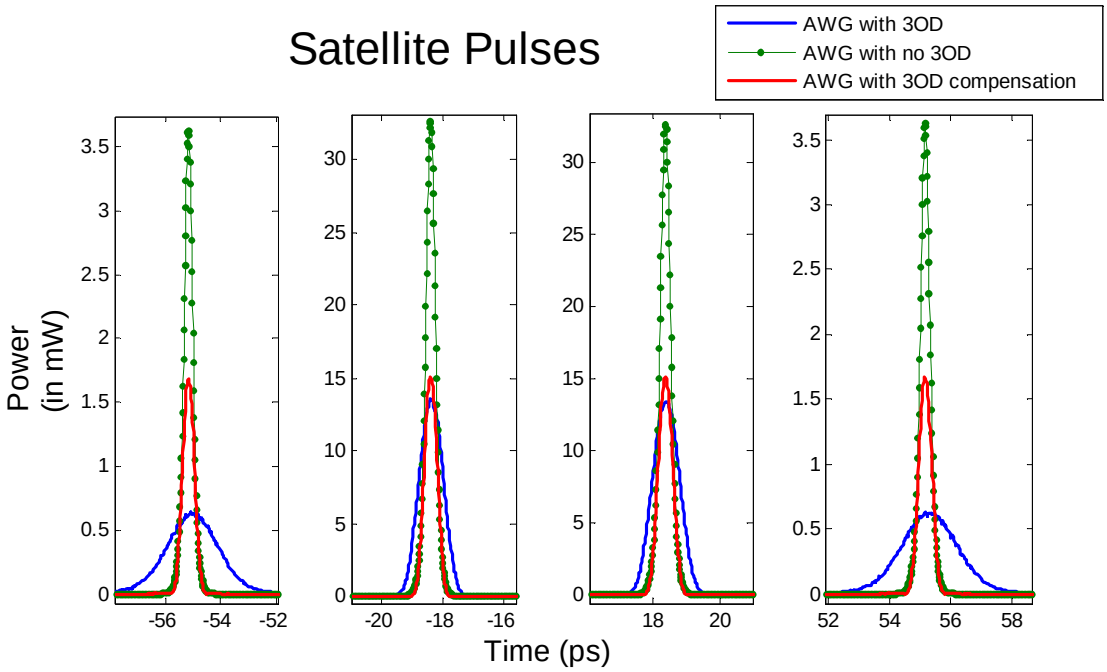

Figure 4.29: Shaped waveforms of OAWG systems with higher-order dispersion, without higher-order dispersion, and with phase-modulated 3OD compensation.

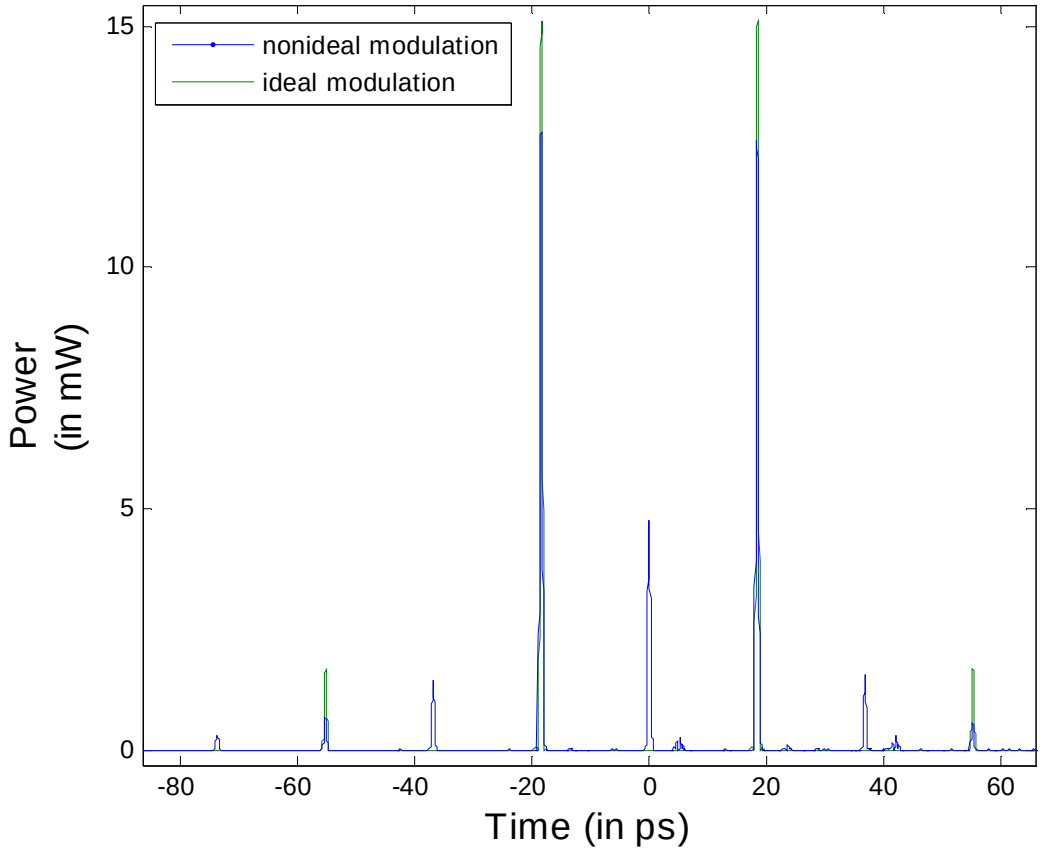

Figure 4.30: Outputs from OAWG system using phase-modulated 3OD compensation with ideal modulation and nonideal modulation.

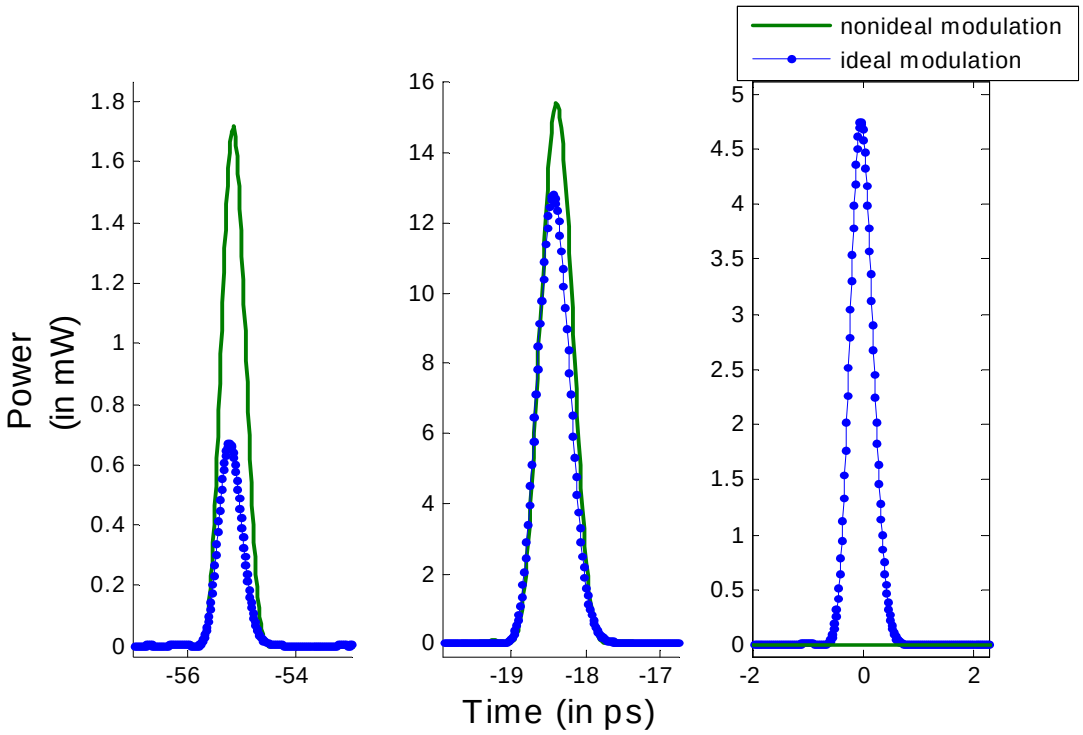

Figure 4.31: Zoomed-in plot of outputs from OAWG system using phase-modulated 3OD compensation with ideal modulation and nonideal modulation.

Summary

In this chapter, results were displayed from the Matlab code that was developed for fiber propagation and OAWG system modeling. The code was useful in studying the various components of the OAWG system such as the optical fiber and the modulator and how the characteristics of each of these components can affect pulse shaping. The simulations discussed above give a good idea of the potential limitations and pulse shaping capabilities of our OAWG system in a real-world setting. The significance of 3OD and higher-order dispersion of the fiber, the power switching ratio (and as a result γ_m) and R parameter of the modulator, the modulation bandwidth and risetime, and the quantization and temporal pixellation of to the EO modulator RF driver can be seen from

the simulations in this chapter. All of these phenomena can have a great impact on the ability to truly generate an arbitrary waveform when considering things such as temporal resolution, potential shaping complexity and TBWP, and pulse shaping fidelity.

Finally, schemes to improve the TBWP of our pulse shaping system were studied. First, the use of a three-fiber system can improve pulse shaping quality and temporal resolution when arbitrary commercial SMF and DCF fibers are used in the pulse shaper. Lastly, 3OD compensation using EO phase modulation in our pulse shaper was also examined. This could potentially improve the TBWP of our OAWG system at the cost of increasing the physical size of the system and having to deal with significant 4OD.

CHAPTER 5

EXPERIMENTAL RESULTS

Introduction

In order to test our OAWG pulse shaping system and demonstrate an initial OAWG system, the setup shown in Figure 5.1 was designed. The use of the EDFAs (erbium-doped fiber amplifier) in the design is to ensure the output waveform can be measured. The placement of the EDFA after the DCF ensures that high peak powers and nonlinear amplification and SPM effects are avoided since the EDFA would be amplifying a broad and dispersed pulse instead of a narrow pulse of high peak power. The $LiNbO_3$ modulator could either be an amplitude modulator or a phase modulator. The DCF fiber is of course used to perform pulse stretching and dispersion. The DCF was chosen as the pulse shaper as opposed to an SMF fiber because of its ability to benefit from any present SPM nonlinearity due to high optical power. If SMF was used as a pulse stretcher with a high power pulse, then the pulse would not disperse as much since the chromatic dispersion and SPM nonlinearity would be working against each other. Pulse compression would be performed by two commercial SMF fibers to perform 2OD and 3OD compensation.

In looking at the modulation, a 10Gb/s or 40Gb/s binary pattern generator can be used to drive the EO modulator as an initial demonstration of the OAWG system. For more robust arbitrary waveform generation in the future, a high-speed electronic arbitrary waveform generator could be used to provide more complex modulation and hence more complicated output waveforms. In order to synchronize the pattern generator with the incoming optical pulses, a phase-locked loop (PLL) with a local voltage-controlled

oscillator (VCO) would be needed to generate a trigger signal for the pattern generator. So, a photodetector converts a split copy of the amplified dispersed optical signal into an electrical signal. A PLL circuit combined with a VCO generates a trigger signal for the pattern generator that is locked to this electrical signal, which has the same frequency as the laser repetition rate. This allows for the pattern generator to provide an electrical signal pattern synchronized to the sequence of pulses propagating through the $LiNbO_3$ crystal. Although the entire system has not been built yet, preliminary experiments are presented in this chapter testing some of the components shown in Figure 5.1.

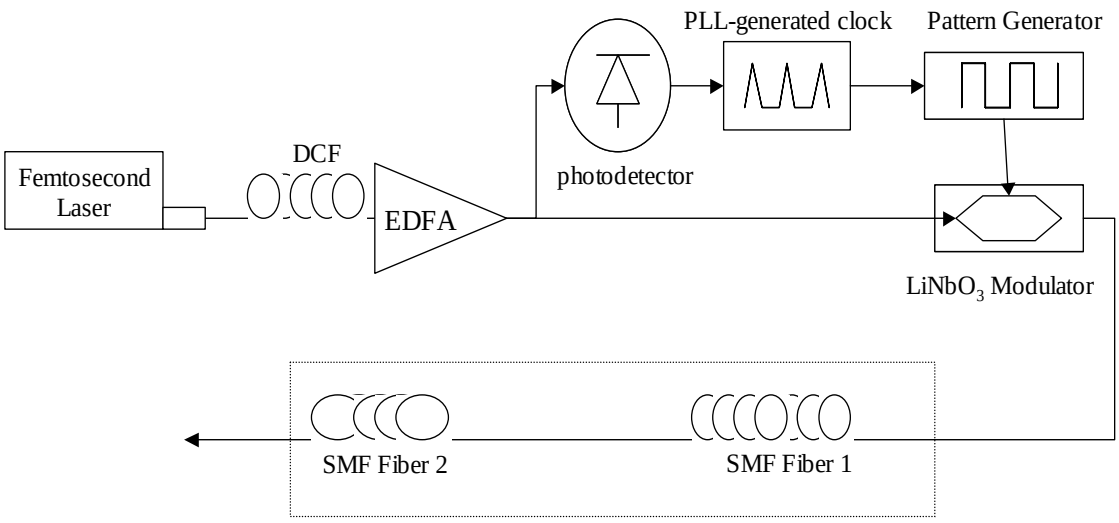

Figure 5.1: Setup for demonstrating an OAWG system with commercial silica fibers.

Phase-locked loop

To provide the desired optical modulation using a pattern generator as a modulator driver, the pattern generator must be able to provide the desired pattern or

electrical signal to the EO modulator simultaneously with the arrival of a dispersed optical pulse. It was assumed that a 10MHz signal locked to the repetition rate of the femtosecond laser was needed to trigger the pattern generator. The pattern generator would then generate a 10Gb/s or 40Gb/s pattern locked to the 10MHz signal. Since the repetition rate of the laser was assumed to be 49MHz, a phase-locked loop (PLL) circuit was designed to generate a 10MHz signal from a VCO locked to 49MHz.

For the PLL and VCO in our system, an Analog Devices AD9511 clock distribution IC evaluation board was used in conjunction with a Universal Microwave Corporation UMJ-559-D14 VCO. A schematic for a general PLL with a VCO is shown in Figure 5.2. The phase frequency detector and charge pump are responsible for generating an error signal dependent on the phase difference between the reference frequency, f_{Ref}, and the VCO frequency divided by N. The loop filter converts this error signal into a voltage that alters the VCO frequency until the error signal is approximately zero. This occurs when the VCO frequency is N times the reference frequency.[28] The frequency of the VCO was limited between 75MHz and 85MHz, so a frequency divider on the AD9511 was used to divide the output VCO frequency by 8 to obtain a 10MHz clock signal. The reference frequency was designed to be 500kHz, meaning that the value for N for the frequency divider in Figure 5.2 could be anywhere between 150 and 170. This required the initial on-chip frequency divider of the AD9511 to divide the initial 49MHz laser repetition rate by about 100 to obtain f_{Ref}, the input into the phase frequency detector.

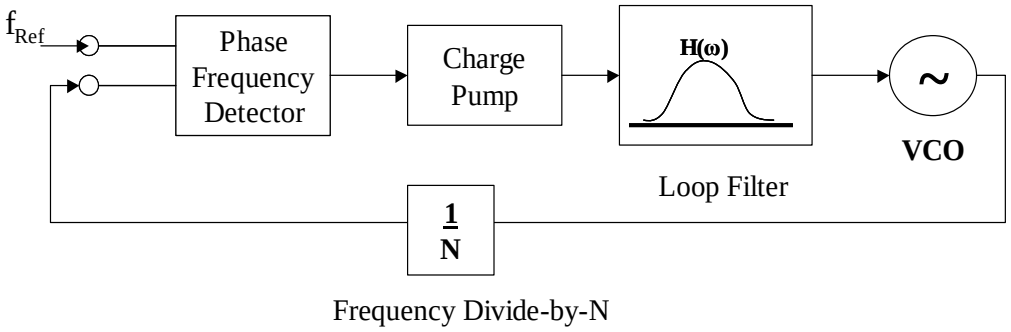

Figure 5.2: General schematic for a divide-by-n phase-locked loop. The phase frequency detector, charge pump, and loop filter are responsible for generating the voltage that alters the frequency of the VCO so that it locks to the reference frequency, f_{Ref}.

The loop filter used for the PLL circuit was designed with the help of Analog Devices ADIsimCLK evaluation software to minimize the timing jitter of the VCO output and the frequency divider (VCO frequency divided by 8) signal when locked to the reference frequency. The loop filter is shown in Figure 5.3. The RMS (root mean-squared) timing jitter was simulated to be at most about 5ps. This amount of timing jitter in the frequency output is acceptable since this is a small enough fraction of the bit period for a 10Gb/s or 40Gb/s pattern.

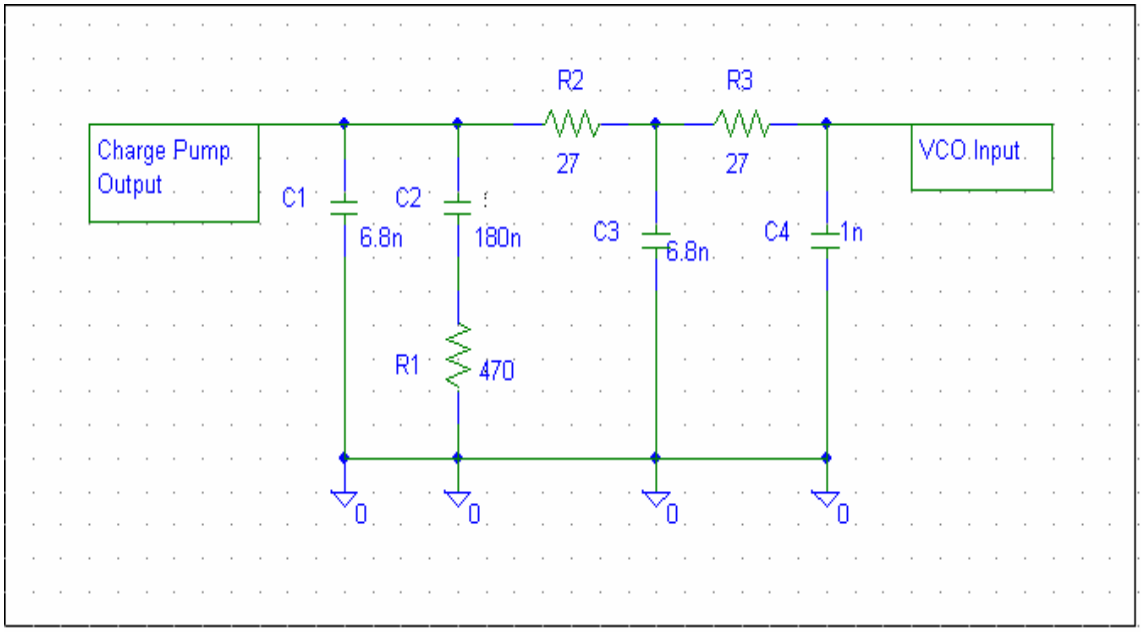

Figure 5.3: Loop filter used for PLL circuit.

PLL Performance

The New Focus IR InGaAs Nanosecond Photodetector output of a pulse train from the IMRA Femtolite 780 femtosecond fiber laser was the input to the AD9511 evaluation board. The onboard input frequency divider was used to divide the frequency of the photodetector output by 98, and the output was provided as the reference frequency of the PLL. The value of N was set to 160 so that the VCO frequency would be 80 MHz. A clock distribution section of the AD9511 chip was used to generate a 10MHz CMOS-level output from the 80MHz VCO frequency. A Tektronix 2440 Digital Oscilloscope was used to observe the photodetector output and the 10MHz CMOS output. The outputs seemed to be phase-locked. Using the status pin of the AD9511, a lock detect signal was monitored to verify that the 10MHz signal was indeed locked to the detected femtosecond pulse train. Unfortunately, the RMS timing jitter could not be measured as

a result of the limited bandwidth of the oscilloscope, but the signals appeared to be synchronized to less than 1ns of each other.

Fiber propagation

The fibers chosen to be used in the OAWG system were EWBDK-DCF fiber, Corning SMF-28 fiber, and TrueWave RS SMF fiber. Due to relatively high β_3/β_2 of the TrueWave RS fiber, 2OD and 3OD compensation should be relatively easy for any length of EWBDK-DCF fiber. In order to compare simulation results and the modeling of the fiber characteristics with experimental results, an IMRA Femtolite 780 femtosecond fiber laser was used to propagate ~200fs 1555.6nm 304.3W peak power (5.95mW average power) soliton-like pulses through about 28.67m of Corning SMF-28 fiber. Figure 5.4 shows a comparison between the FROG (frequency-resolved optical gating) trace of the output using a Newport UPM15-100G Grenouille and a simulation output of the initial pulse (obtained by a FROG trace) after propagating through 28.67m of an SMF fiber (β_2 = -21.6321ps^2/km, β_3 = 0.1284 ps^3/km, β_4 = -3.6068e-4 ps^4/km, α = 0.22dB/km, γ = 1.313W^{-1}/km). The power was normalized so that the peak power for each pulse was one. It can be seen that there is good agreement between the simulation and experiment results.

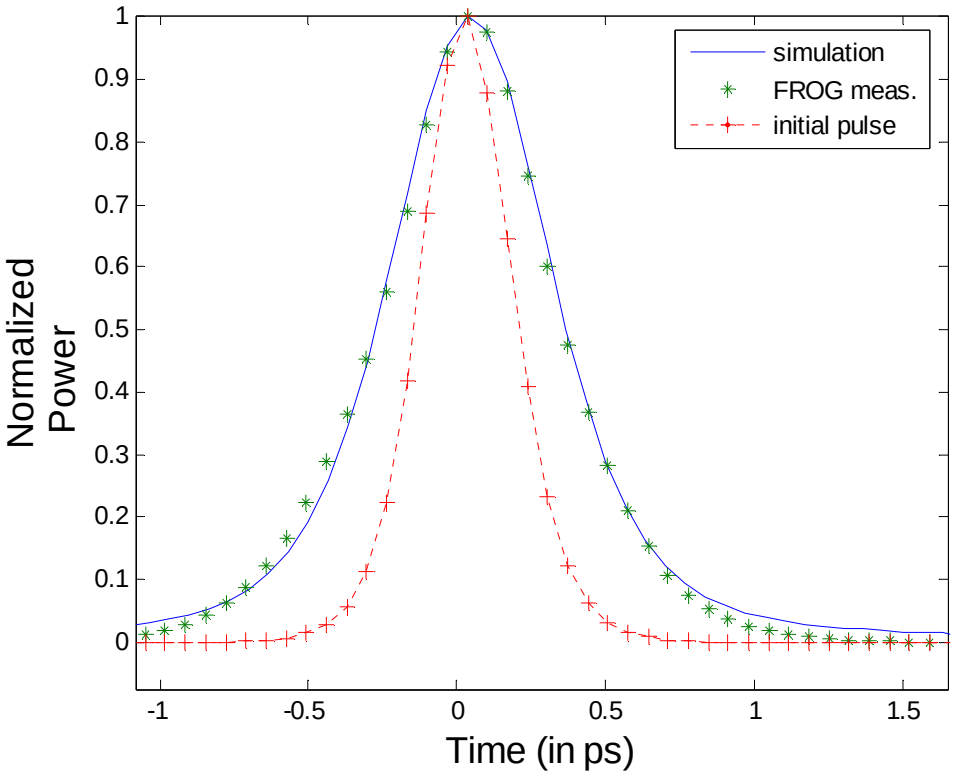

Figure 5.4: Comparison of FROG trace and simulation of initial pulse propagating through 28.67m of SMF fiber.

In order to test a miniature version of the pulse stretcher and pulse compressor that would be used in an actual OAWG system, both a 2-fiber and 3-fiber pulse expansion and compression setup was constructed. Figure 5.5 shows the experimental setup. In the 2-fiber setup, 4.3056m of EWBDK DCF and 30.5m of Corning SMF-28 fiber were used. There were two SMF splices on the ends of the DCF that were estimated to have a loss of 2.75dB each. There were two SMF splices in the SMF that were estimated to have a loss of 0.28dB each. The initial signal for this configuration had an estimated peak power of 302.6W. In the 3-fiber setup, 4.3056m of EWBDK DCF, 29.07m of Corning SMF-28 fiber, and 4.33m of TrueWave RS SMF fiber were used. Each fiber had two SMF splices that were estimated to cause 2.7dB loss each for the

DCF, 0.58dB loss each for the TrueWave fiber, and 0.27dB loss each for the Corning SMF-28. The initial signal for this setup had an estimated peak power of 304.3W.

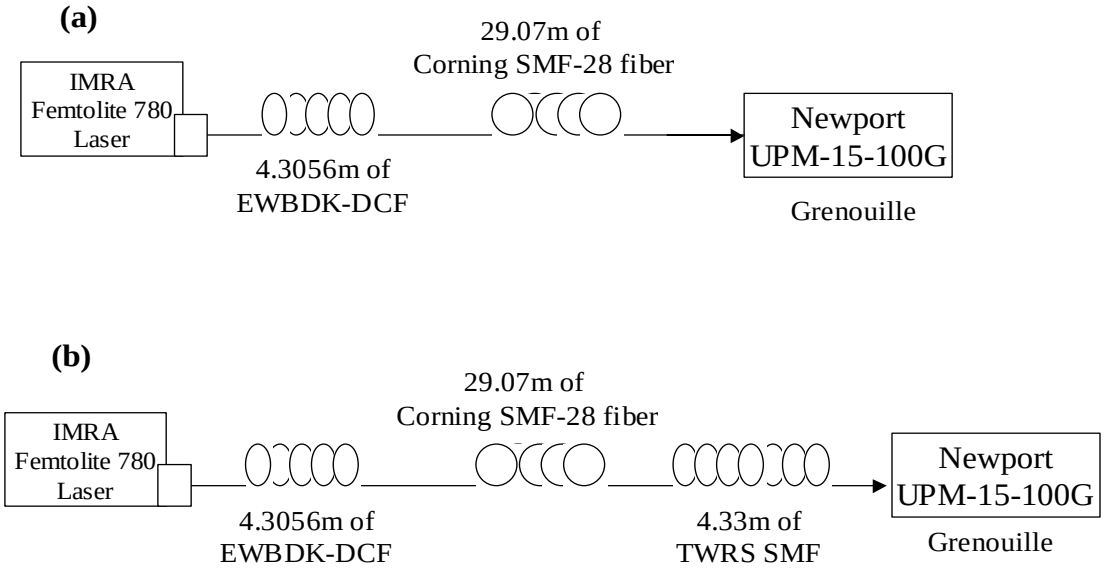

Figure 5.5: (a) Two-fiber setup. (b) Three-fiber setup.

Figures 5.6 and 5.7 show the comparison between the FROG traces and simulation outputs for the two- and three-fiber setups. The fiber characteristics that were used in simulation were β_2 = 152.9479 ps^2/km, β_3 = -0.9533 ps^3/km, β_4 = 2.515e-3 ps^4/km, α = 0.4286dB/km, γ = 5.212W^{-1}/km for the DCF, β_2 = -21.6321ps^2/km, β_3 = 0.1284 ps^3/km, β_4 = -3.6068e-4 ps^4/km, α = 0.22dB/km, γ = 1.313W^{-1}/km for the Corning SMF-28 fiber, and β_2 = -5.7355 ps^2/km, β_3 = 0.0809 ps^3/km, β_4 = -2.4286e-4 ps^4/km, α = 0.22dB/km, γ = 2.445W^{-1}/km for the TrueWave RS SMF fiber. Figure 5.8 compares the initial pulse and outputs from the two- and three-fiber configurations. Figures 5.6 and 5.7 demonstrate that pulse recompression was performed very well and even to less than the

original pulsewidth. This is probably due to SPM effects and the nonzero chirp of the initial pulse. Figure 5.8 shows that there is not too much difference in using the two- and three- fiber dispersion compensation systems. This is because over such a small length, the residual 3OD can be just about negligible, and the ratios of β_2 to β_3 are not too much different in the EWBDK DCF and Corning SMF-28 fibers.

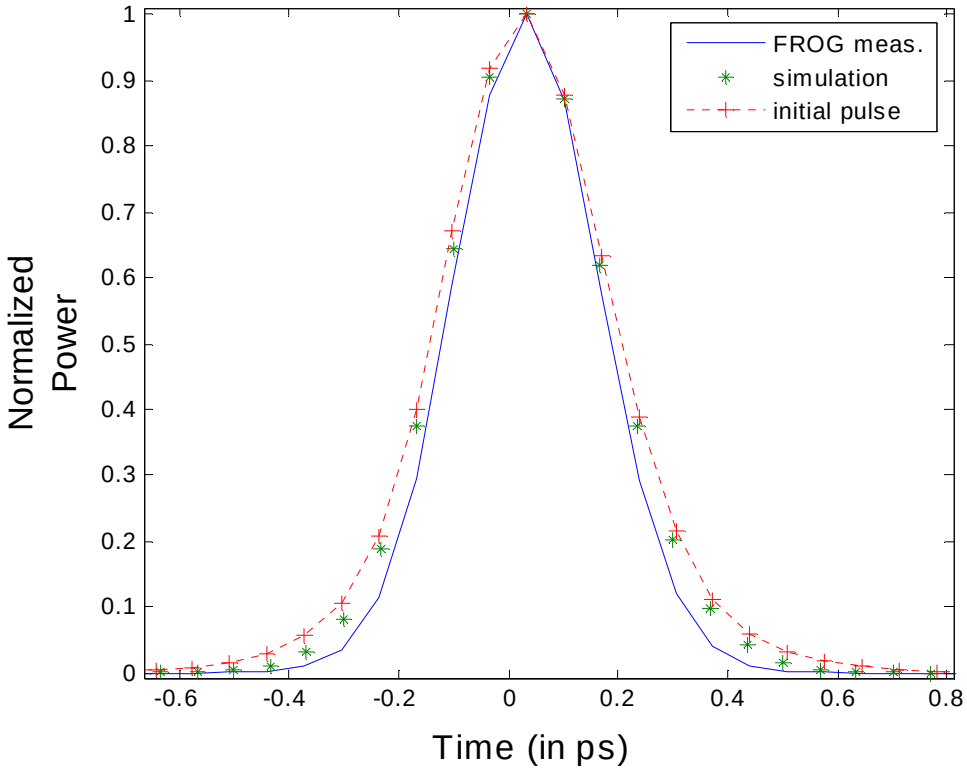

Figure 5.6: Comparison of the simulation and FROG measurement of the output of a two-fiber dispersion compensation system.

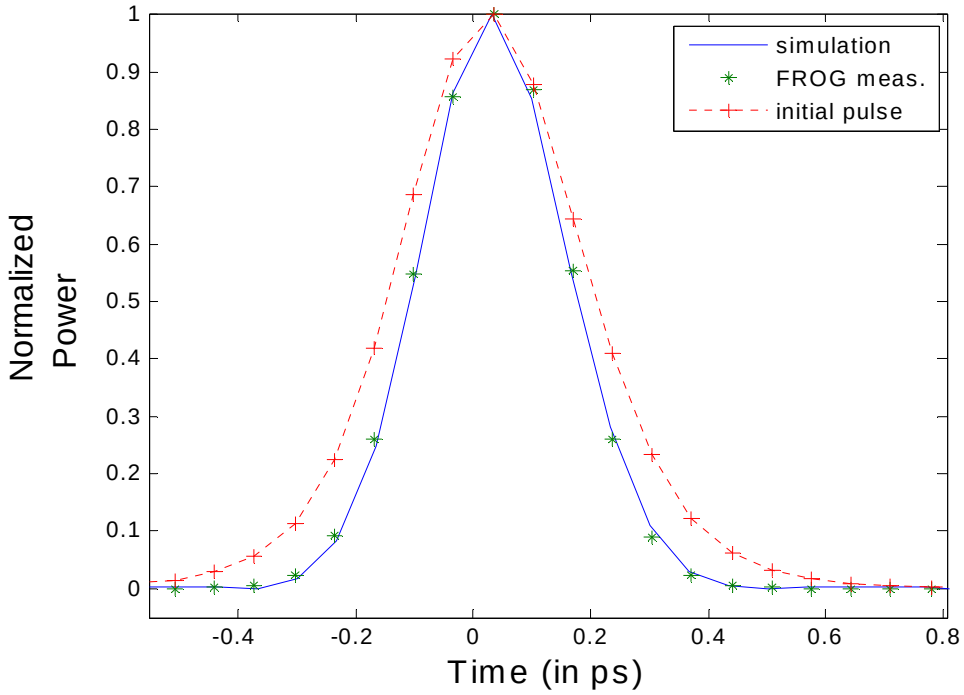

Figure 5.7: Comparison of the simulation and FROG measurement of the output of a three-fiber dispersion compensation system.

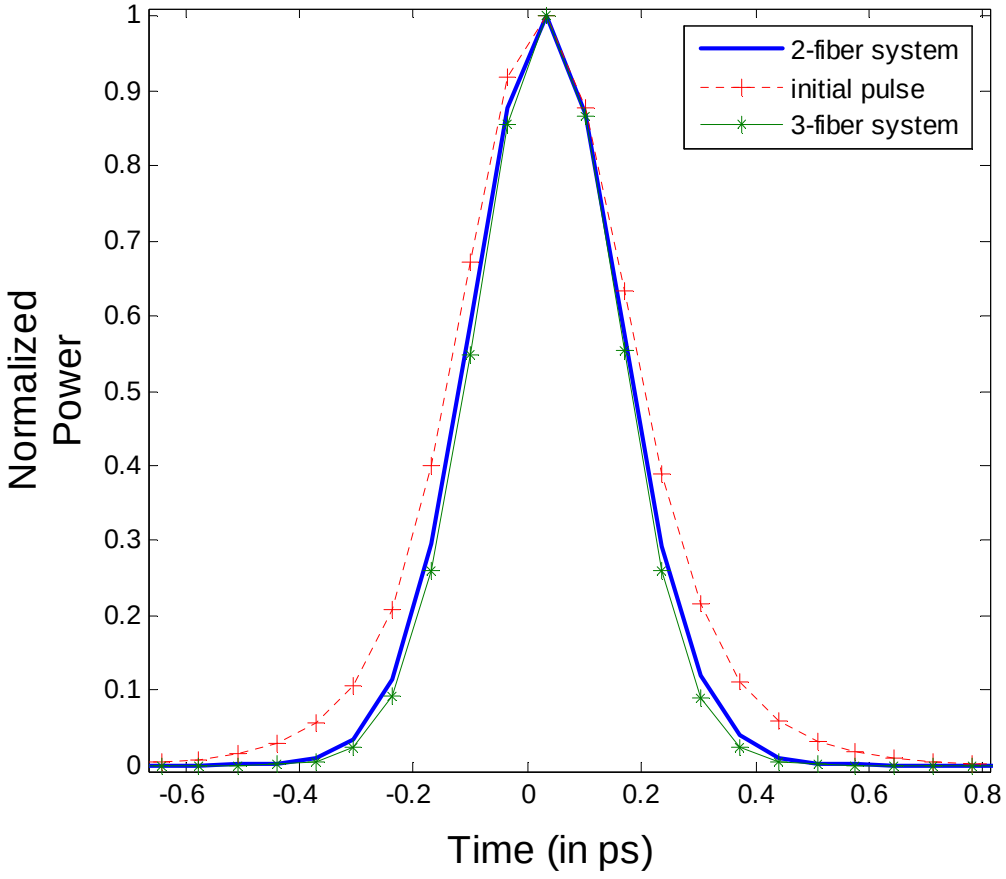

Figure 5.8: Comparison of the FROG traces of the initial signal and the outputs of a two- and three-fiber dispersion compensation system.

CHAPTER 6

APPLICATIONS AND FUTURE WORK

Introduction

Optical arbitrary waveform generation using dispersive silica fibers has now been looked at from a theoretical standpoint and studied in simulation. Although an actual OAWG system is not demonstrated here, the simulation and preliminary experiments provide some initial results that can be looked at to evaluate this OAWG system. In this chapter, possible applications that can benefit from this particular OAWG system are described, and finally, the benefits, disadvantages, and future improvements of this OAWG system are discussed.

Applications

As mentioned before, the presented optical arbitrary waveform generation (OAWG) system has the properties of being fiber-compatible, constructed with commercially available telecommunications components, and capable of high waveform refresh rates. These properties suggest that this method of OAWG would be very useful in optical communications applications, although this OAWG system could be conceivably considered for any pulse shaping application. Some of these applications are described below.

Spectral analysis of microwave signals

The ability to analyze the spectrum of microwave signals with very high spectral resolution can be very beneficial to radar/lidar, imaging, and detection applications.

Using a microwave signal as the input to a modulator for our OAWG system, the output shaped pulse is the approximate spectrum or an indication of the spectrum of the microwave signal. Provided that the TBWP of the OAWG system is large, then this arrangement can resolve very fine spectral features of the microwave signal. This is explained in more detail by Saperstein et al. However, the maximum frequency of the microwave signal that can be used in such a system is limited by the bandwidth of the EO modulator, which is currently less than 100GHz for a very good $LiNbO_3$ modulator. Also, the TBWP for the OAWG system would need to be on the order of 1000 to 10000 to provide excellent spectral resolution for such applications.[29] For our system, this would require very long lengths of fiber due to limited modulation bandwidth and an effective way to negate the effects of higher-order dispersion on the system TBWP. However, if high TBWPs can be achieved, microwave spectral analysis with excellent resolution would be able to be performed in real time at the repetition rate of the optical pulse train.

Optical time-division multiplexing

Considering that sinusoidal amplitude modulation of a broadened pulse can produce a pair of satellite pulses in the shaped output waveform whose time shift is dependent on the modulation frequency, a time-division multiplexing (TDM) or time-division multiple access (TDMA) scheme can be envisioned where users are assigned a time slot that corresponds to a particular sinusoid frequency. If a bit is to be transmitted during a particular time slot, then a sinusoidal signal with the corresponding frequency can be applied to the modulator to generate a satellite pulse during that time slot in the output waveform. This is illustrated in Figure 6.1. As a result, if a variety of frequencies are used that can be coupled into the EO modulator, then the number of frequencies multiplied by the laser repetition rate gives an estimate of the effective data rate of the system. However, the number of usable frequencies depends on the pulse shaping

complexity and TBWP of the system, and the TBWP can be degraded due to the broadening of satellite pulses (a consequence of 3OD) in time slots further deviated from the center time slot. Also, the utilized frequencies must be far enough from each other so that their corresponding satellite pulses can be resolved from each other.

The limitation on the number of frequencies that can be used to generate satellite pulses can also be due to a nonideal modulator switching ratio, the wavelength-dependence of V_π, and the fact that EO amplitude modulation with a sinusoid of significant power can generate additional unwanted satellite pulses as a result of the nature of EO amplitude modulation. These factors have increasingly detrimental effects in this scheme if more sinusoids are used because these sinusoids can produce additional energy into other time slots. The modulation bandwidth also places a limit on the maximum frequency that can be used for a sinusoid. The maximum temporal window or the pulsewidth of the broadened optical pulse before the modulator places a limit on the minimum frequency that can be used. Finally, in order to keep the total applied voltage to the EO modulator to within reasonable levels, either the voltage levels for each sinusoid need or the number of sinusoids needs to be kept reasonably small. Using sinusoids with lower power means that the satellite pulses would have lower power, and this can have a significant effect on the ability to detect the desired signal.

In a multiple access environment, access to a particular slot can be achieved conventionally by the use of an appropriately delayed clock. A TDMA scheme allows for flexibility in increasing the TBWP of the system because users with time slots farther away from the center time slot can use additional fiber to counteract the broadening of the satellite pulse in receiving the data if its time slot is fixed. A similar scheme is described by Saperstein et al. as a solution to the broadening of satellite pulses.[12] In a situation where the TDM signal is to be propagated over a long length of fiber, then decoding the received signal for a particular user can be as simple as providing the correct bandpass filter without the need for dispersion compensation. This is because

propagation over a long length of fiber (provided that it has the same polarity of 2OD as the original pulse stretcher) would perform an approximate Fourier transform of the TDM signal, and the output would be broadened pulses containing frequency components depending on the sinusoidal signals modulated onto the original optical spectrum. Such a simple TDM configuration can have the potential of providing a large number of users access to data over a common medium at a relatively high data rate.

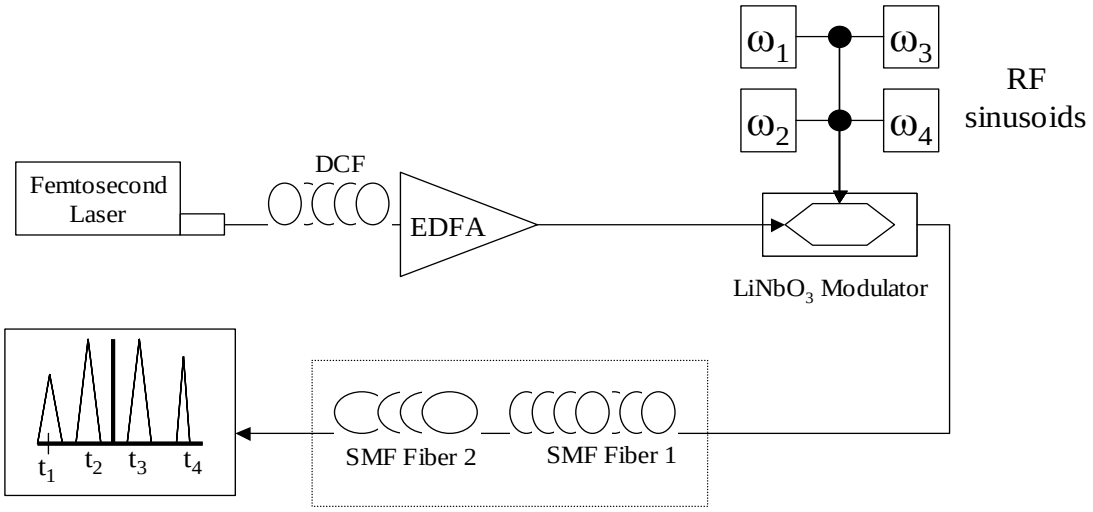

Figure 6.1: Illustration of optical TDM using fiber OAWG system. The time delay, t_i, corresponds to the i^{th} RF sinusoid.

Wavelength-division multiplexing

Since Fourier-based pulse shaping techniques rely on spectral modulation, it is natural to consider these types of pulse shapers as a form of a WDM (wavelength-division multiplexing) filter. So a number of pulse shaper configurations have been looked at to determine their capabilities for WDM. WDM allows for multiple signals to

share a common medium since each signal has a different wavelength, and access to a particular signal requires the appropriate wavelength filter or a device that selects its specific wavelength. Most currently used WDM systems use multiple sources and modulators to provide data signals of different wavelengths. A cost-effective way to perform WDM is to use a femtosecond laser with a broad spectrum and directly modulate the spectrum serially with a single modulator using TDSS. This is referred to as chirped pulse WDM (CPWDM).[11] An illustration of the operation of CPWDM is shown in Figure 6.2. This has been studied with the use of chirped FBGs as well as with a dispersive SMF fiber.[30]

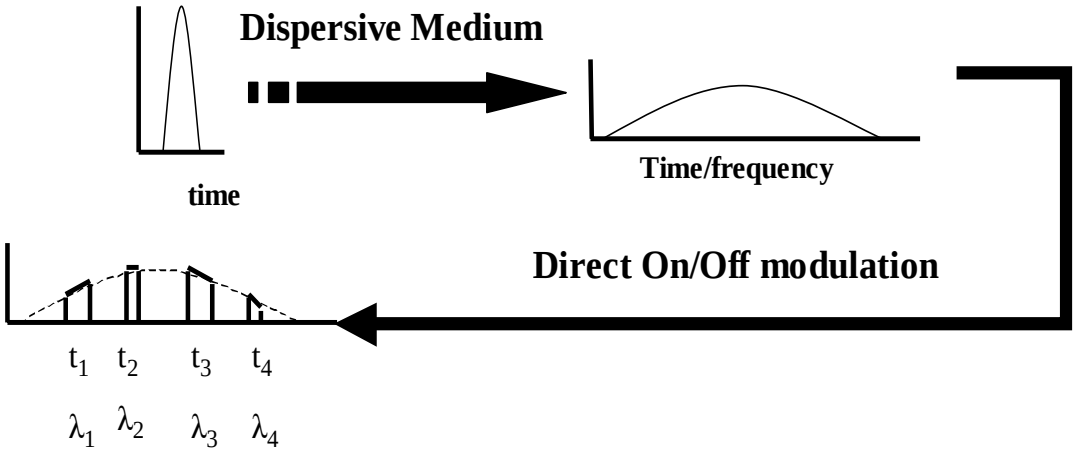

Figure 6.2: Schematic of CPWDM showing on/off temporal modulation on a dispersed chirped pulse is equivalent to wavelength demultiplexing.

In a paper presented by Boivin et al., a dispersive SMF fiber was used to disperse an initial 100fs optical signal to ~20.7ns pulsewidth, and a pattern generator was used to drive an electro-absorption modulator with a 9.94Gb/s binary pattern to modulate the dispersed optical pulse. This binary modulation effectively separated the initial pulse

spectrum into 206 channels and modulated different parts of the spectrum with bits at the data rate equal to the repetition rate of the femtosecond laser, which was 36.7MHz. Essentially, the binary pattern for a given optical pulse determined the wavelengths that received a one-bit (or were passed) and those that received a zero-bit. This demonstrated the capability of using fiber dispersion and serial modulation to provide optical signals at different wavelengths with the use of only one source and one modulator. A passive wavelength splitter could be used to separate the different optical signals. This same idea could be applied to use WDM in our system, the only difference being that our system would use an EO modulator and recompress the spectrally modulated signal using a medium with the opposite dispersion. Wavelength selection could then be performed using a WDM filter or wavelength splitter or even possibly another fiber pulse shaper. In using another OAWG system as a WDM filter, binary amplitude modulation that attenuates all but a small duration of the dispersed optical signal can be used as a narrowband filter of a WDM system.

A disadvantage of using this system as a WDM source or filter is that amplitude modulation is required and can reduce the measured power of the output. This is not too much of a problem since a good amount power is not needed to detect the signal for a particular wavelength, and an EDFA can be used to amplify the chirped pulse, which can reduce amplified noise and the possibility of nonlinear effects. The main disadvantage of this technique is that since a long length of fiber is used for significant dispersion, temperature variations can slightly alter the dispersion characteristics but noticeably affect the total fiber dispersion. The temporal location of the dispersed wavelengths can change as a result, and a particular set of bits that were designed for a particular wavelength would instead correspond to and send bits to the incorrect wavelength. Also, the number of wavelength channels depends on the length of the dispersive fiber.

Code-division multiple access

Optical Code Division Multiple Access (CDMA) has been studied extensively since the development of Fourier-based pulse shaping techniques. This can be useful for short distance and local area network applications. CDMA is another optical communications scheme that can allow multiple users to communicate with each other over a common medium with minimal interference. In optical CDMA, spectral phase coding is used to shape the initial high peak-powered pulse into a low-powered pseudonoise burst. This signal can then be transmitted to a CDMA receiver that uses a pulse shaper arrangement to perform spectral phase coding again. If the spectral phase code used by the CDMA receiver is the conjugate of that used by the transmitter, then the output signal of the pulse shaper is the initial high peak-powered pulse since spectral phase modulation is approximately lossless. However, if the spectral code is significantly different from this conjugate phase code, then a pseudonoise burst is received.

If multiple CDMA receivers and transmitters are used over a fiber-optic medium, then minimally interfering codes can be assigned to each receiver and transmitter so that a particular transmitter can communicate with a particular receiver over the shared medium if it shares the same code without being significantly affected by other transmitted signals. The other transmitted signals will appear to be pseudonoise bursts.[5] Then by using a nonlinear thresholder, a receiver can discriminate between a high peak-powered pulse from its matched transmitter and pseudonoise bursts from other transmitters.

Periodic repetitions of maximal length sequences[13] or Hadamard-Walsh codes[32] are examples of methods to obtain minimally interfering spectral codes for a CDMA system. Various optical CDMA testbeds[31], [32] have been constructed using the diffraction grating-based pulse shaper that have demonstrated the ability to use CDMA in a single user and multi-user environment to increase overall data transmission. Our fiber OAWG system could also be used for CDMA, where the modulator can perform the spectral coding and decoding. A possible implementation is given in Figure 6.3. Since

the broadening of satellite pulses does not affect the ability of a CDMA receiver to decode a transmitted encoded signal correctly, the potential length of the spectral code is dependent only on the total 2OD of the fiber media, the modulation bandwidth or speed, and the repetition rate of the laser.

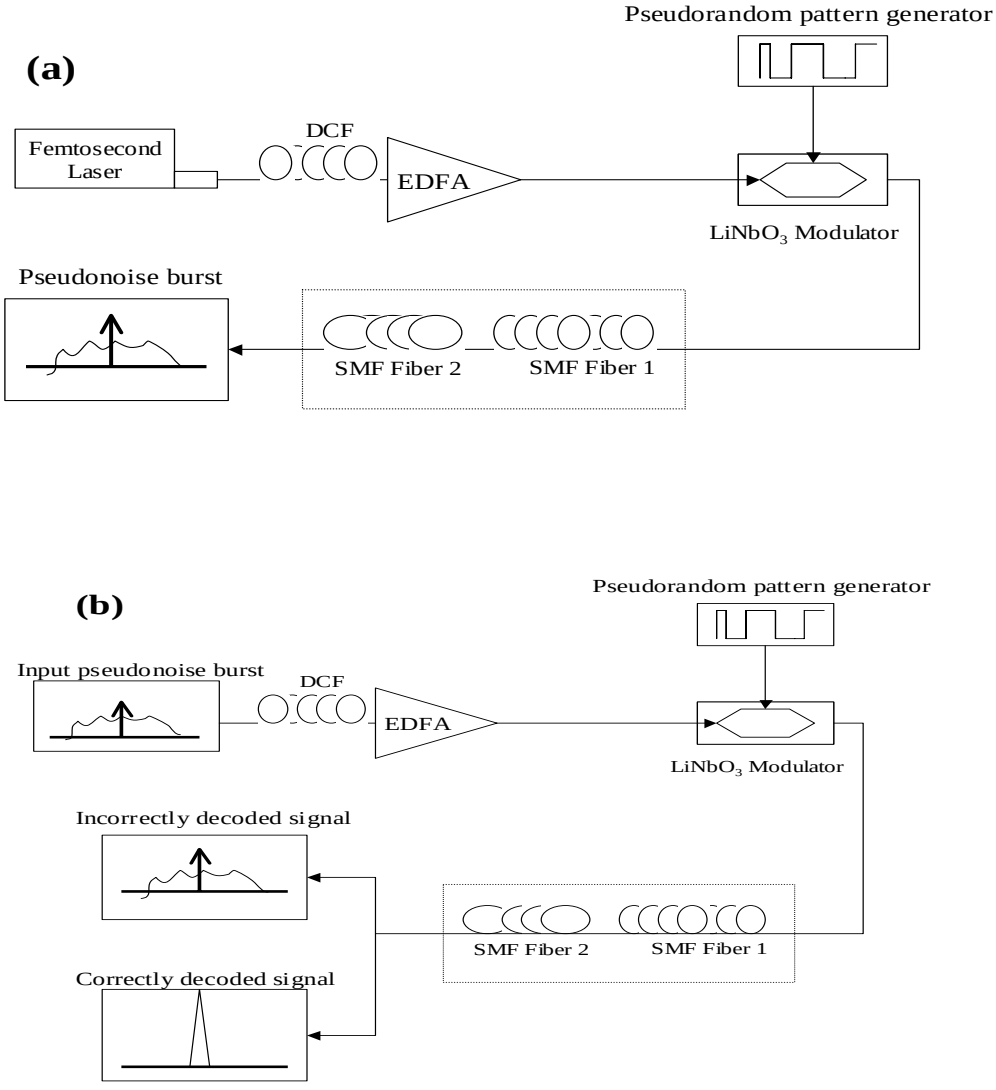

Figure 6.3: (a) Schematic of a CDMA transmitter that generates a pseudonoise burst as an output signal from a femtosecond pulse. (b) Schematic of a CDMA receiver that reproduces the initial femtosecond pulse if a received pseudonoise burst is decoded correctly.

This fact could mean that a pulse shaper employing chromatic dispersion in fibers can potentially achieve very long CDMA codewords with a large minimum distance, provided that the pulse repetition rate is low. If shorter codewords are acceptable for higher pulse repetition rate, then a fiber OAWG has the advantage of being able to refresh the spectral code from pulse to pulse. However, the number of users in this system is limited by the receiver's ability to discriminate between the sum of all low intensity pseudonoise bursts generated by almost all of the users and the sole correctly decoded high intensity pulse. The potential problems of using our OAWG system for CDMA are ensuring that the spectral phase code provided by the electronic pattern generator is locked to the arrival of the dispersed optical pulse at the EO modulator and the dependence of the code length on the fiber length. However, fiber compatibility, the ability to produce long spectral phase codes, and the ability to have a high waveform refresh rate can prove to be useful in implementing our OAWG system in a fiber-optic CDMA system.

Future work

Adaptive pulse shaping

A commonly proposed technique to improve any OAWG system is to employ a computer-controlled closed-loop feedback scheme to perform adaptive pulse shaping and find the optimum parameters to match the output waveform as closely as possible to the target waveform.[5], [15] In quantum and molecular control applications that demand adaptive pulse shaping, a computer algorithm can be used to find the optimum parameters

to yield the desired quantum or molecular reaction instead of trying to determine a particular desired waveform.[10] Adaptive pulse shaping could be used to improve the ability of our pulse shaping technique to perform OAWG in a setting where excellent shaping fidelity is much more important than waveform refresh rate. Feedback control of the electronic waveform driving the EO modulator could be a valuable tool in providing well-shaped waveforms for our OAWG system as well as finding an optimal modulation signal that can overcome the degradation of TBWP due to 3OD effects to generate complicated output waveforms.

Overcoming present limitations

Currently, the limiting factors of our OAWG system demonstrated by simulation and theory are modulation bandwidth, finite on-off ratio, variation in V_π for an EO modulator, higher-order fiber dispersion, and long lengths of fiber needed to provide a large temporal window for modulation and high TBWP. The modulation bandwidth can be improved by the development of faster electronic modulator drivers and by increasing the bandwidth of the EO crystal. Since this has been consistently an active area of research, faster devices will probably be available in the near future. The on-off ratio and modulator V_π are again properties of the EO modulator. Depending on the pulse shaping needed, it would be extremely beneficial to use EO modulators that have on-off ratios and V_π characteristics as close to ideal as possible. As for the limitations due to the dispersive characteristics of fiber including the necessity to use longer lengths of fiber, chirped FBGs is an alternative that can provide high 2OD with very low higher-order dispersion over short fiber lengths. However, these devices are very temperature-sensitive and rely on reflective and polarization effects that can affect the quality of the overall pulse shaping system. Using commercial fibers, specially designed fibers, or FBGs represents a tradeoff between commercial availability and cost and desirable dispersive properties.

Schemes can be implemented to overcome the effect of higher-order dispersion in commercial fibers such as the use of multiple fibers of specified lengths and quadratic, cubic, and quartic phase modulation to perform higher-order dispersion compensation. These schemes may be useful in providing a simple all-fiber OAWG system capable of high TBWP and temporal resolution and compatibility with optical communications systems. However, the disadvantages of these techniques must be realized such as the need for longer lengths of fiber, which can introduce higher loss and make our system more sensitive to higher-orders of dispersion. Depending on the pulse shaping application, some techniques in overcoming the problem of higher-order dispersion are more beneficial than others.

Conclusion

The concept of OAWG using chromatic dispersion in silica fibers was presented, and the pulse shaping capabilities was examined both in theory and in simulation. The possible benefits of using this type of OAWG system is its ability to be constructed with standard telecommunications equipment, a simple modulation scheme, the possibility of increasing TBWP without a significant increase in size as in the case of spatial-domain techniques, compatibility with fiber-optic systems, and the possibility of updating shaped waveforms at a very high rate. This makes this system very attractive to optical communications applications such as WDM, TDM, and CDMA. The disadvantages are the need for synchronization of the spectral modulation with the arrival of the dispersed optical pulse, the dependence on TBWP on the length of fiber, and the limitation on the achievable TBWP due to 3OD effects. The nonideal properties of a $LiNbO_3$ EO modulator can also add other complications to using this technique for OAWG.

With the use of spectral phase modulation and three or more fibers for dispersion compensation, the TBWP can be significantly improved. Nonlinearity and SPM can also have a desirable effect for our system in increasing the number of addressable temporal pixels of the dispersed pulse. Feedback control of the optical modulation can also be future enhancement to our OAWG system. However, even with these modifications, very long lengths of fiber, very fast modulation schemes, or extremely ultrashort pulses would be needed in order to realize excellent TBWPs and pulse shaping complexities. Also, increasing the TBWP in this scheme would place a limit on the maximum waveform refresh rate. In spite of these issues, an OAWG system using standard telecommunications fibers remains to be a promising solution in future high-speed and high-resolution pulse shaping applications.

APPENDIX A

BENCHMARK SIMULATIONS

Dispersion benchmarks

In the benchmarking exercise shown in Figure A.1, the ability of the propagation program code to simulate the dispersion of a 14.14ps (half-width 1/e intensity point) Gaussian pulse over dispersal lengths, L_D, of $2L_D$ and $4L_D$ in the absence of nonlinearity and fiber loss was examined and compared with the analytical result from Equation 3.10. Since the effect of β_3 is usually negligible over these distances, the program code was run with the β_3 (but without β_4) of an SMF fiber (β_2 = -21.6321 ps^2/km; β_3 = 0.1282ps^3/km; β_4 = 0 ps^4/km; λ_0 = 1550 nm). As can be seen in Figure A.1, the dispersed pulse given by the program code matches perfectly that predicted by the analytical formula even with the use of nonzero β_3.

In this simulation shown in Figure A.2, a 14.14ps Gaussian pulse was dispersed over a distance of $5L_D'$ (where $L_D' = T_0^3/\beta_3$) of a specified SMF fiber (β_2 = 0; β_3 = 0.1282 ps^3/km; β_4 = 0 ps^4/km; λ_0 = 1550 nm) in the absence of loss and nonlinearity. For the case of a 14.14ps, this corresponds to a length of 110, 313 km. This plot was compared to a known plot of the same parameters. Although it is not shown here, the simulated output shown in Figure A.2 is in complete agreement with the benchmarked plot shown in Agarwal.[19]

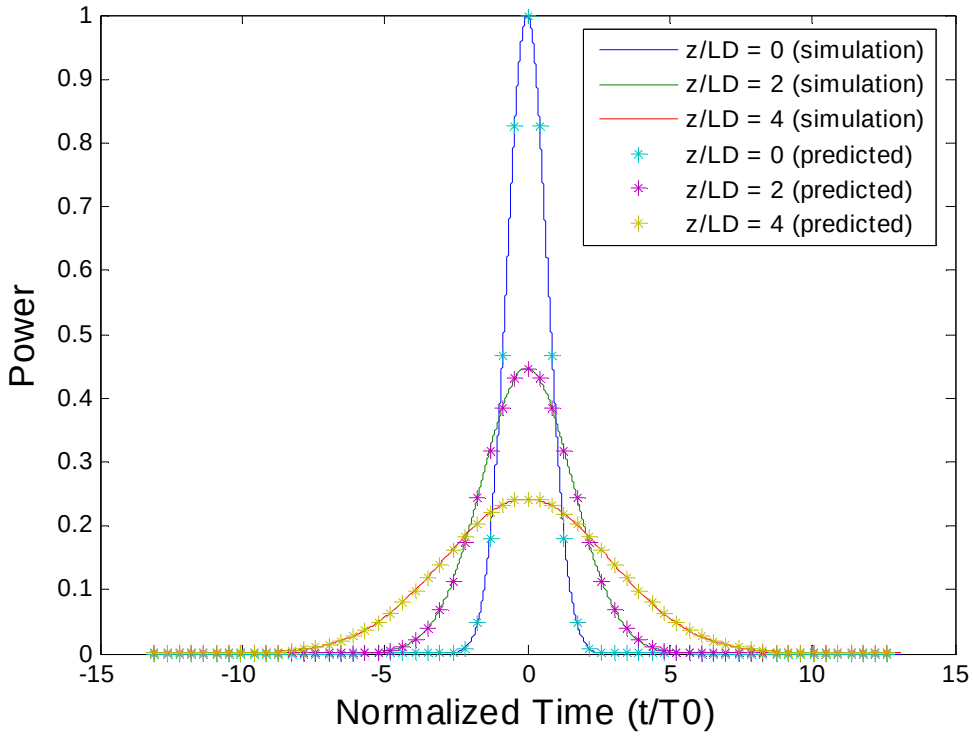

Figure A.1: Simulation showing the dispersion of a 14.14ps Gaussian pulse after propagating various multiples of the second-order dispersal length.

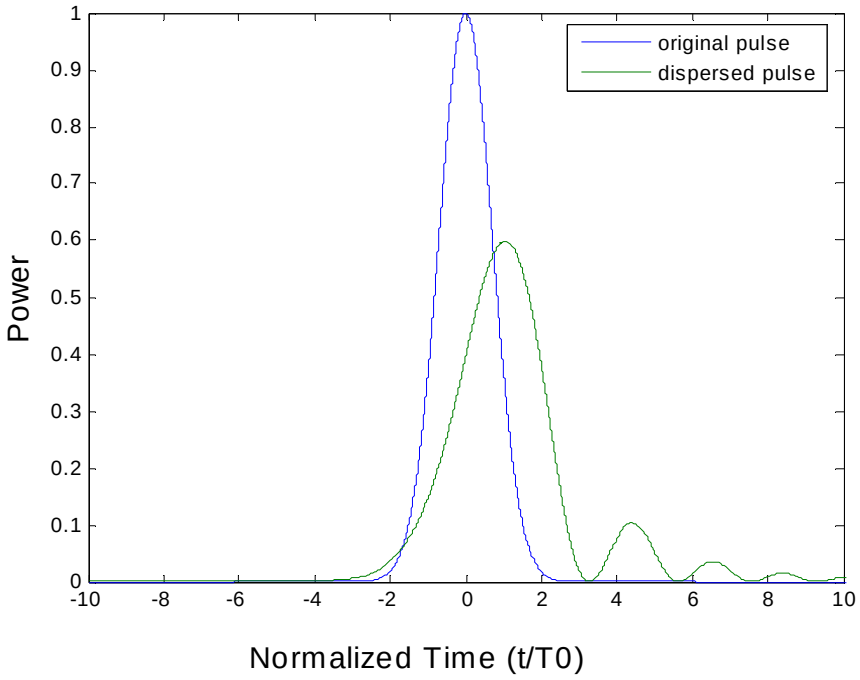

Figure A.2: Simulation showing the dispersion of a 14.14ps Gaussian pulse after propagating five times the third-order dispersal length.

Nonlinearity benchmarks

Figure A.3 shows a comparison of the spectrum obtained by a using the Fourier split-step technique to simulate a 14.14ps 1550nm 1W peak power Gaussian pulse propagating through 10km of a nonlinear optical fiber (α = 0.22dB/km; γ = 2.1018W^{-1}/km, λ_0 = 1550 nm) with no chromatic dispersion. Assuming the delayed nonlinear and Raman response to be negligible (which is usually a very safe assumption), the expected Gaussian pulse spectrum is given by the formulas in Equation A.1 below.[19] In Equation A.1, z is the propagation distance, t is the retarded time propagating through the fiber at the group velocity of the optical signal, and A(z, t) is the slowly-varying complex pulse envelope. Once again, the simulation is in total agreement with the theoretical result.

$$A(z,t) = A(0,t)\exp(-\frac{\alpha z}{2} + i\gamma \mid A(0,t) \mid^2 \frac{(1-\exp(-\alpha z))}{\alpha}) \qquad (A.1)$$
$$A(z,\varpi) = FFT(A(z,t))$$

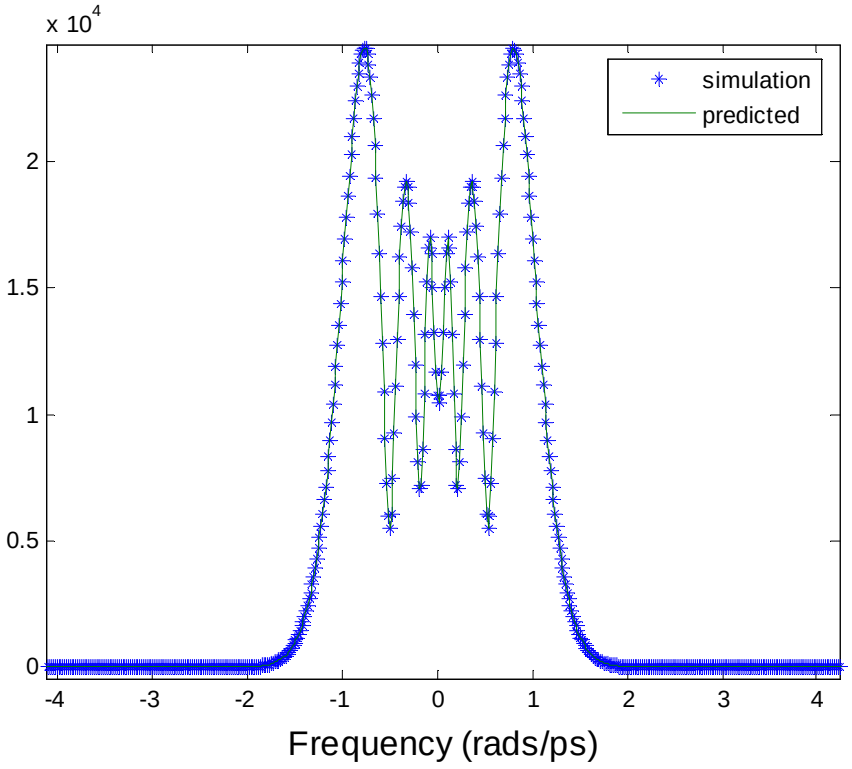

Figure A.3: Frequency spectrum of the output after propagating a 14.14ps 1W Gaussian pulse through 10km of dispersionless nonlinear fiber. The y-axis has arbitrary units.

Figure A.4 shows the agreement between the predicted and simulation maximum phase shifts of a pulse going through a nonlinear non-dispersive SMF fiber (α = 0.22dB/km, γ = 2.1018W^{-1}/km, λ_0 = 1550 nm) using the split-step Fourier technique. The pulse that was used was a 1W peak power 14.14ps Gaussian pulse. Equation A.2 gives

the predicted maximum phase shift. In Equation A.2, P_0 is the peak power of the pulse, and z is the propagation distance.

$$\varphi_{\max} = \gamma P_0 \frac{(1-\exp(-\alpha z))}{\alpha}. \qquad \text{(A.2)}$$

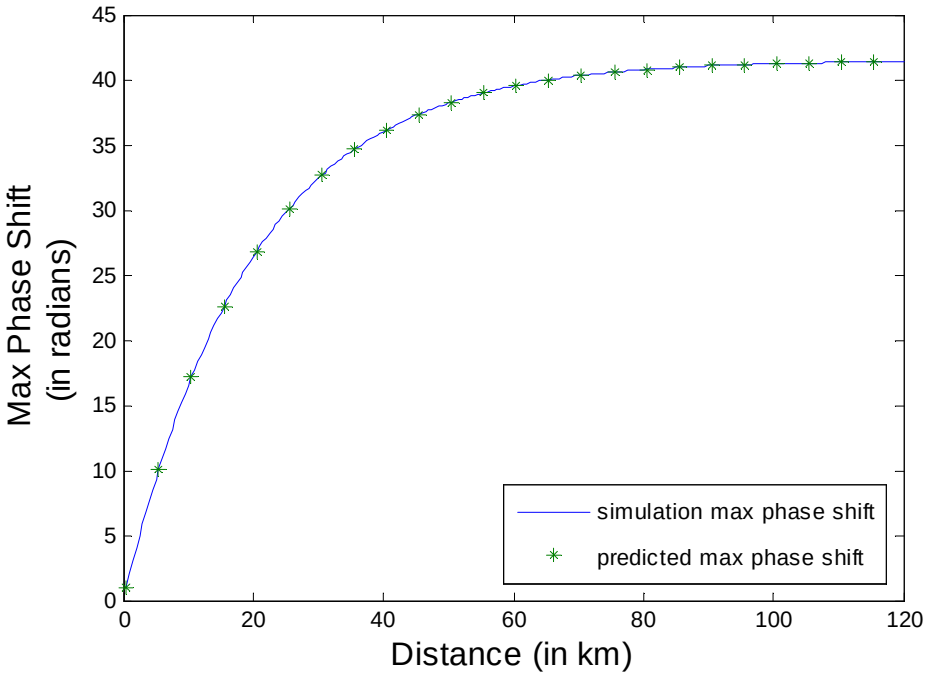

Figure A.4: Maximum phase shift versus the propagation distance of a 14.14ps 1W Gaussian pulse in the absence of dispersion.

In the above benchmark exercises, the nonlinear Schrödinger equation (NLSE – Equation 3.1), instead of the more general propagation equation (Equation 3.2), acted as the basic underlying formula that governed the behavior of the output pulses and the

corresponding simulations. In almost all practical situations where the pulsewidth is above 30 to 50fs, the NLSE is an excellent approximation of the propagation equation. In the following simulations, the more generalized propagation equation including the self-steepening and intrapulse Raman scattering terms (delayed nonlinear response) was studied, and the code incorporating these nonlinear effects into the split-step Fourier method was benchmarked.

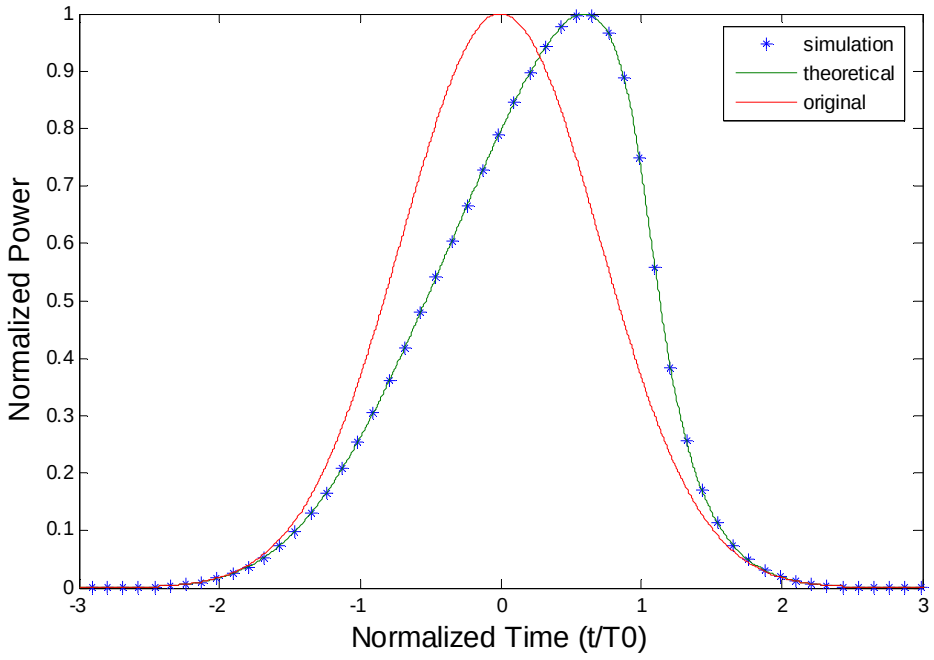

Figure A.5: Generation of an optical shock due to propagation of 1W 82.23fs 1550nm Gaussian pulse through 15.748km of lossless dispersionless fiber.

Figure A.5 shows a plot of an initial 1W peak power 82.23fs Gaussian pulse and the simulated (using the split-step Fourier technique) and predicted output pulses after propagation through 15.748km of lossless dispersionless fiber (γ = 1.27W^{-1}/km, λ_0 = 1550 nm, f_R = 0). In this simulation, a delayed nonlinear response was assumed, and as a result, an optical shock front can be seen in the output. The theoretical output pulse can be obtained by solving the following differential equation (Equation A.3) given by the propagation equation:

$$\frac{\partial A(z,t)}{\partial z} = i\gamma\left(1+\frac{i}{\omega_0}\frac{\partial}{\partial t}\right)\left(A(z,t)\left|A(z,t)\right|^2\right)$$
$$A(0,t) = \sqrt{P_0}\,\exp(-\frac{t^2}{2T_0}) \qquad \text{(A.3)}$$

The output intensity is given by the following relations (Equation A.4). As shown in Figure A.5, there is total agreement between the theoretical and simulation intensities.

$$\left|A(z,t)\right|^2 = P_0 I;$$
$$I(z,t) = \exp\left[-\left(\frac{t}{T_0}-\frac{3I\gamma P_0 z}{\omega_0 T_0}\right)^2\right] \qquad \text{(A.4)}$$

Combined nonlinearity and dispersion benchmarks

In Figure A.6, a 251.903kW 82.23fs Gaussian pulse was dispersed through 125.03mm of lossless DCF fiber (β_2 = 21.6321 ps^2/km, γ = 1.27W^{-1}/km, λ_0 = 1550 nm, f_R = 0) with no higher-order dispersion using the split-step Fourier technique. Again, a

delayed nonlinear response was assumed as in the propagation equation (3.2). As a result of the dispersive medium, the effect of the optical shock is not as severe as the one shown in Figure A.5. This output was shown to be in good agreement with the benchmarked plot (not shown here) in Agarwal.[19]

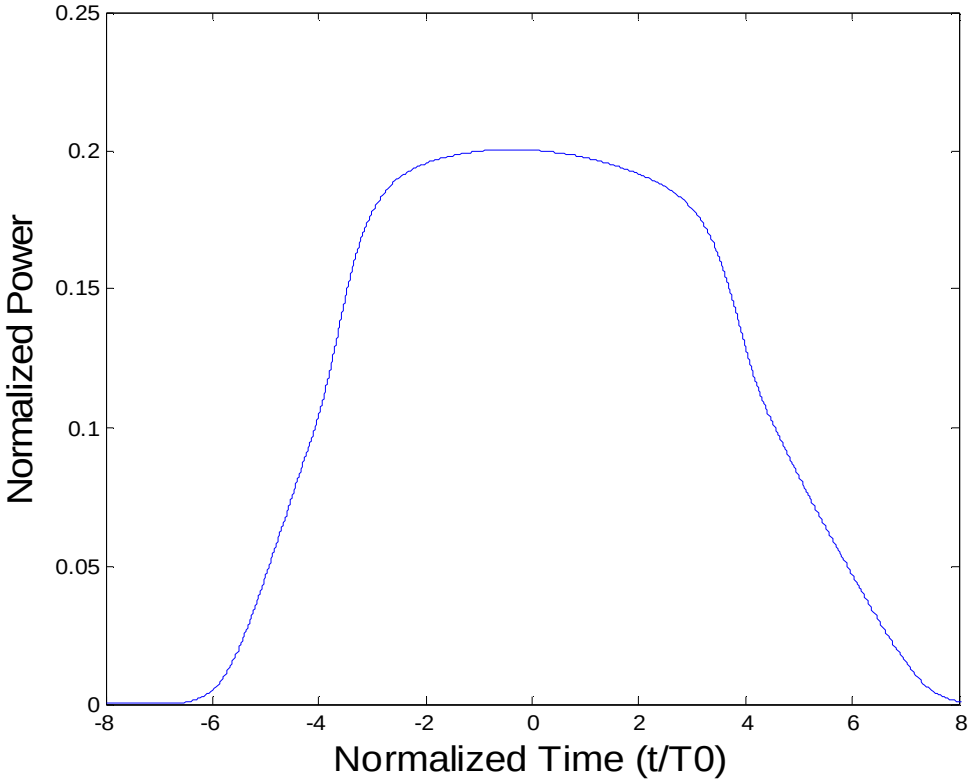

Figure A.6: Generation of an optical shock due to propagation of 251.903kW 82.23fs 1550nm Gaussian pulse through 125.03mm of lossless DCF fiber.

In order to benchmark the operation of β_4 in the split-step code, the ability to propagate a soliton in a nonlinear lossless dispersive medium (β_2 = -21.6321 ps^2/km; β_3 =

0 ps^3/km; β_4 = -3.6068 ps^4/km; α = 0dB/km; γ = 1.2W^{-1}/km λ_0 = 1550 nm) in the absence of third-order dispersion was tested. In such a case, a stable soliton, whose intensity parameters are given in Equation A.5, is able to propagate.[33] The result after propagation of the soliton in 10cm of an anomalously dispersive medium is shown in Figure A.7.

$$|A(z,t)|^2 = \frac{9\beta_2^{\,2}}{5\gamma|\beta_4|} sech^4\left(\frac{t}{\sqrt{5\beta_4/3\beta_2}}\right) \qquad \text{(A.5)}$$

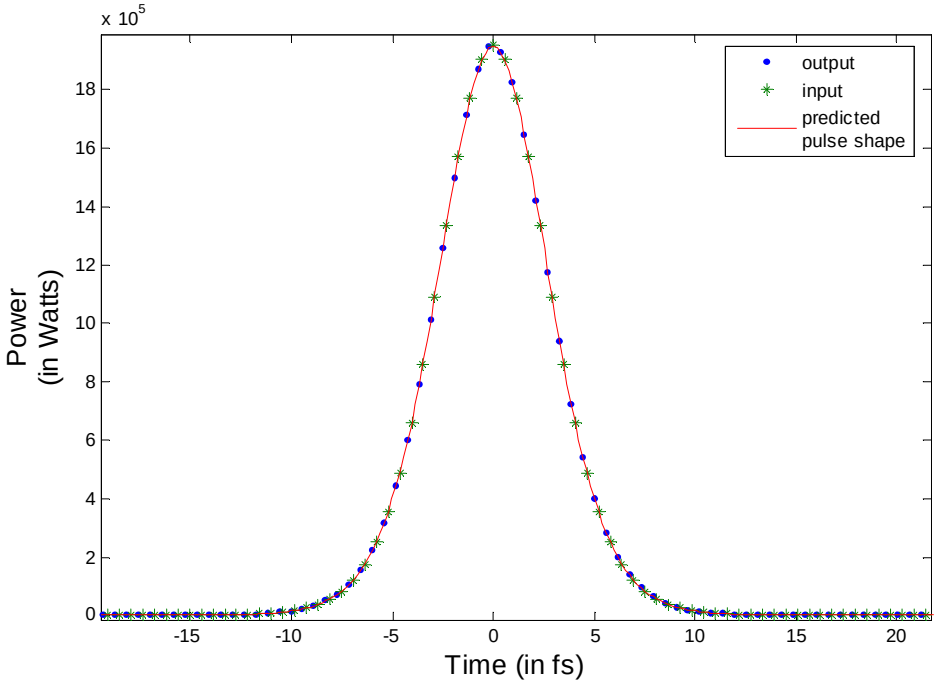

Figure A.7: Propagation of a 1.95megawatt peak power bright optical soliton in 10cm of a lossless medium.

REFERENCES

[1] Tektronix. “Arbitrary Waveform Generator,” http://www.tek.com/site/ps/0,,76-19779-INTRO_EN,00.html (Accessed December 29, 2006).

[2] WEINER, A. M., “Femtosecond optical pulse shaping and processing,” Prog. Quant. Electr., vol. 19, pp. 161-237, 1995.

[3] WEINER, A. M., SILBERBERG, Y., FOUCKHARDT, H., LEAIRD, D. E., SAIFI, M. A., ANDREJCO, M. J., and SMITH P. W., “Use of femtosecond square pulses to avoid pulse breakup in all-optical switching,” IEEE J. Quant. Electr., vol. 25, no. 12, pp. 2648-2655, 1989.

[4] LEAIRD, D. E. and WEINER, A. M., “Femtosecond direct space-to-time pulse shaping,” IEEE J. Quant. Electr., vol. 37, no. 4, pp. 494-504, 2001.

[5] WEINER, A. M., “Femtosecond pulse shaping using spatial light modulators,” Review of Scientific Instruments, vol. 71, no. 5, pp. 1929-1960, 2000.

[6] KUROKAWA, T., TSUDA, H., OKAMOTO, K., NAGANUMA, K., TAKENOUCHI, H., INOUE, Y., and ISHII, M., “Time-space-conversion optical signal processing using arrayed-waveguide grating,” Electron. Lett., vol. 33, pp. 1890-1891, 1997.

[7] MIYAMOTO, D., MANDAI, K., KUROKAWA, T., TAKEDA, S., SHIODA, T., and TSUDA, H., “Waveform-controllable optical pulse generation using an optical pulse synthesizer,” IEEE Photon. Tech. Lett., vol. 18, no. 5, pp. 721-723, 2006.

[8] VERLUISE, F., LAUDE, V., CHENG, Z., SPIELMANN, CH., and TOURNOIS, P., “Amplitude and phase control of ultrashort pulses by use of an acousto-optic programmable dispersive filter: pulse compression and shaping,” Opt. Lett., vol. 25, no. 8, pp. 575-577, 2000.

[9] KITAYAMA, K., OSAWA, S., WADA, N., and CHUJO, W., “Optical pulse train synthesis of arbitrary waveform using weight/phase-programmable 32-tapped delay

line waveguide filter," Optical Fiber Communication Conference and Exhibit, 2001, vol. 3, pp. WY3/1-WY3/3, 2001.

[10] WARREN, W. S., RABITZ, H., and DAHLEH, M., "Coherent control of quantum dynamcs: the dream is alive," Science, vol. 259, no. 5101, pp. 1581-1589, 1993.

[11] CHOU, P. C., HAUS, H. A., and BRENNAN III, J. F., "Reconfigurable time-domain spectral shaping of an optical pulse stretched by a fiber Bragg grating," Opt. Lett., vol. 25, pp. 524-526, 2000.

[12] SAPERSTEIN, R. E., ALIĆ N., PANASENKO, D., ROKITSKI, R., and FAINMAN, Y., "Time-domain waveform processing by chromatic dispersion for temporal shaping of optical pulses," J. Opt. Soc. Am. B., vol. 22, no. 11, pp. 2427-2436, 2005.

[13] WEINER, A. M., HERITAGE, J. P., and KIRSCHNER, E. M., "High-resolution femtosecond pulse shaping," J. Opt. Soc. Am. B., vol. 5, pp. 1563-1572, 1988.

[14] TSUDA, H., OKAMOTO, K., ISHII, T., INOUE, Y., TAKENOUCHI, H., and KUROKAWA, T., "Second- and third- order dispersion compensator using a high-resolution arrayed-waveguide grating," IEEE Photon. Tech. Lett., vol. 11, no. 5, pp. 569-571, 1999.

[15] OHNO, K., TANABE, T., and KANNARI, F., "Adaptive pulse shaping of phase and amplitude of an amplified femtosecond pulse laser by direct reference to frequency-resolved optical gating traces," J. Opt. Soc. Am. B., vol. 19, no. 11, pp. 2781-2790, 2002.

[16] AZAÑA, J. and CHEN, L. R., "Synthesis of temporal optical waveforms by fiber Bragg gratings: a new approach based on space-to-frequency-to-time mapping," J. Opt. Soc. Am. B, vol. 19, no.11, pp. 2758–2769, 2002.

[17] UDESHI, K., LIAO, K-H, LONG, Q., GIANCHANDANI, Y. B., and GALVANAUSKAS, A., "Programmable optical wave form shaper on a microchip," Appl. Phys. Lett., vol. 89, 031120, 2006.

[18] RAMASWAMI, R. and SIVARAJAN, K. N., Optical Networks: A Practical Perspective, 2nd ed., Academic Press, San Diego, CA, 2002.

[19] AGARWAL, G. P., Nonlinear Fiber Optics (Optics and Photonics Series), 2nd ed., Academic Press, London, 1995.

[20] Centellax. “Arbitrary Waveform Generator,” http://www.centellax.com/products/testmeas/pdf/TG1P4A.pdf (Accessed April 11, 2007).

[21] SHASHI, K. and YEATES, A. (ed.), Nonlinear Optical Materials: Theory and Modeling, American Chemical Society, Washington, DC, 1996.

[22] DUBOVITSKY, S., STEIER, W. H., KUO, Y-H., YEGNANARAYANAN, S., and JALALI, B., “A novel technique for wavelength independent bias of Mach-Zehnder modulators,” International Topical Meeting on Microwave Photonics, pp. 57-60, 2002.

[23] REFI, J. R., "Mixing TrueWave RS Fiber with other single-mode fiber designs within a network," OFS White Paper 1002-0702, pp. 1-7, 2002.

[24] LI, J-S and HE, S-L, “Electro-optic modulator based on Si_2N_2O substrate,” Optical Engineering, vol. 45, no. 1, pp.14603-1-4, 2006.

[25] SINKIN, O. V., HOLZLÖHNER, R., ZWECK, J., and MENYUK, C. R., "Optimization of the split-step Fourier method in modeling optical-fiber communications systems," J. Lightwave Tech., vol. 21, no. 1, pp. 61-68, 2003.

[26] SHEN, S., CHANG, C. C., SARDESAI, H. P., BINJRAJKA, V., and WEINER, A. M., "Effects of self-phase modulation on sub-500 fs pulse transmission over dispersion compensated fiber links," J. Lightwave Tech., vol. 17, no. 3, pp. 452-461, 1999.

[27] WEINER, A. M., HERITAGE, J. P., and SALEHI, J. A., "Encoding and decoding of femtosecond pulses," Opt. Lett., vol. 13, no. 4, pp. 300-302, 1988.

[28] CURTIN, M. and O'BRIEN, P., "Phase-locked loops for high-frequency receivers and transmitters-part 1," Analog Dialogue 33-3, pp. 1-4, 1999.

[29] SAPERSTEIN, R. E., XIE, X. B., YU, P. K. L., and FAINMAN, Y., "Demonstration of a microwave spectrum analyzer based on time domain processing

of ultrafast pulses," Conference on Lasers and Electro-Optics, vol. 2, pp. 1109-1111, 2005.

[30] BOIVIN, L., NUSS, M. C., STARK, J. B., KNOX, W. H., and CUNDIFF, S. T., "206-channel chirped-pulse wavelength-division-multiplexed source," Conference on Lasers and Electro-Optics, vol. 11, p. 280, 1997.

[31] SARDESAI, H. P., CHANG, C. C., and WEINER, A. M., "A femtosecond code-division multiple-access communication system test bed," J. Lightwave Tech., vol. 16, no. 11, 1998.

[32] CONG, W., YANG, C., SCOTT, R. P., HERNANDEZ, V. J., FONTAINE, N. K., KOLNER, B. H., HERITAGE, J. P., BEN YOO, S. J., "Demonstration of 160- and 320-Gb/s SPECTS O-CDMA network testbeds," IEEE Photon. Tech. Lett., vol. 18, no. 15, pp. 1567-1569, 2006.

[33] PICHÉ, M., CORMIER, J-F., and ZHU, X., "Bright optical soliton in the presence of fourth-order dispersion," Opt. Lett., vol. 21, no. 12, pp. 845-847, 1996.